BUCKLING RESISTANCE OF PARTIALLY ENCASED COLUMNS UNDER FIRE

Amari Soufyane

Final Report of the Thesis Presented to the

School of Technology and Management

Polytechnic Institute of Bragança

To the Fulfilment of the Requirements for the Master of Science Degree
in

Construction Engineering

July 2017

This page was intentionally left in blank

BUCKLING RESISTANCE OF PARTIALLY ENCASED COLUMNS UNDER FIRE

Amari Soufyane

Final Report of the Thesis Presented to the

School of Technology and Management

Polytechnic Institute of Bragança

To the fulfilment of the Requirements for the Master of Science Degree in

Construction Engineering

Supervisor at IPB: Prof. Dr.Paulo Alexandre Gonçalves Piloto

Supervisor at UHBC: Prof. Dr. Noureddine Benlakehal

July 2017

This page was intentionally left in blank

ACKNOWLEDGMENT

I start by thanking the God for having given us the courage, the will, the love of knowledge and above all patience in order to produce this modest work.

My thanks and my deepest gratitude goes to my parents who supported me from the beginning since my early days in school until this point. Also my brother and sister and also my girlfriend.

My first thanks go to my supervisors Dr. Paulo Piloto, coordinator Professor from the Department of Applied Mechanics, School of Technology and Management, Polytechnic Institute of Bragança, and Dr. Nourredine Benlakehal, Department of Civil Engineering, Faculty of Civil Engineering and Architecture, University Hassiba Benbouali of Chlef.

I thank all my professors especially from IPB Dr. Luís Mesquita, Dra. Elza Fonseca and Dr. Manuel Minhoto. And from UHBC Dr Lamri Belkacem, Dr. Kada Abdelhak and Dr Abdellah Benarous for helping, support and encouragement.

I also thank all my family, all my friends Leonardo Calió and Ricardo Hoffstater from Brazil and Mohamed form Tunisia. And also my friends from Algeria Habbar Ghania, Nechab Khadouma, Khetata Mohamed Seddik and Zourkane Abdelkader, I wish a better futur for them.

Finally, my sincere thanks to all those who helped me, I say to them “thank you”.

Amari Soufyane

This page was intentionally left in blank

ABSTRACT (EN)

The fire resistance of partially encased columns depends on the temperature evolution during fire exposure. This work aims to evaluate the effect of the balanced summation model on the design of the buckling load of Partially Encased Columns under fire situation. New improvements will be presented to assess fire resistance, suggesting some modification in the Annex G of Eurocode EN 1994-1-2.

The advanced calculation method presented herein is based on the 3D modelling of the Partially Encased Column, using steel profiles ranging from IPE200 to IPE500 and HEB160 to HEB500, and using different buckling lengths. An incremental and interactive procedure is used to solve the geometric and material non-linear behaviour. The temperature effect is taken into account, using the uncouple thermal-structural analysis.

The results obtained by the numerical simulations are in good agreement with the new simple calculation method and are also useful to prescribe the buckling curve that best fits the 3D simulation results.

KEY WORDS

Partially encased column; Fire resistance; Simplified and advanced calculation methods; Buckling load.

This page was intentionally left in blank

RESUMO (PT)

A resistência ao fogo de pilares parcialmente revestidos com betão, dependem da evolução da temperatura durante o tempo de exposição ao fogo. Este trabalho visa avaliar o efeito do Método da Soma Pesada na conceção da carga resistente à encurvadura de pilares parcialmente revestidos em situação de incêndio, de acordo com as normas europeias. Serão apresentadas novas formulações para avaliar a resistência ao fogo, no qual se sugere alterações de alguns aspetos prescritos no Anexo G do Eurocode EN 1994-1-2.

O método avançado de cálculo apresentado nesta tese é baseado na modelação 3D da coluna parcialmente revestida, utilizando perfis estruturais na gama compreendida desde IPE200 ao IPE500 e HEB160 ao HEB500, e usando diferentes comprimentos de encurvadura. Um processo incremental e interativo é utilizado para resolver um problema não lienar geométrico e material.. O efeito da temperatura é considerado utilizando a análise sem acoplamento termo-estrutural.

Os resultados obtidos pelas simulações numéricas serão utilizados para comparar com os valores do método de cálculo simplificado e também será útil para prescrever uma curva de flexão que melhor se adeque para os resultados das simulações em 3D.

PALAVRAS CHAVE

Colunas mistas parcialmente revestidas, Resistência ao fogo, Método avançado e simplificado de cálculo, Carga resistente à encurvadura

This page was intentionally left in blank

INDEX

ANNEX

This page was intentionally left in blank

INDEX OF FIGURES

INDEX OF TABLES

NOTATIONS

Latin upper case letters

A_c	Cross-sectional area of the concrete.
A_s	Cross-sectional area of the reinforcement.
A_m/V	Section factor.
E	Modulus of elasticity.
E_a	Modulus of elasticity of the structural steel at room temperature.
$E_{a,\theta}$	Modulus of elasticity of the structural steel at elevated temperature.
E_c	Effective modulus of elasticity of the concrete at room temperature.
E_{cm}	Secant modulus of elasticity of the concrete at room temperature.
$E_{c,\sec,\theta}$	Characteristic value for the secant modulus of concrete in the fire situation.
$(EI)_{fi,c,z}$	Effective flexural stiffness of the concrete around the z-axis exposed to fire
$(EI)_{fi,eff,z}$	Effective flexural stiffness of a composite section around the z-axis exposed to fire.
$(EI)_{fi,f,z}$	Effective flexural stiffness of the flange around the z-axis exposed to fire.
$(EI)_{fi,w,z}$	Effective flexural stiffness of the web around the z-axis exposed to fire.
$(EI)_{fi,s,z}$	Effective flexural stiffness of the reinforcement around the z-axis exposed to fire.
E_s	Modulus of elasticity of the steel reinforcement at room temperature.
$E_{s,\theta}$	Characteristic value for the slope of the linear elastic range of the stress-strain relationship of reinforcing steel at elevated temperatures.
H_t	Factor.
I_y	Moment of inertia relative to the axis y-y.
I_z	Moment of inertia relative to the axis z-z.

Q_c	Is the convective part of the rate of heat release.
$[K]$	The element stiffness matrix.
$[S]$	Geometric stiffness matrix of the element.
L	Length of the column.
L_{cr}	Buckling length.
$N_{fi,cr,z}$	Elastic critical load (≡ Euler buckling load) around the axis Z in the fire situation.
$N_{fi,pl,Rd}$	Normal plastic stress resistant exposed to fire.
$N_{fi,b,Rd}$	Buckling resistant exposed to fire.
T,θ	Temperature.
W_{pl}	Plastic section modulus.

Latin lower case letters

b	Width of the cross section.
b_w	Width of the web element.
$b_{c,fi}$	Neglected external layer of concrete.
$b_{c,fi,horizontal}$	Neglected external layer of concrete in horizontal directions.
$b_{c,fi,vertical}$	Neglected external layer of concrete in vertical directions.
$c_a(\theta)$	Specific heat of steel.
$c_p(\theta)$	Specific heat of concrete.
f_{cd}	Design value of the yield strength of the steel at room temperature.
f_{cm}	The average design value of the yield strength of the steel at room temperature.
f_{sk}	Characteristic value of the yield strength of the steel reinforcement at room temperature
f_{ck}	Characteristic value of the compressive strength of the concrete at room temperature.
$f_{u,\theta}$	The ultimate strength at elevated temperature, allowing for strain-hardening.

h	Total height of a cross section.
h_1	Height between web.
$\dot{h}_{net}$	Net heat flow per unit area.
$\dot{h}_{net,c}$	Net convective heat flux per unit surface area.
$\dot{h}_{net,d}$	Design value of the density of heat flow per unit area.
$\dot{h}_{net,r}$	Net radioactive heat flux per unit surface area.
$h_{w,fi}$	Height reduction of the web.
$k_{E,\theta}$	Reduction factor for the slope of linear elastic range at the steel temperature θ_a reached at time t.
$k_{c\theta}$	Reduction factor for the tensile strength of concrete.
$k_{p,\theta}$	Reduction factor of the yield point of structural steel giving the proportional limit at temperature θ_a reached at time t.
$k_{y,\theta}$	Reduction factor for effective yield strength at the steel temperature θ_a reached at time t.
t	Time.
t_f	Flange thickness.
t_w	Web thickness.
u	Geometric mean of the distances u_1 u_2 .
u_1 u_2	Shortest distance between the reinforcing steel centre and inner face of the flange or the nearest end of concrete.
z	Height along the flame axis.

Greek upper case letters

$\nabla\theta$	$\nabla\theta=\langle d\theta/d_x \quad d\theta/d_y \quad d\theta/d_z\rangle^t$
ϕ	Configuration factor.
ϕ_{LT}	Value to determine the reduction factor χ_{LT} .
$\phi_{LT,\theta,com}$	Value to determine the reduction factor χ_{LT} at elevated temperature θ.

Greek lower case letters

α	Imperfection factor, thermal elongation coefficient.
α_c	Coefficient of heat transfer by convection.
β	Parameters to take into account the effect of biaxial bending.
ε	Emissivity of material.
$\varepsilon_{c,\theta}$	Thermal strain of concrete.
$\varepsilon_{p,\theta}$	Thermal strain of pressurising steel.
$\varepsilon_{s,\theta}$	Thermal strain of reinforcing steel.
ε_f	Emissivity of the fire.
ε_m	Surface emissivity of the member.
$\eta_{fi,t}$	Amplitude charging for fire resistance calculation.
θ_a	Temperature of steel profile [°C].
θ_c	Temperature of concrete [°C].
θ_s	Temperature of reinforcement [°C].
θ_g	Gas temperature in the vicinity of the element or in the fire compartment.
θ_r	Effective radiation temperature of the fire environment.
$\theta_{c,t}$	Average temperature in the concrete at time t.
$\theta_{f,c}$	Average temperature in the flange at time t.
$\theta_{w,c}$	Average temperature in the web at time t.
$\theta_{s,c}$	Average temperature in the reinforcement at time t.
λ_a	Thermal conductivity of steel.
λ_c	Thermal conductivity of concrete.
$\lambda_{(\theta)}$	Thermal conductivity.
$\overline{\lambda}_{LT}$	Relative slenderness for lateral torsional buckling.

ρ	Density.
ν	Poisson coefficient in elastic regime.
σ	Stefan Boltzmann constant.
σ_x	Principal stress in the x direction.
χ_{LT}	Reduction factor for lateral torsional buckling.
$\chi_{LT,fi}$	Reduction factor for buckling torsional lateral sections exposed to fire.

This page was intentionally left in blank

CHAPTER.1 INTRODUCTION

Economic and social development in the world today is so great that it would be impossible to imagine everyday life without the use of steel and concrete. Every day new infrastructure works such as ports, airports, highways, railways, buildings, among others, show the evolution that society is going through at the moment. The peculiar characteristics of steel and concrete made possible the advances in the process of systematization of construction methods. The use of these materials transformed the construction industry into a gigantic market, placing technological development and scientific research on these materials on another level.

For the dimensioning of structural elements subjected to compression, which is the focus of this work, special attention must be paid to normative prescriptions, since if its collapse occurs it can trigger the overall instability of the structure. National and international standards present simplified methods that do not always refer to economic projects. In this way, advanced calculation methods allow a better evaluation of the structural performance with a more rigorous analysis of the structure in a fire situation.

Figure 1 - Composite building.

The partially encased concrete and steel columns have a higher fire resistance when compared to the bare steel columns. However, it is not possible to calculate the resistance of all members of their composition taking into account only the temperature of the steel. The resistance of these elements when subjected to fire conditions depends on the evolution of the temperature during the period exposed to fire.

The annex G of CEN - EN 1994-1-2, [1]. Through the simplified calculation method, allows the calculation of the buckling resistant load of partially encased columns in a fire

situation for different resistance times R30, R60, R90 and R120 when subjected to the standard fire. Proposal was suggested for the calculation of the plastic compression load and stiffness of each cross-section component. This work aims to evaluate and validate the new formulas proposed, and if necessary to propose an improvement of them.

1.1- Advantages and disadvantages of partially concrete encased sections

Composite elements made of steel and concrete combine the advantages of each of the materials in just one element. The association of structural steel profiles with simple or reinforced concrete forms a composite and solid structure, giving great resistant capacity without increasing the dimension of the cross section. The element can be prefabricated or moulded in place. The main advantages are: High bearing resistance, especially in case of welded steel sections; No need of formwork; Simple solution for joints and load introduction; Easy solution for later strengthening and additional later joints; No need for edge protection. The main inconvenient is a lower fire resistance in comparison with concrete encased sections.

1.2- Objective and methodology

The main objective of this work is to study the behaviour of partially encased columns in a fire situation, by means of an approximated simple method and numerical simulations, to determine the buckling resistance.

A three-dimensional (3D) numerical model will be presented, using finite elements, considering not only the thermal action, but also the static loading simulating the service conditions. For the verification of the buckling resistance, twenty-four cross-sections will be analysed, based on 14 HEB profiles and 10 IPE profiles, considering the length of 3m and 5m.

The fire resistance of partially encased columns depends on the evolution of temperature during exposure to fire. This work aims to evaluate the effect of the balanced summation model on the design of the buckling load of partially encased columns under fire situation, in accordance with European standards. New formulas will be presented to assess fire resistance, suggesting changes in some aspects prescribed in Annex G of CEN - EN 1994-1-2, [1].

The simplified method of calculation is based on new formulations for specific rating times of resistance to fire: R30, R60, R90 and R120 minutes.

The new formulae proposed to determine the buckling load and to evaluate with more accuracy the temperature effect, consequently the strength of the cross-section components will

be used to improve the balanced summation method. This method includes a new average value for the calculation of the assumed constant flange temperature, includes the new 400ºC isothermal criterion to determine the residual height of the web, includes the new 500 ºC isothermal criterion to determine the residual area of the concrete and also includes the new average uniform temperature for the reinforcement.

The advanced calculation method, using the ANSYS software, is based on the 3D modelling of the column with perfect contact between all the components. The Finite Element Method uses incremental and interactive process to define the buckling resistance. The thermal-structural uncouple analysis is considered herein, which is, not only the thermal action in the element totally involved by the fire, but also the static load to be supported in service conditions. The thermal effect as a result of the deformation of the material is not consider to modify the temperature field of the column, because the effect of the fire is much higher.

The results obtained by the numerical simulations will be used to compare with the values of the elastic critical load and the buckling resistant load obtained from the Simplified Calculation Method - New Proposal, and from the current version of the EN 1994-1-2 Annex G, [1].

1.3- Work characterization

Fire resistance of partially encased columns (HEB, IPE, other non-European cross section) depends on the temperature evolution during fire exposure. This work aims to assess de effect of the balanced summation model into the design of the axial buckling load of partially encased columns under fire, according to CEN - EN 1994-1-2, [1]. New formulae will be proposed to evaluate the fire resistance, based on new simple formulas to determine the flange temperature, the residual height and temperature of the web, the residual cross section and temperature of concrete, and finally the reduced stiffness and strength of reinforcement. An advanced calculation method with (ANSYS) software will used to validate new and safe formulae, based on the analysis of the column totally engulfed in fire for different fire ratings.

Two different methods of analysis are to be used: The simplified calculation method, based on new simple formulae for several fire ratings R30, R60, R90 and R120; The advanced calculation method, based on 3D finite element method to determine the buckling resistance of columns under fire, for several fire ratings R30, R60, R90 and R120. This requires the result of the nonlinear, unsteady thermal analysis, to define the static temperature field required for the

incremental and iterative solution method to each fire rating. The numerical analysis is used with material and geometric nonlinearities.

1.4- Fire safety Engineering

Fire safety engineering can be considered as the field of engineering dedicated towards the adequate design of structures in case of a fire, such that the elements surrounding the building compartment containing the fire are able to fulfil its function, whether it is structural, insulating or partitioning. The aim of the fire safety engineering is to prevent or reduce the loss of lives and avoid significant damage to the structure through the implementation of adequate preventive, protective and/or suppression systems, [2].

In the event of a fire, a building is subjected to both mechanical and thermal actions (fire load). Thermal actions correspond to the rise in temperature of the hot gases within the room and are dominated by the heat transfer conditions at the surface of the building elements. Under the impact of thermal actions, the temperature of the structure increases. This phenomenon is due to the "heat transfer" and potentially leads to thermal expansion and deterioration of mechanical properties in the heated parts of the construction elements.

According to Algerians regulation, [3], and depending on the type of structural elements, fire resistance requirements depends on the classification of buildings under analysis. Two types of buildings are considered (housing and office building):

1.4.1- Housing

The type of building houses are dividing in 4 families.

The first family may be considered detached or semi-detached, single-detached dwelling house, not including cellars and underground or semi-buried floors as we can see in Figure 2.

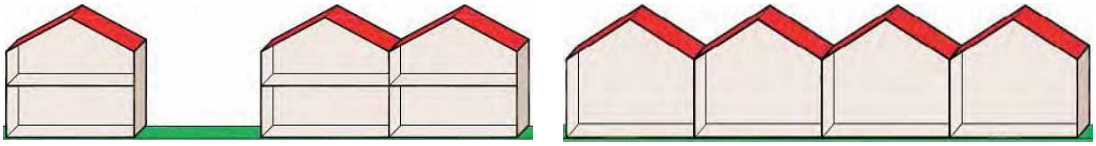

a) Detached or semi-detached dwelling-house (one floor on the ground floor) at most.

b) Single-family dwellings on the ground floor grouped in strips.

Figure 2 – The first family of building classification.

The second family may be considered single-detached or semi-detached dwellings with more than two levels, inhabitable, single-family dwellings and collective dwellings with the lowest floor of the highest dwelling located less than 8 meters from the ground as we can see in Figure 3.

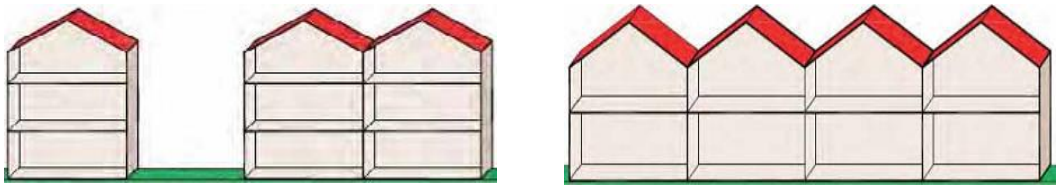

a) Detached or semi-detached dwellings of more than one floor on the ground floor.

b) Single-storey dwellings on the ground floor only.

Figure 3 – The Second family of building classification.

The third family is considered for the collective buildings with the high of the building corresponding to a number of floors h, higher than 7 floors $h = R + 7\,\text{max}$, being R the number of floors.

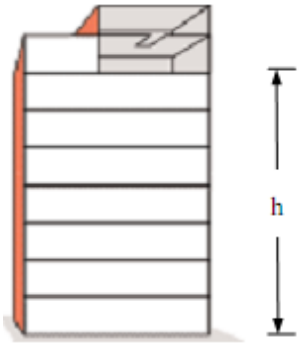

Figure 4 – The third family of building classification.

The Fourth family considers collective buildings with high bigger than 28 m and smaller than 50 m.

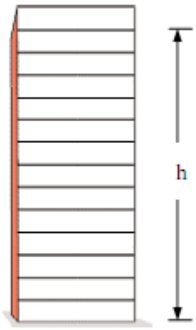

Figure 5 - The fourth family of building classification.

The Table 1 presents the fire requirements for each of the load bearing element used in housing building in fire situation.

Table 1 – The fire ratings times of housing resistance.

Family	1 Family	1st Family	2nd Family	2nd Family	2nd Family	3rd Family	4re Family
	individual or paired	Strip	individual or paired	Strip	Collective	h <28m	28m<h<50m
Structural Requirement	R 15	R 15	R 30	R 30	R 30	R 60	R 90

1.4.2- Office building

The fire stability of the structure for office buildings is defined as follows see Table 2 .

Table 2 - The fire ratings times of office building resistance.

High floor height	$h \leq 8$ m	8 m < $h \leq 28$ m
Structural Requirement	No requirement	R 60
floor Requirement	No requirement	R 60

1.5- State of the art

In 1964 Malhotra and Stevens, [4], presented the results of fourteen fire resistance tests on totally encased steel sections with free thermal elongation, The results show that the concrete cover has a significant effect on the fire resistance, and the lightweight concrete has higher fire resistance compared to normal gravel concrete which has more spalling. Given the fact that the load level is known to play a very important role in the fire resistance of columns.

In 1987, J. B. Schleich, [5], was the project leader of an important experimental and numerical campaign developed to test and analyse the behaviour of Partially Encased Columns (PEC) and Beams (PEB) with and without connection to the slab. This project demonstrated the possibilities of the computer code CEFICOSS, able to cover most structural fire applications. This programme CEFICOSS has to be considered as a general thermo-mechanical numerical Computer code allowing predicting the behaviour under fire conditions of structural building parts such as columns, beams or frames. These structural elements could be composed either of bare steel profiles or partially protected.

In 1990 Lie and Chabot, [6], tested five concrete-filled circular hollow columns and proposed a mathematical model to predict the temperature distribution within the cross-section and the structural response to fire. The heat transfer analysis is based on a division of the circular section into annular elements, while gas temperature around the section was considered uniform. The effect of moisture in the concrete was considered, by assuming that when an element within the cross section reaches the temperature of 100ºC or above, all the heating to that element drives out moisture until it is dry. This mathematical model was later applied to composite steel-concrete columns with rectangular cross-section and circular composite

columns with fibre-reinforced concrete. The same authors presented another study in 1996 on the behaviour of fibre-reinforced concrete-filled hollow columns. The benefit of this type of concrete on the fire resistance of the columns was compared with those of the plain and bar-reinforced concrete.

In 2000 Stefan Winter and Jörg Lange, [7], present tests on partially encased columns using high-strength steel. Special emphasis was laid on strength tests of high-tensile-steel under fire condition because the steel of the flanges would be directly exposed to high temperatures in the event of a fire. With the currently available data it is not possible to give exact proof of the reliability of the design formulae of the German codes for high strength steel in Partially Encased Composite Columns. Furthermore the extreme weakening of the yield strength under high temperatures severely reduces the efficiency of these columns.

In 2006 A.A. Marinopoulou, V.D. Balopoulos, C.N. Kalfas, [8], developed a simulation of partially encased composite steel–concrete columns. This research presents a method for simulating composite steel-concrete columns of double-symmetrical, partially encased cross-sections, as equivalent steel columns to fictitious cross-section, for the purposes of linear elastic analysis. Plate dimensions are chosen to match the compression resistance and principal bending stiffness of the composite section. Section equivalence results in three algebraic equations for the dimensions of the additional plates, in terms of the geometry of the actual section and the material properties of steel, concrete, and reinforcement bars. The proposed method combines accuracy, efficiency, and convenience; it takes advantage of widely available software for linear elastic steel structure analysis and obviates the need for finite-element simulation.

In 2010 Ehab Ellobody and Ben Young, [9], presented an investigation of concrete encased steel composite columns at elevate temperatures. The behaviour of the composite columns was investigated using a nonlinear 3D finite element model. A thermal 3D finite element analysis was performed using the software ABAQUS. The structure was simulated using uncoupled structural-thermal analysis. The research presented the comparison between the fire test results and finite element results. The authors concluded that the model is capable to predict the behaviour of concrete steel columns at elevated temperatures, and also shown that the Eurocode 1994-1-2 predictions are generally conservative for the concrete encased steel composite columns at elevated temperatures, except for the columns with high load ratio.

In 2013, Paulo A.G. Piloto et al, [10], conducted an experimental investigation using partially encased beams to test its fire resistance and found that the beams attained the ultimate

limit state by lateral torsional buckling mode. The results show the dependence of the fire resistance on the load level. The results for critical temperature are also presented. The results have provided essential data to the calibration and validation of new simplified design methods, tabulated data and advanced numerical methods.

In 2014 Sadaoui Arezki and Illouli Said, [11], proposed a practical and theoretical evaluation of the resistance of partially encased composite steel-concrete columns in fire situation according to Eurocode EN 1994-1-2 subjected to eccentric loading. The practical method is based on Campus-Massonet criteria adapted for the calculations of the buckling resistance of eccentrically loaded columns, and combines accuracy, efficiency and convenience regarding the interactions with combined compression and bending loads process as EC4 procedure. The design of the procedure is codified in a program, used to investigate the effects of load level, slenderness ratio, and reinforcement cover on the fire resistance of the column. The work present some examples of application and results and shows that the design for fire becomes critical for classes of fire resistance above R60.

In 2016, A. Piquer and D. Hernandez-Figuerido, [12], describes a study of partially encased composite (PEC) columns of an I-shaped steel section. These columns were built with a standard size rolled steel sections with additional longitudinal steel reinforcing bars in an attempt to improve their behaviour. A range of geometric cross-sections and material properties have been used to show the cheapest columns with the best performance. The structure of this article is firstly presented with a presentation of the problem, defining variables, variables ranges and the considered constraints. Then, it has been shown the cost of each solution. Afterwards, a presentation to verify the resistance and stability of steel columns with or without fire protection and (PEC) columns at ambient temperature. Finally, the results obtained are presented with some analyses. During the analyses, the steel columns demonstrated worst performance in fire conditions, therefore the resistance of steel columns with protection and PEC columns is quite good at high temperatures. The author concludes that (PEC) columns offer the best option of three typologies of columns studied and the recommended combination of materials for an economical design of a (PEC) column is high strength concrete with low strength steel.

1.6- Thesis structure

The thesis is organised in seven chapters. In the following paragraphs, a brief description of the contents of each is presented.

Chapter 1 is an introduction to the research work presented in this thesis, where the objective and motivation is also presented. The state of the art is also included.

Chapter 2 presents the Partially Encased Columns (PEC), with a definition of the mechanical and thermal properties of materials. The fire curves and thermal actions are also presented.

In chapter 3, the simple calculation method is presented and applied to (PEC) when submitted to fire by four sides. This method is based on the Balanced summation method applied to the four components, according to CEN - EN 1994-1-2, [1], used to determine the buckling resistance of PEC under standard fire ISO834, [13]. The effective flexural stiffness around the weak axis and the plastic resistance of the cross section, are the most important parameters to be calculated.

Chapter 4 presents new formulas to be used for the balanced summation method presented in EN1994-1-2 - ANNEX G, used to calculate the plastic resistance to axial compression and the effective flexural stiffness. These two parameters are required to calculate the buckling resistance of the partially encased columns.

Chapter 5 presents the advanced calculation method for the analysis of the axial buckling load and the plastic resistance of PEC. Numerical simulations use the finite element ANSYS software with an uncoupled thermal and mechanical analysis.

This page was intentionally left in blank

CHAPTER.2 COLUMNS UNDER FIRE

From the thermal actions defined by a fire model (nominal, parametric, natural), the effect of the heating the structural elements (columns, beams…) is determined by analytical methods described in CEN - EN 1993-1-2, [14], or by advanced calculation methods. These methods are based on the theory of heat transfer.

The simplest way to represent a fire is to use nominal curves, which is a relation giving the time evolution of the temperature of the gases. Curves have been established to develop experimental tests from building construction elements and to compare them, to evaluate the behaviour under real fires. The most frequently used are described below.

2.1- Fire curves

2.1.1- Nominal fire curves

These are conventional curves given by the CEN - EN 1991-1-2, [15], and adopted for the classification or verification of the fire resistance, for example the standard temperature - time curve ISO 834, [13], the external fire curve, hydrocarbon. These three nominal fire curves are presented below.

Figure 6 represents the variation of the gas temperature versus time for the nominal fire curves.

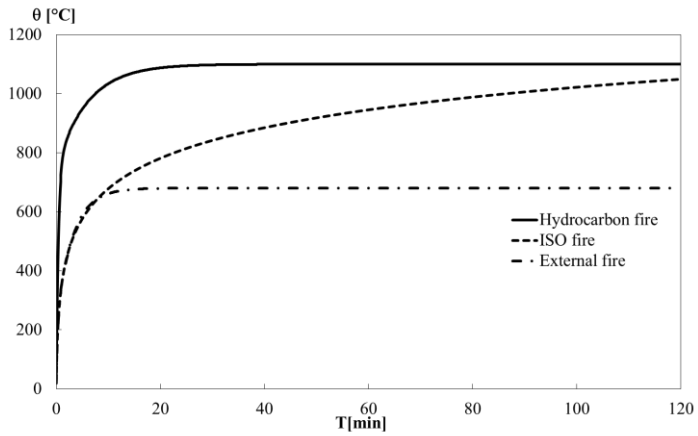

Figure 6 - Nominal fire curves

In 1981, Margaret Law, [16], presented the visionary paper regarding a summary of novel work developed at Arup Fire division. This group of research evaluate the structural fire safety of some innovative and architecturally exciting buildings – such as the Pompidou Centre

in Paris. Among the many topics covered in this paper, stated a number of criticisms of the standard fire resistance test and proposed the way forward using knowledge-based analytical approaches.

Natural fire (more real definition of fire) is a trend of investigation and a must to future designing rules (performance based design). This requires a better understanding of the element or structure under cooling. The material behaviour under cooling also requires knowledge, but this behaviour depends essentially on the cooling rate. Research on structural behaviour after the time for maximum temperature are very scarce and focus mainly on residual load-bearing capacity. Element failure under natural fire depends also on its severity. A new indicator was already suggested by Thomas Gernay and Jean-Marc Franssen, [17].

2.1.1.1- Standard curve ISO 834

For the modelling of a fire in a building, the ISO 834, [13], curve constitutes a conventional reference. The evolution of the temperature as a function of time is given according to the following formula Eq (1):

$$\theta_g = 20 + 345\log_{10}(8t + 1) \ [°C] \tag{1}$$

Where θ_g is the gas temperature in the fire compartment [°C], t is the time [min], assuming the coefficient of heat transfer by convection equal to $\alpha_c = 25 \left[W/m^2K\right]$.

2.1.1.2- Hydrocarbon curve

Developed in the 1970 by the oil company Mobil, it shows a very rapid increase in temperature with a temperature to 900 °C in the first five minutes. This research was initiated to develop a test procedure to evaluate fire protection materials for offshore rigs and oil structures.

The curve of the temperature - time hydrocarbons is given by Eq (2).

$$\theta_g = 20 + 1080\left(1 - 0{,}325e^{-0{,}167t} - 0{,}675e^{-2{,}5t}\right) \ [°C] \tag{2}$$

Where θ_g is the gas temperature in the fire compartment [°C], t is the time [min] and the coefficient of heat transfer by convection is consider equal to $\alpha_c = 50 \left[W/m^2K\right]$.

2.1.1.3- External fire curve

If the structure for which fire resistance is to be known is considered to be an external structure or a compartment located below or adjacent to an external wall, an external fire curve may be used according to the formula below see Eq (3).

$$\theta_g = 20 + 660.\left(1 - 0{,}687.e^{-0{,}32t} - 0{,}675.e^{-0{,}38t}\right) \left[°C\right] \tag{3}$$

Where θ_g is the gas temperature in the fire compartment [°C], t is the time [min] and the coefficient of heat transfer by convection is consider equal to $\alpha_c = 25 \left[W/m^2K\right]$.

2.1.2- Localized fire curves and parametric curves

In a localized fire, there is an accumulation of smoke and hot gas in a layer below the ceiling (upper layer) when the flames touch the ceiling. The flow creates a horizontal interface between this layer and the cold lower layer, where the gas temperature remains much lower. The thermal action of a localized fire can be assessed using the method Heskestad or the Hasemi, [15].

The localized fire depends of the fire load density. Usually this load can be defined by the heat release rate. The localized fire creates a plume and can also create a ceiling jet that can affect the structure (columns, beams, portal frames, or the complete structure), see Figure 7.

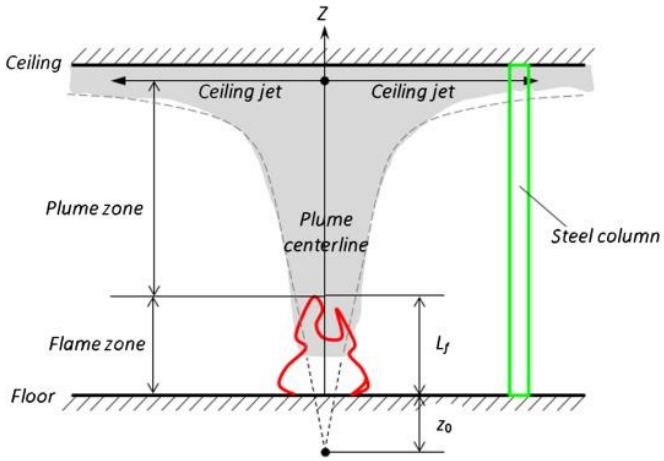

Figure 7 – Parameters of localized fire.

Localized fire temperature-time curve may be calculated according to Eq (4).

$$\theta_z = 20 + 0{,}25 Q_c^{2/3} \left(z - z_0\right)^{-5/3} \tag{4}$$

Where θ_z is the temperature of the plume along the vertical flame axis [°C], Q_c is the convective part of the heat release rate [W], z is the height along the flame axis and z_0 is the virtual origin of the fire.

Parametric fires are a simple way to account for important physical phenomena that can influence the development of a fire in a particular building, see Figure 8. They are nevertheless a significant step towards the consideration of the real nature of a particular fire in relation to nominal fires.

The use of parametric curves is limited to maximum surface compartments of 500m² and a ceiling height not exceeding 4 m. The heating and cooling phase can be defined by the next equations, respectively. Eq (5) and Eq (6) represents the variation of temperature versus time for natural fire curves.

$$\theta_g = 20 + 1325\left(1 - 0.324 e^{-0{,}2t^*} - 0.204 e^{-1{,}7t^*} - 0.472 e^{-19t^*}\right) \tag{5}$$

$$\theta_g = \theta_{\max} - 250\left(t^* - t^*_{\max}\right) \tag{6}$$

Where θ_g is the gas temperature in the fire compartment [°C], t is the time [min]; t^* is the time parameter that depends on the time factor, which itself depends on the opening factor and on the thermal absorptivity.

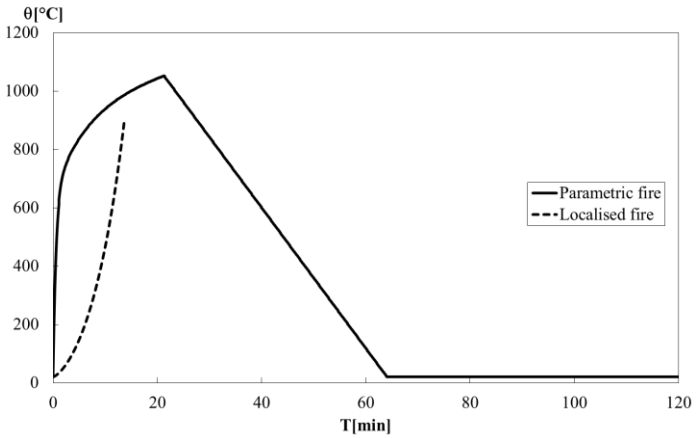

Figure 8 - Natural fire curves.

2.2- Heat transfer

The heat flux $\dot{h}_{net}\left[W/m^2\right]$ produced by the fire depends on two heat transfer mechanisms: radiation and convection. The net heat flux value is given by the following relation see Eq (7).

$$\dot{h}_{net,d} = \dot{h}_{net,c} + \dot{h}_{net,r} \quad \left[W/m^2\right] \tag{7}$$

Convective heat transfer, often referred to simply as convection, is the transfer of heat from one place to another by the motion of fluid particles, see Figure 9. Convection is usually the dominant form of heat transfer in liquids and gases. Although often discussed as a distinct method of heat transfer, convective heat transfer involves the combined processes of unknown conduction and advection. The rate at which this exchange of energy occurs is given by Newton's law of cooling, shown Eq (8) .

$$\dot{h}_{net,c} = \alpha_c(\theta_g - \theta_m) \quad \left[W/m^2\right] \tag{8}$$

Where, α_c is the heat transfer coefficient by convection $\left[W/m^2K\right]$, θ_g is the gas temperature in the vicinity of the fire exposed member $\left[^oC\right]$, and θ_m is the surface temperature of the member $\left[^oC\right]$.

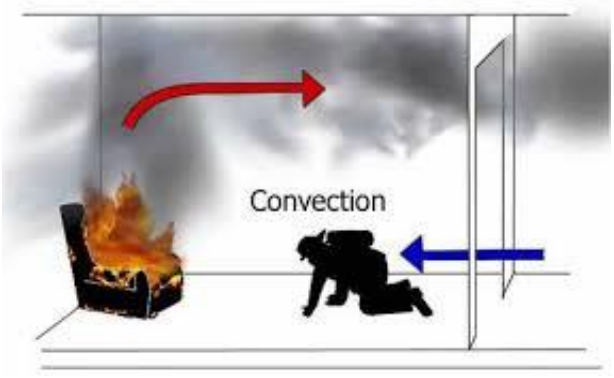

Figure 9 - Convective heat transfer.

The convection coefficient value depends on the velocity of the fluid or gas and can be considered equal to 9, 25 and 50 for cases of non-exposed surface, exposed surface with ISO834 curve, [13], and exposed surface with hydrocarbons.

Radiation is a method of heat transfer that does not rely upon any contact between the heat source and the heated object, as is the case with conduction and convection. Heat can be transmitted through empty space by thermal radiation often called infrared radiation. This is a type electromagnetic radiation, see Figure 10. No mass is exchanged and no medium is required in the process of radiation. It can even occur in a vacuum. The amount of energy that can be radiated by a surface is given by the Stefen-Boltzmann law can be calculated by Eq (9).

$$\dot{h}_{net,r} = \phi \times \varepsilon_f \times \varepsilon_m \times \sigma[(\theta_r + 273)^4 - (\theta_m + 273)^4] \quad [W/m^2] \tag{9}$$

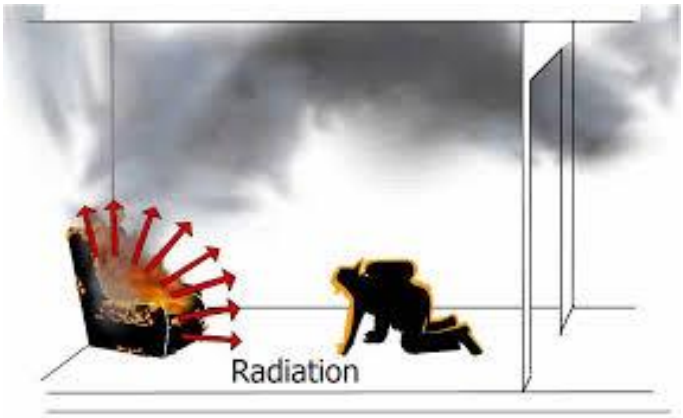

Figure 10 – Radiation heat transfer.

Where ϕ represents the view factor; ε_f represents the emissivity of the fire; ε_m is the emissivity of the surface of the element; σ is the Stephan Boltzmann constant $5{,}67\times10^{-8}\left[W/m^2K^4\right]$; θ_r represents is the effective radiation temperature of the fire environment $[^oC]$; θ_m represents the surface temperature of the member $[^oC]$.

The emissivity of the material for steel and concrete is equal to $\varepsilon_m = 0{,}7$. The emissivity of the fire (flames) is assumed $\varepsilon_f = 1{,}0$ and the view factor can be assumed equal to 1,0 when not specified.

2.3- Materials properties at elevated temperatures

2.3.1- Thermal properties

2.3.1.1- Steel profile and reinforcing

Specific heat is the measure of the materials ability to absorb heat. For steel, specific heat is a function of temperature and is independent of the composition of steel. The variation of specific heat with temperature is represented in Figure 11. The specific heat of steel Ca defined in accordance to CEN - EN 1993-1-2, [14], as the following:

$20[^oC] \le \theta_a < 600[^oC]$:

$$c_a = 425 + 7{,}73\times10^{-1}\theta_a - 1{,}69\times10^{-3}\theta_a^2 + 2{,}22\times10^{-6}\theta_a^3 \left[J/k_gK\right] \quad (10)$$

$600[^oC] \le \theta_a < 735[^oC]$:

$$c_a = 666 + \frac{13002}{738-\theta_a}\left[J/k_gK\right] \quad (11)$$

$735[^oC] \le \theta_a < 900[^oC]$:

$$c_a = 545 + \frac{17820}{\theta_a - 731}\left[J/k_gK\right] \quad (12)$$

$900[^oC] \le \theta_a < 1200[^oC]$:

$$C_a = 650\ \left[\text{J/kg.k}\right] \quad (13)$$

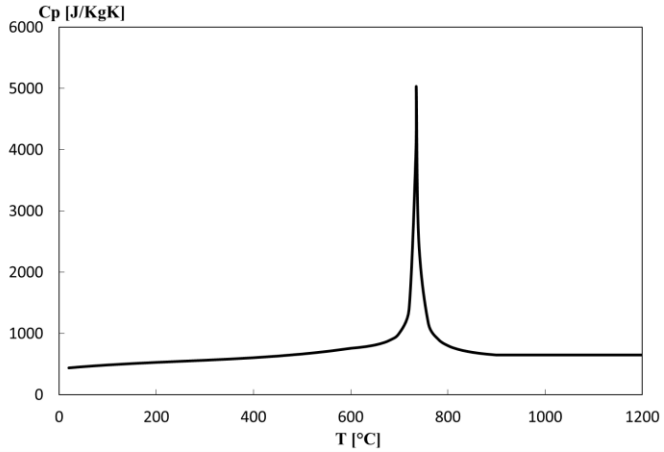

Figure 11 - Specific heat at elevated temperature.

Thermal conductivity is the measure of how rapidly the given material will conduct heat. For steel; thermal conductivity is a function of both temperature and the composition of the steel. The variation of thermal conductivity with temperature is represented in Figure 12 .The

CEN - EN 1993-1-2, [14], suggests the following linear approximation for thermal conductivity for most structural steel.

$20[°C] \le \theta < 800[°C]$:

$$\lambda_a = 54 - 3{,}33.10^{-2}\theta_a \ [\mathrm{w/mk}] \tag{14}$$

$800[°C] \le \theta \le 1200[°C]$:

$$\lambda_a = 27{,}3 \ [\mathrm{w/mk}] \tag{15}$$

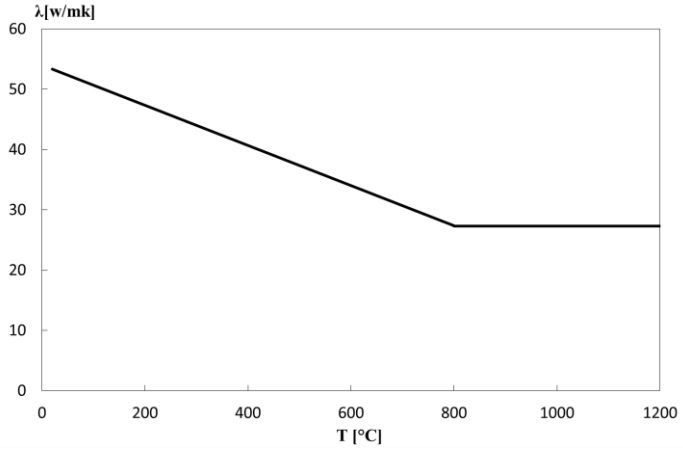

Figure 12 - Thermal conductivity at elevated temperature.

The density of steel is constant ρ=7850 kg/m^3, even when the temperature is modified. According to CEN - EN 1993-1-2, [14], the variation of thermal conductivity is represented in Figure 13.

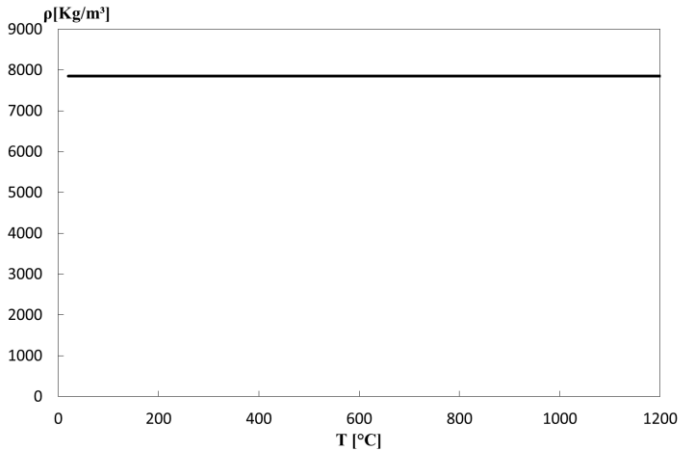

Figure 13 - Density of steel at elevated temperature.

2.3.1.2- Concrete

The specific heat $c_p(\theta)$ of concrete varies mainly with the moisture content. The moisture within the concrete causes a peak between $100[°C]$ and $200[°C]$ due to the water being driven off. Figure 14 depicts the variation of this property with temperature The peak value depends on the amount of moisture, in this case $\mu = 3\%$ was assumed, The CEN - EN 1992-1-2, [18], recommends the following relationship for calculation of concrete specific heat.

$20[^oC] \le \theta \le 100[^oC]$:

$$c_p(\theta) = 900[J/k_g K] \tag{16}$$

$100[^oC] < \theta \le 200[^oC]$:

$$c_p(\theta) = 900 + (\theta - 100)[J/k_g K] \tag{17}$$

$200[^oC] < \theta \le 400[^oC]$:

$$c_p(\theta) = 1000 + (\theta - 200)/2\,[J/k_g K] \tag{18}$$

$400[^oC] < \theta \le 1200[^oC]$:

$$c_p(\theta) = 1100[J/k_g K] \tag{19}$$

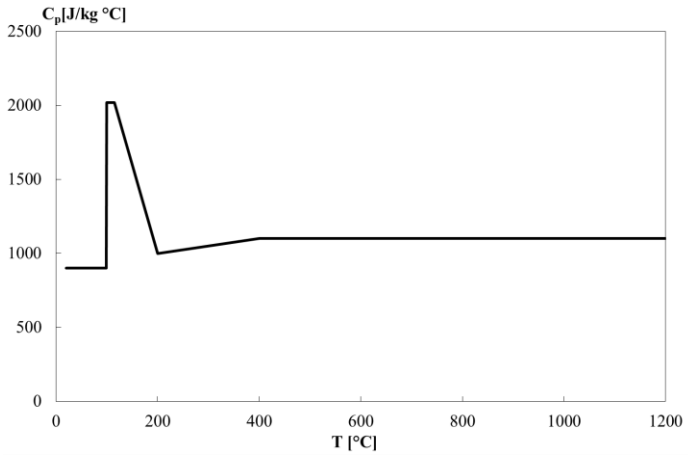

Figure 14 - Specific heat at elevated temperature.

Thermal conductivity depends upon the aggregate type and the temperature of the concrete. The thermal conductivity λ_c of concrete may be determined between lower and upper limit values. The following equation defined in CEN - EN 1992-1-2, [18], recommends the upper limit of thermal conductivity of normal weight concrete may be determined from:

$20[^oC] \le \theta \le 1200[^oC]$:

$$\lambda_c = 2 - 0.2451(\theta/100) + 0.0107(\theta/100)^2 \ \ [\mathrm{w/mk}] \tag{20}$$

The following equation defined in CEN - EN 1992-1-2, [18], recommends also the lower limit of thermal conductivity for normal weight concrete.

$20[^oC] \le \theta \le 1200[^oC]$:

$$\lambda_c = 1.36 - 0.136(\theta/100) + 0.0057(\theta/100)^2 \ \ [\mathrm{w/mk}] \tag{21}$$

Where θ *is* the concrete temperature. The variation of the upper limit and lower limit of thermal conductivity with temperature is illustrated in Figure 15.

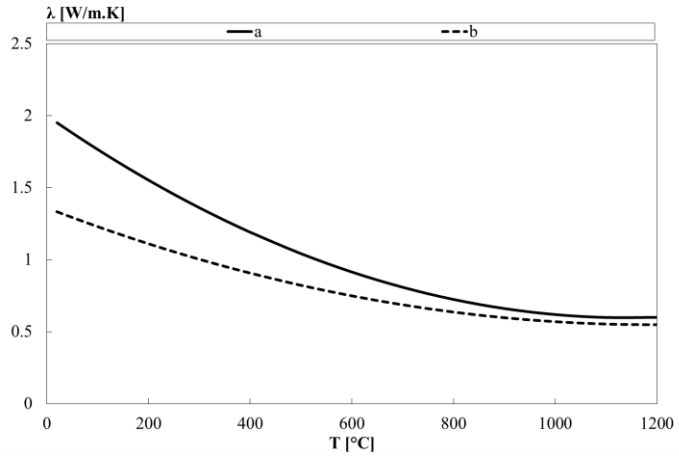

Figure 15 - Thermal conductivity at elevated temperature.

The density is a physical property of matter. In a qualitative manner, density is defined as the heaviness of objects with a specific volume. It is represented as ρ. Common unit of density is kg/m^3. Figure 16 represents the variation of density with temperature. The specific mass at room temperature is $\rho(20°C) = 2300 kg/m^3$, The CEN - EN 1992-1-2, [18], recommends the following relationship for calculation of concrete density.

$20[°C] \le \theta \le 115[°C]$:

$$\rho(\theta) = \rho(20°C) \tag{22}$$

$115[°C] < \theta \le 200[°C]$:

$$\rho(\theta) = \rho(20°C).(1 - 0{,}02(\theta - 115)/85) \tag{231}$$

$200[°C] < \theta \le 400[°C]$:

$$\rho(\theta) = \rho(20°C).(0{,}98 - 0{,}03(\theta - 200)/200) \quad (24)$$

$400[°C] < \theta \leq 1200[°C]$:

$$\rho(\theta) = \rho(20°C).(0{,}95 - 0{,}07(\theta - 400)/800) \quad (25)$$

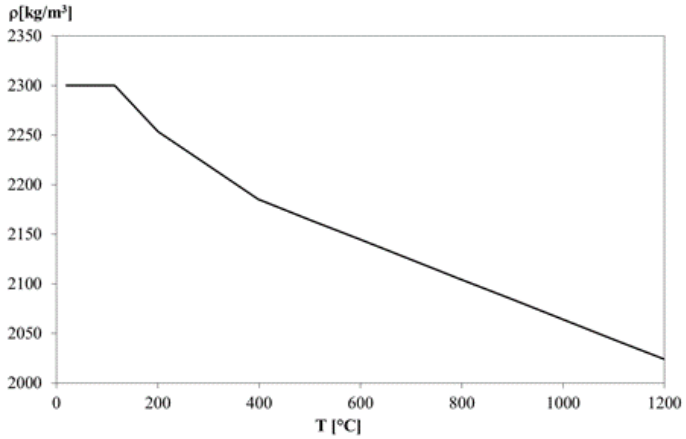

Figure 16 - Density of concrete at elevated temperature.

2.3.2- Mechanical properties

The mechanical properties of steel change with temperature. Both strength and stiffness steel drop with increased temperature. The nominal resistance of steel profiles is characterized in European standards CEN - EN 1993-1-1, [19], for room temperature and CEN - EN 1993-1-2, [14], for elevated temperatures (the action of fire).

2.3.2.1- Steel profile S275

The values of the yield and ultimate stress, f_y and f_u, are presented herein. Under normal conditions the S275 steel, with thickness less than 40 mm, the mechanical properties are described in Table 3 and Figure 17 shows the variation of the stress-strain relationship at different temperature levels.

The temperature dependence of these properties were collected from the CEN - EN 1993-1-2, [14]. These reduction factors should be applied to the proportional limit $k_{p,\theta}$, to the effective yield strength $k_{y,\theta}$ and to the slope of the linear elastic range $k_{E,\theta}$, as shown in Figure 18. The stress-strain relationship for steel at elevated temperatures is represented in Table 4

Table 3 – Mechanical characteristics of steel (S275).

$E_a\,[GPa]$	$f_y\,[MPa]$	$f_u\,[MPa]$	$G_a\,[GPa]$	ν
210	275	430	81	0,3

Table 4 - Stress-strain relationship for steel at elevated temperatures.

Strain range	Stress σ	Tangent modulus
$\varepsilon \le \varepsilon_{p,\theta}$	$\varepsilon\, E_{a,\theta}$	$E_{a,\theta}$
$\varepsilon_{p,\theta} < \varepsilon < \varepsilon_{y,\theta}$	$f_{p,\theta} - c + (b/a)\left[a^2 - (\varepsilon_{y,\theta} - \varepsilon)^2\right]^{0.5}$	$\frac{b(\varepsilon_{y,\theta} - \varepsilon)}{a\left[a^2 - (\varepsilon_{y,\theta} - \varepsilon)^2\right]^{0.5}}$
$\varepsilon_{y,\theta} \le \varepsilon \le \varepsilon_{t,\theta}$	$f_{y,\theta}$	0
$\varepsilon_{t,\theta} < \varepsilon < \varepsilon_{u,\theta}$	$f_{y,\theta}\left[1 - (\varepsilon - \varepsilon_{t,\theta})/(\varepsilon_{u,\theta} - \varepsilon_{t,\theta})\right]$	-
$\varepsilon = \varepsilon_{u,\theta}$	0,00	-
Parameters	$\varepsilon_{p,\theta} = f_{p,\theta}/E_{a,\theta}$ $\quad \varepsilon_{y,\theta} = 0{,}02$ $\quad \varepsilon_{t,\theta} = 0{,}15$ $\quad \varepsilon_{u,\theta} = 0{,}20$	
Functions	$a^2 = (\varepsilon_{y,\theta} - \varepsilon_{p,\theta})(\varepsilon_{y,\theta} - \varepsilon_{p,\theta} + c/E_{a,\theta})$ $b^2 = c(\varepsilon_{y,\theta} - \varepsilon_{p,\theta})E_{a,\theta} + c^2$ $c = \frac{(f_{y,\theta} - f_{p,\theta})^2}{(\varepsilon_{y,\theta} - \varepsilon_{p,\theta})E_{a,\theta} - 2(f_{y,\theta} - f_{p,\theta})}$	

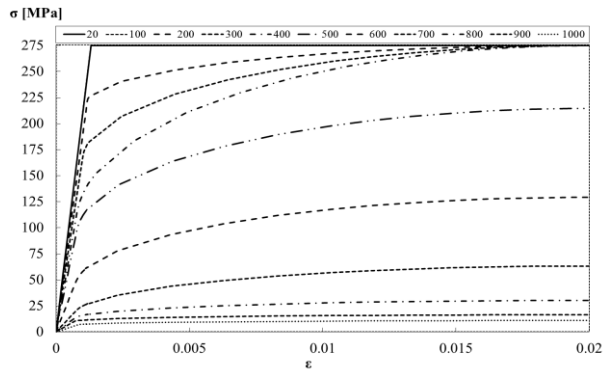

Figure 17 - Curve stress-strain of steel under tension.

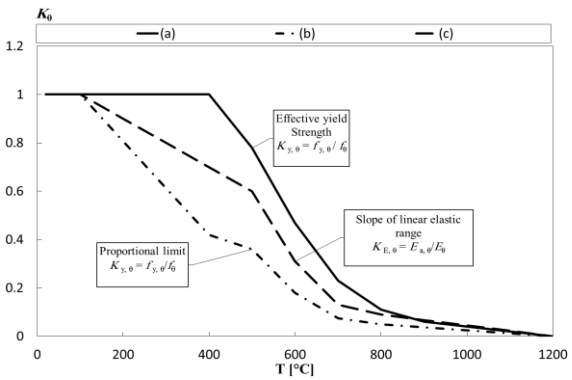

Figure 18 - Reduction factors for the stress strain relationship of steel at elevated temperatures.

2.3.2.2- Concrete C20 / 25

The concrete strength at room temperature is defined in CEN - EN 1992-1-1, [20], and for elevated temperature in CEN - EN 1992-1-2, [18]. This is the reference document for the behaviour of this material under fire conditions. The material properties of concrete C20 / 25 at room temperature are shown in Table 5 the stress-strain relationship for concrete at elevated temperatures is illustrated in Table 6 and Figure 19 showing the expected nonlinear variation.

The reduction of the characteristic compressive strength of siliceous aggregate concrete as a function of the temperature T, is allowed by the coefficient $k_{c,t(\theta)}$, this coefficient is represented in Figure 20 .

Table 5 - Mechanical characteristics of the concrete C20 / 25.

$f_{ck}\,[MPa]$	$f_{ck,cube}\,[MPa]$	$f_{cm}\,[MPa]$	$f_{ctm}\,[MPa]$	$E_{cm}\,[GPa]$	$\varepsilon_{c1}\,[‰]$	$\varepsilon_{cu1}\,[‰]$
20	25	28	2,2	30	2,0	3,5

Table 6 - Stress-strain relationship for concrete at elevated temperatures.

Range	Stress σ(θ)
$\varepsilon \le \varepsilon_{c1,\theta}$	$3.\varepsilon.f_{c\theta} \Big/ \varepsilon_{c1,\theta}\left(2+\left(\frac{\varepsilon}{\varepsilon_{c1,\theta}}\right)^3\right)$
$\varepsilon_{c1,\theta} < \varepsilon \le \varepsilon_{cu1,\theta}$	For numerical purposes, a descending branch should be adopted. Linear or nonlinear models are permitted.

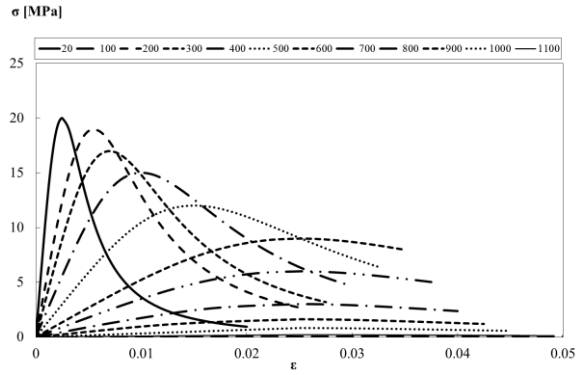

Figure 19 - Curve stress-strain of concrete under compression.

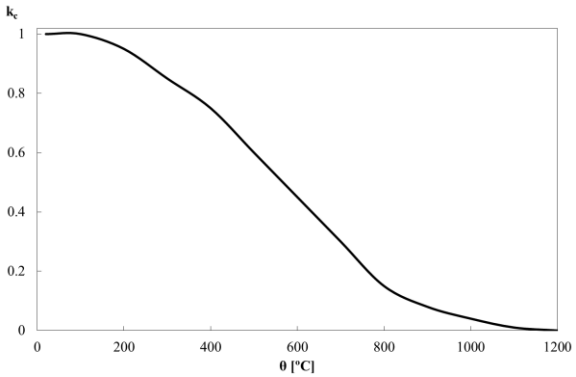

Figure 20 - Reduction factor for the stress-strain relationship of concrete at elevated temperatures.

The Figure 19 presents the graphics of the idealized curve stress-strain of concrete under compression and submitted to different temperatures. The Figure 20 presents the reduction factor for the stress-strain of the concrete at elevated temperatures based on siliceous aggregate.

2.3.2.3- Reinforcing steel S500

The characteristics of the steel reinforcement is described in CEN - EN 1992-1-1, [20], according to the steel grade selected, Steel S500 NR. The class B of this material has the properties described in Table 7.

When subjected to high temperatures, CEN - EN 1992-1-2, [18], defines reduction factors to be applied to the mechanical properties. The value of the yield stress $f_{sy,\theta}$, the value

of proportional limit $f_{sp,\theta}$ and the value of the modulus of elasticity $E_{s,\theta}$ varies with temperature as can be seen in Figure 20 the factors are represented to reduce the effective yield strength, and the modulus of elasticity. The stress-strain relationship for reinforcement at elevated temperatures is defined by Table 8 and Figure 21 represents the curve variation of stress-strain.

Table 7 - Mechanical characteristics of steel S500.

$E_s\,[GPa]$	$f_{yk}\,[MPa]$	$f_{uk}\,[MPa]$	$G\,[GPa]$	k	ν
210	500	540	81	1,08	0,3

Table 8 - Stress-strain relationship for reinforcement at elevated temperatures.

Strain range	Stress σ	Tangent modulus
$\varepsilon_{sp,\theta}$	$\varepsilon E_{s,\theta}$	$E_{s,\theta}$
$\varepsilon_{sp,\theta} < \varepsilon < \varepsilon_{sy,\theta}$	$f_{sp,\theta} - c + (b/a)\left[a^2 - (\varepsilon_{sy,\theta} - \varepsilon)^2\right]^{0.5}$	$\dfrac{b(\varepsilon_{sy,\theta} - \varepsilon)}{a\left[a^2 - (\varepsilon - \varepsilon_{sy,\theta})^2\right]^{0.5}}$
$\varepsilon_{sy,\theta} \le \varepsilon \le \varepsilon_{st,\theta}$	$f_{sy,\theta}$	0
$\varepsilon_{st,\theta} < \varepsilon < \varepsilon_{su,\theta}$	$f_{sy,\theta}\left[1 - (\varepsilon - \varepsilon_{st,\theta})/(\varepsilon_{su,\theta} - \varepsilon_{st,\theta})\right]$	-
$\varepsilon = \varepsilon_{su,\theta}$	0,00	-
Parameters	$\varepsilon_{sp,\theta} = f_{sp,\theta}/E_{s,\theta}$ $\quad \varepsilon_{sy,\theta} = 0{,}02$ $\quad \varepsilon_{st,\theta} = 0{,}15$ $\quad \varepsilon_{su,\theta} = 0{,}20$	
Functions	$a^2 = (\varepsilon_{sy,\theta} - \varepsilon_{sp,\theta})(\varepsilon_{sy,\theta} - \varepsilon_{sp,\theta} + c/E_{s,\theta})$ $b^2 = c(\varepsilon_{sy,\theta} - \varepsilon_{sp,\theta})E_{s,\theta} + c^2$ $c = \dfrac{(f_{sy,\theta} - f_{sp,\theta})^2}{(\varepsilon_{sy,\theta} - \varepsilon_{sp,\theta})E_{s,\theta} - 2(f_{sy,\theta} - f_{sp,\theta})}$	

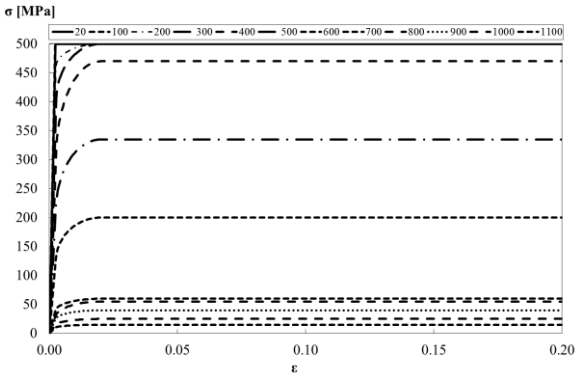

Figure 21 - Curve stress-strain of reinforcement under tension.

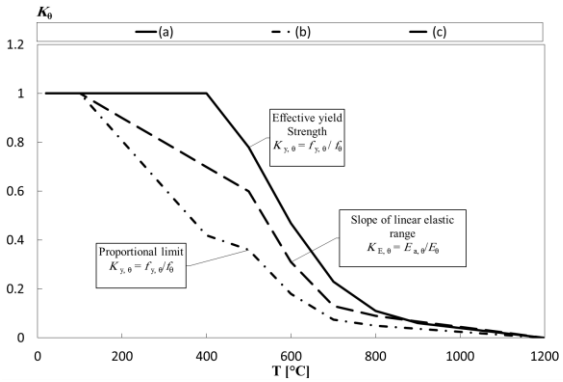

Figure 22 - Reduction factors for the stress-strain relationship of rebar's at elevated temperatures.

2.4- Tests under fire for columns

The completed test time (in minutes) is time at which the test specimen continues to maintain its ability to support the test load during the test. Support of the test load is determined by both the amount of maximum displacement and the rate of deflection. Since relatively rapid

deflections can occur until stable conditions are reached, the rate of deflection criterion is not applied in the first 10 min of the fire test. The criterion to stop the test is defined for vertically loaded elements, based on contraction or rate of contraction, [21]. According to the revised document in 2012, the test can be stopped if one of the limitations for the displacement and rate of displacement is achieved. The limiting vertical contraction for displacement is "c" (negative elongation) $C = h/100 mm$ or the limiting rate of vertical contraction (negative elongation) is $dC/dt = 3h/1000 \quad mm/\min$. Where h is the initial height (in millimetres) of the test specimen once the load has been applied.

This section justifies the maximum vertical displacement allowed during the numerical simulations. This decision was made to reduce the computation time during the post buckling of the (PEC).

This page was intentionally left in blank

CHAPTER.3 SIMPLIFIED CALCULATION METHOD USING EUROCODE 4- ANEEX G

The Eurocode CEN - EN 1994-1-2, [1], is used for the calculation of the design value of the plastic resistance to axial compression and of the effective flexural stiffness in the fire situation. The simplified calculation method was originally developed Jungbluth, [22], and was defined to determine the capacity of the (PEC). The cross section is divided into four components: The flanges of the steel profile; the web of the steel profile; the concrete contained by the steel profile and the reinforcing bars, assuming the section exposed to the standard R30, R60, R90 and R120 for fire action by the four sides. Each component should be evaluated based on the evolution of the temperature in each component and the effect that it produces in the reduction of the resistant characteristics, the reduction of the modulus of elasticity and the effective geometry. The design value of the plastic resistance to axial compression and the effective flexural stiffness of the cross section obtained by a balanced summation of the corresponding values of the four components. Strength and deformation properties of steel and concrete at elevated temperatures complies with the corresponding principles and rules of CEN - EN 1993-1-2, [14], and CEN - EN 1992-1-2, [18].

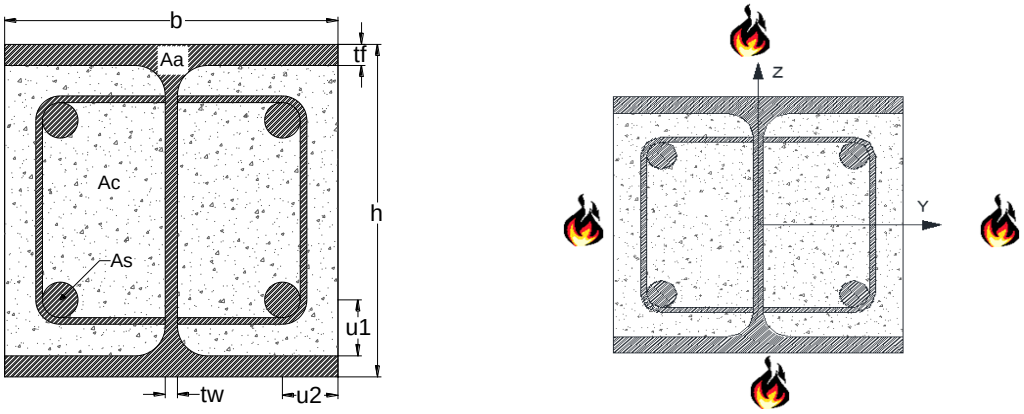

Parameters of the cross section Four sides exposed

Figure 23 – Partially encased section.

Figure 23 presents the four components of the cross section: the flange component, the web component, the concrete and reinforcement components. This calculation method takes into consideration the effect of the fire in four components of the cross section.

The stability of (PEC) requires the calculation of the critical load and the effective flexural stiffness. These quantities depend on the temperature effect on the elastic modulus and on the second order moment of area of each component, according to Eq (26).

$$(EI)_{fi,eff,z} = \varphi_{f,\theta}(EI)_{fi,f,z} + \varphi_{w,\theta}(EI)_{fi,w,z} + \varphi_{c,\theta}(EI)_{fi,c,z} + \varphi_{s,\theta}(EI)_{fi,s,z} \quad (26)$$

In this equation $(EI)_{fi,eff,z}$ represents the effective flexural stiffness of the composite section in fire, $(EI)_{fi,f,z}$ represents effective flexural stiffness of the flange, $(EI)_{fi,w,z}$ represents effective flexural stiffness of the web, $(EI)_{fi,c,z}$ represents the effective flexural stiffness of the concrete and $(EI)_{fi,s,z}$ represents the effective flexural stiffness of reinforcement. The contribution of each part is going to be weighted according to φ factors, a reduced modulus of elasticity and a reduced cross-section. These values depend on the fire rating, according to Table 9.

Table 9 - Reduction coefficients for bending stiffness around the week axis.

Standard fire resistance class	$\varphi_{f,\theta}$	$\varphi_{w,\theta}$	$\varphi_{c,\theta}$	$\varphi_{s,\theta}$
R30	1,0	1,0	0,8	1,0
R60	0,9	1,0	0,8	0,9
R90	0,8	1,0	0,8	0,8
R120	1,0	1,0	0,8	1,0

The elastic buckling load $N_{fi,cr,z}$ requires the calculation of the effective flexural stiffness of the composite section in fire $(EI)_{fi,eff,z}$. The non-dimensional slenderness ratio $\bar{\lambda}_\theta$ and $N_{fi,cr,z}$ are calculated according to Eqs. (27)-(28), when the safety partial factors are assumed equal to 1.0. The buckling length of the column under fire conditions is represented by L_θ. The calculation of the axial plastic resistance under fire $N_{fi,pl,Rd}$ the cross-section is divided into four components according to Eq. (29).

$$N_{fi,pl,Rd} = N_{fi,pl,Rd,f} + N_{fi,pl,Rd,w} + N_{fi,pl,Rd,c} + N_{fi,pl,Rd,s} \quad (27)$$

$$\bar{\lambda}_\theta = \sqrt{N_{fi,pl,Rd} / N_{fi,cr,z}} \quad (28)$$

$$N_{fi,cr,z} = \pi^2 / L_\theta^2 \times (EI)_{fi,eff,z} \quad (29)$$

3.1- Definition of partially encased column

Partially encased columns (PEC) are normally made of hot rolled steel profiles, reinforced with concrete between the flanges, see Figure 24. The composite section is responsible to increase the torsional and bending stiffness without increasing the section dimension, when compared to the same section of steel profile, being the concrete part very

significant to increase the fire resistance. Since the thermal conductivity of concrete is relatively small, the temperature field in the composite cross section is highly non-uniform. There is no simplified method available to the heat transfer analysis, therefor the numerical simulation is required to analyse the fire effect.

The cross sections were defined according to the tabulated data, [1], to design partially encased columns under fire conditions. This led to the minimum dimensions and minimum distances between components. The design of these profiles depends on the applied load and the relations between the thickness of the web and the thickness of the flange, see Table 10. These tabulated data are also applied to other different steel grades, such as S235 and S355, for a minimum reinforcement value between 1 and 6%. The tabulated data specifies values for the most common cross sections, based on experimental and empirical results. These results are usually conservatives and may be used for a preliminary design.

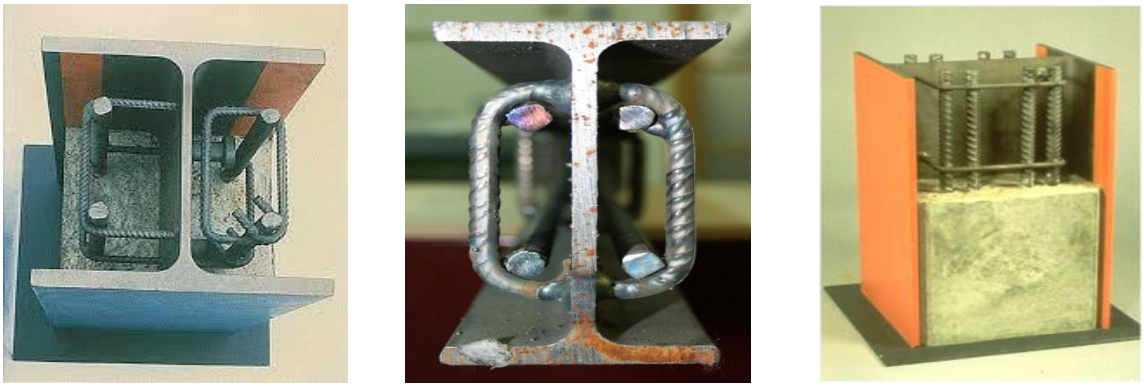

Figure 24 - Example of partially encased column.

The materials used for the calculations were selected according to the most commonly used in practice, being the steel grade S275 selected for the cross section of the profile, steel grade B500 for the reinforcement and concrete grade C20/25 for the concrete. Twenty-four different cross sections were selected to analyse the effect of fire (Ten steel IPE profiles ranging from 200 to 500 and fourteen steel HEB ranging from 160 to 500). These columns were tested under standard fire ISO834, [13], using three buckling lengths explained in Figure 25, using 3m and 5m column height.

The effective length of the column L_θ for the ultimate limit state may be different from that considered at room temperature. Eurocode takes into consideration the fact that the surrounding cold part of the structure can provide unchanged rotation stiffness, leading to effective buckling lengths of 0.5L (fixed ends) and 0.7L (mixed ends). Nevertheless, authors decided to evaluate the effective buckling length of 1.0L (pinned extremities).

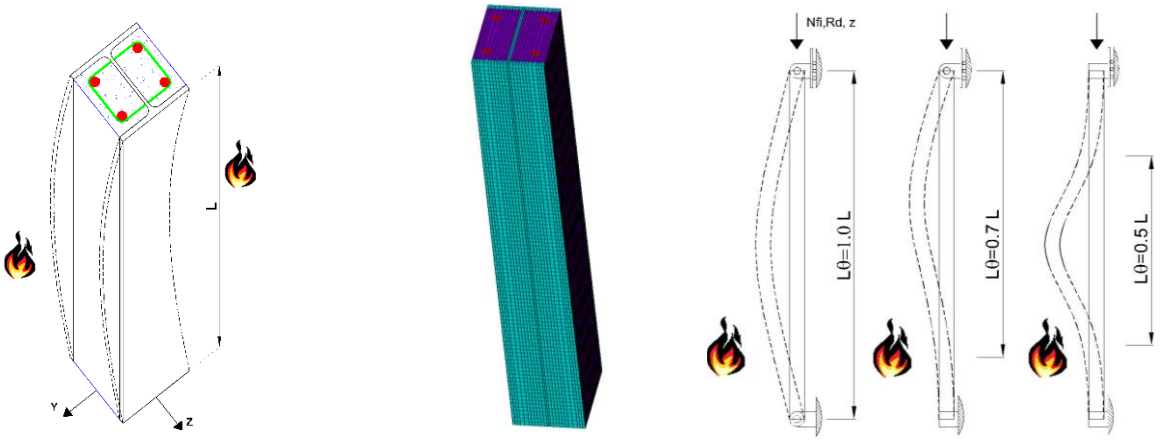

a) Buckling deformed shape b) .Finite element (ANSYS). c) Buckling length in fire

Figure 25 - Partially encased column under fire.

Table 10 presents the main dimensions of the cross section, in particular the number of rebar's, the diameter of each rebar, the cover dimensions in both principal directions.

Table 10 - Characteristics of the sections under study.

Profile	Bars (n)	h_i	Φ (mm)	A_s (mm^2)	A_c (mm^2)	u_1 (mm)	u_2 (mm)	u (mm)	$A_s / A_s + A_c$	t_w / t_f	A_m/V (m^{-1})
HEB160	4	134.0	12	452	19916	40	40	40	2.22	0.62	25.00
HEB180	4	152.0	12	452	25616	40	40	40	1.74	0.61	22.22
HEB200	4	170.0	20	1257	31213	50	50	50	3.87	0.60	20.00
HEB220	4	188.0	25	1963	37611	50	50	50	4.96	0.59	18.18
HEB240	4	206.0	25	1963	45417	50	50	50	4.14	0.59	16.67
HEB260	4	225.0	32	3217	53033	50	50	50	5.72	0.57	15.38
HEB280	4	244.0	32	3217	62541	50	50	50	4.89	0.58	14.29
HEB300	4	262.0	32	3217	72501	50	50	50	4.25	0.58	13.33
HEB320	4	279.0	32	3217	77275	50	50	50	4.00	0.56	12.92
HEB340	4	297.0	40	5027	80509	50	50	50	5.88	0.56	12.55
HEB360	4	315.0	40	5027	85536	50	50	50	5.55	0.56	12.22
HEB400	4	352.0	40	5027	95821	70	50	55	4.98	0.56	11.67
HEB450	4	398.0	40	5027	108801	70	50	55	4.42	0.54	11.11
HEB500	4	444.0	40	5027	121735	70	50	55	3.97	0.52	10.67
IPE200	4	183.0	12	452	16823	50	40	45	2.62	0.66	30.00
IPE220	4	201.6	20	1257	19730	50	40	45	5.99	0.64	27.27
IPE240	4	220.4	20	1257	23825	50	40	45	5.01	0.63	25.00
IPE270	4	249.6	25	1963	30085	50	40	45	6.13	0.65	22.22
IPE300	4	278.6	25	1963	37848	50	40	45	4.93	0.66	20.00
IPE330	4	307.0	25	1963	44854	50	40	45	4.19	0.65	18.56
IPE360	4	334.6	32	3217	50988	50	40	45	5.93	0.63	17.32
IPE400	4	373.0	32	3217	60715	70	40	45	5.03	0.64	16.11
IPE450	4	420.8	32	3217	72779	70	40	45	4.23	0.64	14.97
IPE500	4	468.0	40	5027	83800	70	50	55	5.66	0.64	14.00

3.2- Flange of the steel profile

The average flange temperature $\theta_{f,t}$ must be determined according to the next formula. The value depends on the empirical coefficient k_t, on the reference value $\theta_{0,t}$ and on the section factor A_m/V see Eq (30).

$$\theta_{f,t} = \theta_{0,t} + k_t (A_m/V) \tag{30}$$

The empirical coefficient shown in this Table 11:

Table 11 - Parameters for the flange temperature

Standard Fire Resistance	$\theta_{0,t}$ $[m^o C]$	k_t $[m^o C]$
R30	550	9,65
R60	680	9,55
R90	805	6,15
R120	900	4,65

The average temperature of the flange allows the calculation of the fire effect on the mechanical properties. This effect is defined by the reduction coefficients, $K_{y,\theta}$, $K_{E,\theta}$ used for the modulus of elasticity and to the yield stress, being determined from Eq (31) and Eq (32).

$$f_{ay,f,t} = f_{ay,f} K_{y,\theta} \tag{31}$$

$$E_{ay,f,t} = E_{ay,f} K_{E,\theta} \tag{32}$$

The plastic resistance to axial compression and the flexural stiffness of the two flanges of the steel profile in the fire situation are determined from Eq (33) and Eq (34).

$$N_{fi,pl,Rd,f} = 2\left(b_{ef}\, f_{ay,f,t}\right)/\delta_{M,fi,a} \tag{33}$$

$$(EI)_{fi,f,z} = E_{a,f,t}\left(e_f b^3\right)/6 \tag{34}$$

3.3- Web of the steel profile

The part of the web to be neglected is defined by $h_{w,fi}$. The fire effect is responsible to decrease the height of the resistant web, starting at the inner edge of the flange see Figure 28. This part is determined from Eq (35).

$$h_{w,fi} = 0{,}5\left(h - 2e_f\right)\left(1 - \sqrt{1 - 0.16\left(H_t / h\right)}\right) \tag{35}$$

The parameter H_t it's given according to the Table 12:

Table 12 - Parameter for height reduction of the web.

Standard Fire Resistance	$H_t[mm]$
R30	350
R60	770
R90	1100
R120	1250

The yield stress is modified from Eq (36)

$$f_{ay,w,t} = f_{ay,w,t}\sqrt{1 - 0.16\left(H_t / h\right)} \tag{36}$$

The residual area of the web will affect the calculation of the effective flexural stiffness, but the elastic modulus should be consider with the same value at room temperature. The plastic resistance to axial compression is affected by the reduction of the geometry and also by the reduction coefficient for the yielding stress.

The design value of the plastic resistance to axial compression and the flexural stiffness of the web of the steel profile in the fire situation are determined from Eq (37) and Eq (38).

$$N_{fi,pl,rd,w} = \left[ew\left(h - 2e_f - 2h_{w,fi}\right)\right] f_{ay,w,t} / \delta_{M,fi,a} \tag{37}$$

$$\left(EI\right)_{fi,w,t} = \left[E_{a,w}\left(h - 2e_f - 2h_{w,fi}\right)\right]e_w^3 / 12 \tag{38}$$

3.4- Partially encased concrete

An external layer of concrete with a thickness $b_{c,fi}$ is going to be neglected in the calculation see Figure 28. The thickness $b_{c,fi}$ is given in Table 13, and depends on the section

factor A_m/V , of the entire composite cross-section, only for fire ratings of 90 minutes and 120 minutes.

Table 13 - Thickness reduction of the concrete area.

Standard Fire Resistance	$b_{c,\,fi}\ [mm]$
R30	4.0
R60	15.0
R90	$0.5(\mathrm{A_m}/V)+22.5$
R120	$2.0(\mathrm{A_m}/V)+24.0$

The average temperature in concrete $\theta_{c,t}$ is given in Table 14 and depends on the section factor A_m/V of the entire composite cross-section and on the fire rating class.

Table 14 - Average concrete temperature.

R30		R60		R90		R120	
$A_m/V[m^{-1}]$	$\theta_{c,t}[^oC]$	$A_m/V[m^{-1}]$	$\theta_{c,t}[^oC]$	$A_m/V[m^{-1}]$	$\theta_{c,t}[^oC]$	$A_m/V[m^{-1}]$	$\theta_{c,t}[^oC]$
4	136	4	214	4	256	4	265
23	300	9	300	6	300	5	300
46	400	21	400	13	400	9	400
		50	600	33	600	23	600
				54	800	38	800
						41	900
						43	1000

The calculation of the average temperature of the concrete allows the calculation of the reduction factor for the compressive strength of concrete $k_{c,\theta}$ and the secant modulus$E_{c,sec,\theta}$, both affecting the effective flexural stiffness and plastic resistance to axial compression. The secant modulus of concrete at elevated temperature is obtained from the next expression and is going to affect the effective flexural stiffness see Eq (39).

$$E_{c,\mathrm{sec},\theta} = f_{c,\theta} / \varepsilon_{cu,\theta} = f_c K_{c,\theta} / \varepsilon_{cu,\theta} \tag{39}$$

The design value of the plastic resistance to axial compression considers the effect of the material temperature and the residual cross section. The effective flexural stiffness of the concrete in the fire considers the residual area of concrete, being both parameters determined from Eq (40).

$$N_{fi,pl,Rd,c} = 0{,}86\left[\left(\left(h-2e_f-2b_{c,\,fi}\right)\left(b-e_w-2b_{c,\,fi}\right)\right)-A_s\right]f_{c,\theta}/\delta_{M,\,fi,c} \tag{40}$$

Where A_s is the cross-section of the reinforcing bars.

$$(EI)_{fi,c,z} = E_{c,\sec,\theta}\left[\left(h - 2e_f - 2b_{c,fi}\right)\left(\left(b - 2b_{c,fi}\right)^3 - e_w^3\right)/12\right) - I_{s,z}\right] \quad (41)$$

Where $I_{s,z}$, is the second moment of area of the reinforcing bars related to the central axis Z of the composite cross-section.

3.5- Reinforcing bars

The reduction factor $k_{y,t}$ of the yield stress and the reduction factor $k_{E,t}$ of the modulus of elasticity of the reinforcing bars depend on the fire rating and on the position of the reinforcement, being the geometrical average $_u$ representative of the distances of the reinforcement to the outer borders of the concrete see Table 15 and Table 16.

Table 15 - Reduction factor $k_{y,t}$ for the yield point $f_{s,y}$ of the reinforcing bars.

	Standard Fire Resistance			
u [mm]	R30	R60	R90	R120
40	1	0,789	0,314	0,17
45	1	0,883	0,434	0,223
50	1	0,976	0,572	0,288
55	1	1	0,696	0,367
60	1	1	0,822	0,436

Table 16 - Reduction factor $k_{E,t}$ for the modulus of elasticity of the reinforcing.

	Standard Fire Resistance			
u [mm]	R30	R60	R90	R120
40	0,83	0,604	0,193	0,11
45	0,865	0,647	0,283	0,128
50	0,888	0,689	0,406	0,173
55	0,914	0,729	0,522	0,233
60	0,935	0,763	0,619	0,285

The geometrical average u of the axial distance u_1 and u_2 is obtained from $u = \sqrt{u_1.u_2}$, being u_1 the distance from the outer reinforcing bar to the inner flange edge in [mm] and u_2 is the distance from the outer reinforcing bar to the concrete surface [mm]. There are a few restraints to the calculation of the geometrical average u, see next equations Eq (42) and Eq (43).

$$\left(u_1 - u_2\right) > 10mm, \quad u = \sqrt{u_2\left(u_2 + 10\right)} \quad (42)$$

$$\left(u_2 - u_1\right) > 10mm, \quad u = \sqrt{u_1\left(u_1 + 10\right)} \quad (43)$$

The design value of the plastic resistance to axial compression and the flexural stiffness of the reinforcing bars takes into account the effect of the temperature into the mechanical properties in the fire condition and are obtained from Eq (44) and Eq (45).

$$N_{fi,pl,Rd,s} = A_s k_{y,t} f_{s,y} / \delta_{M,fi,s} \quad (44)$$

$$(EI)_{fi,s,z} = k_{E,t} E_s I_{s,z} \quad (45)$$

The partial safety factor can be considered equal to 1.

This page was intentionally left in blank

CHAPTER.4 NEW PROPOSAL FORMULA FOR ANNEX G

4.1- Introduction

A new formulae is proposed to determine the buckling resistance and to evaluate with more accuracy the temperature, [23], consequently the strength of the cross-section components. A new proposal is presented for the calculation of the average temperature of the flange. A new proposal is proposed to calculate the residual height of the web, based on 400ºC isothermal, [24]. A new proposal is presented for the calculation of the external layer of concrete to be neglected, based on 500ºC isothermal, [1]. The reduced stiffness and strength of reinforcement is also proposed based on a new approximation for the average temperature. Figure 26 present the Isothermal criteria used for new proposal.

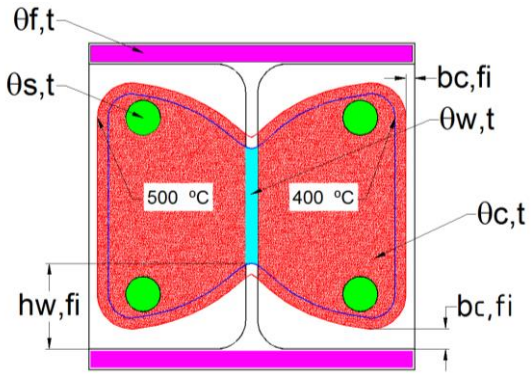

Figure 26 - Isothermal criteria in the cross section.

4.2- Fire effect for the flange component

The flange component requires a bilinear approximation for the calculation of the average temperature instead of the linear approximation currently proposed in CEN - EN 1994-1-2, [1], using a new empirical coefficient k_t and a new reference value $\theta_{0,t}$. This new proposal differentiates the type of the profile to be used in the partially encased column (HEB and IPE) see Eq (46) and Table 17.

Figure 27 represents the average temperature of the flange, depending on the section factor and on the standard fire resistance class. Each graph depicts the results of the simplified calculation method based on the current version of the Eurocode, the results of the advanced calculation method based on a 2D analysis (ANSYS) and the results of the new formulae by approximation to the numerical simulation results.

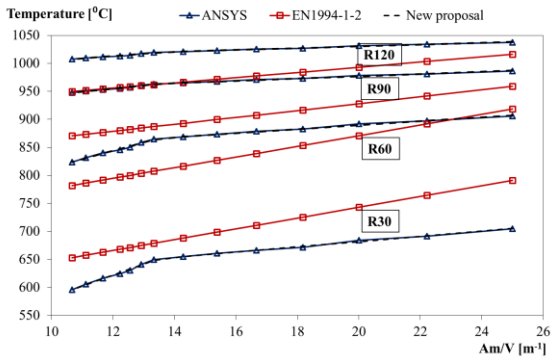

a) HEB sections

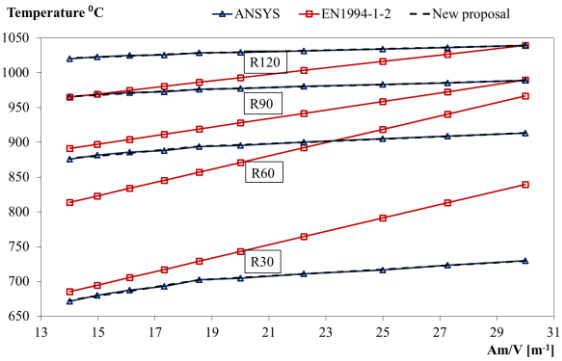

b) IPE section

Figure 27 - Average temperature of the flange.

The temperature is affecting the elastic modulus of the material without any other reduction that could affect the second order moment of area.

$$\theta_{f,t} = \theta_{0,t} + k_t\left(A_m/V\right) \tag{46}$$

The new proposal presents a new value for the reference temperature and a new value for the empirical coefficient.

Table 17 - Parameters for determining the temperature in the flange.

Sections	10<Am/V<14		14<=Am/V<25		10<Am/V<19		19<=Am/V<30	
	HEB		HEB		IPE		IPE	
Standard Fire	$\theta_{0,t}$ [^{0}C]	k_t [m^{0}C]	$\theta_{0,t}$ [^{0}C]	k_t [m^{0}C]	$\theta_{0,t}$ [^{0}C]	k_t [m^{0}C]	$\theta_{0,t}$ [^{0}C]	k_t [m^{0}C]
R30	387	19,55	588	4,69	582	6,45	656	2,45
R60	665	14,93	819	3,54	824	3,75	862	1,72
R90	887	5,67	936	2,04	935	2,20	956	1,09
R120	961	4,29	998	1,62	997	1,68	1010	0,96

4.3- Fire effect on the web component

The effect of the fire on the web of the steel section is determined by the 400 °C isothermal criterion, [24].This procedure defines the affected zone of the web and predicts the web height reduction $h_{w,fi}$.

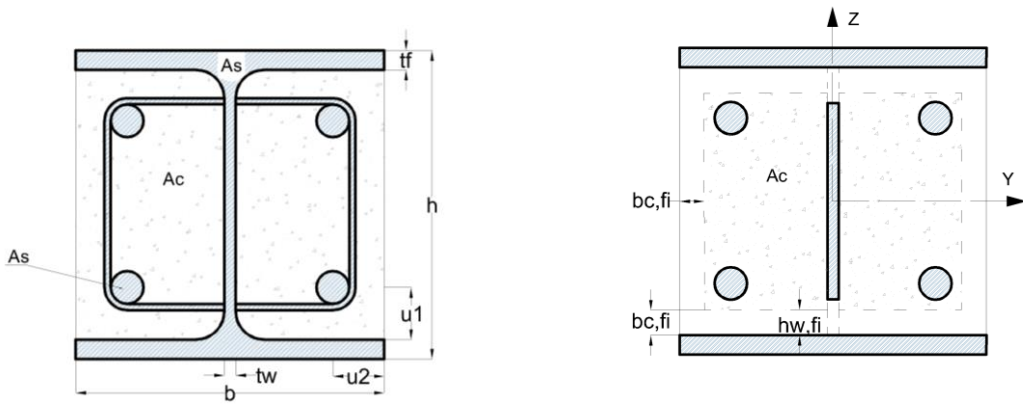

Figure 28 – Balanced summation model for partially encased columns under fire.

This new formulae presents a strong dependence on the section factor A_m/V , see Figure 29, regardless of the fire resistance class (t in minutes), unlike the current version of the CEN - EN 1994-1-2, [1].

The results of the current version of CEN - EN 1994-1-2, [1], are unsafe for all fire resistance classes and for all section factors. The new proposal presents a parametric expression that depends on section factor and on the standard fire resistance class, Eqs (47)-(48). Both equations have the application limits defined in Table 18. This calculation is affecting the second order moment of area of the web, without considering any temperature effect on the reduction of the elastic modulus.

$$2h_{w,fi}/h_i \times 100 = 0.0035 \times t^2 \times (A_m/V) - 0.03 \times t^{2.02} + (A_m/V)/2 \text{ for (HEB)} \quad (47)$$

$$2h_{w,fi}/h_i \times 100 = 0.002 \times t^2 \times (A_m/V) - 0.03 \times t^{1.933} + (A_m/V) \text{ for (IPE)} \quad (48)$$

Table 18 - Application limits (HEB and IPE profiles).

Standard fire resistance	Section factor (HEB)	Section factor (IPE)
R30	A_m/V <22,22	A_m/V <30
R60	A_m/V <15,38	A_m/V <18,56
R90	A_m/V <12,22	A_m/V <14,97
R120	A_m/V <11,11	-

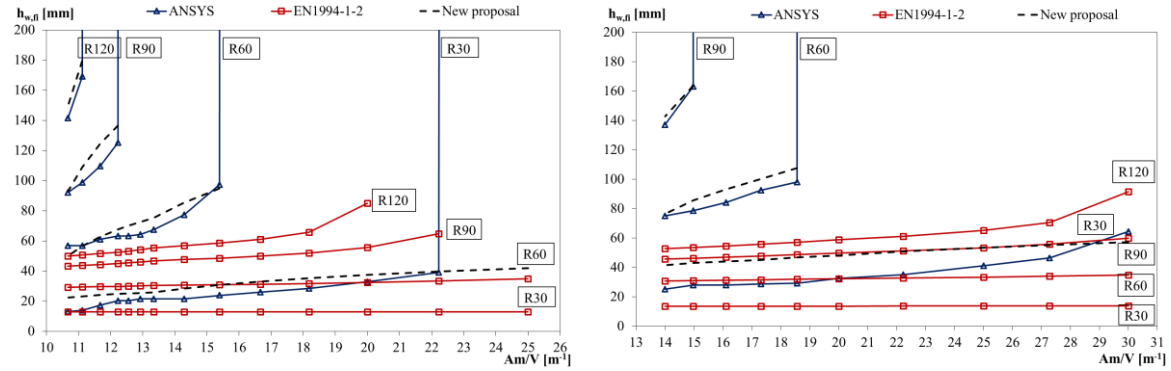

a) HEB sections b) IPE section

Figure 29 - Web height reduction.

The residual area of the web will affect the calculation of the effective flexural stiffness and the plastic resistance to axial compression, but the elastic modulus and the yield stress are not affected by the temperature.

The arithmetic average temperature of the effective web section is also depicted in Figure 30 and was defined by the nodal position under the limiting condition, see Eq.(49) , Table 19 and Table 20. Temperature results of CEN - EN 1994-1-2, [1], presented on this graph were determined by the inverse method, using the reduction factor of the yielding stress. The new proposal was adjusted to numerical results and a big difference between the current version and the new proposal is presented.

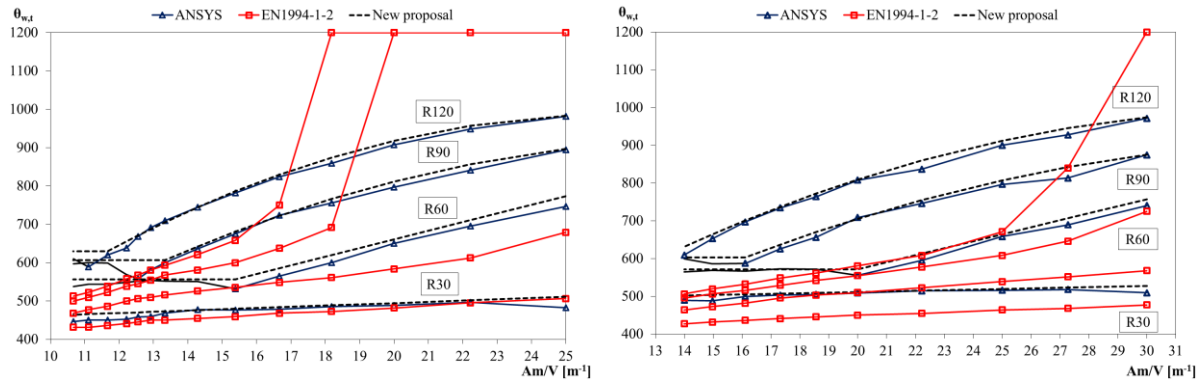

a) HEB sections b) IPE section

Figure 30 - Average web temperature for different standard fire resistance classes.

$$\theta_{w,t} = a \times \left(A_m/V\right) \times 2 + b \times A_m/V + c \tag{49}$$

Table 19 - Parameters and application limits for HEB cross sections.

Standard fire resistance	a (HEB)	b (HEB)	c (HEB)	Section factor (HEB)
R30	0.0000	3.2285	430.0000	10<Am/V<25
R60	0.0000	0.0000	566.6500	10<Am/V<15
	0.0000	22.5320	210.0000	15<Am/V<25
R90	0.0000	0.0000	606.4000	10<Am/V<13
	1.1823	70.2440	120.0000	13<Am/V<25
R120	0.0000	0.0000	629.8661	10<Am/V<11
	-1.6136	85.6710	-150.0000	11<Am/V<25

Table 20 - Parameters and application limits for IPE cross sections.

Standard fire resistance	a (IPE)	b (IPE)	c (IPE)	Section factor (IPE)
R30	0.0000	1.5708	480.0000	14<Am/V<30
R60	0.0000	0.0000	571.5400	14<Am/V<20
	0.0000	18.5770	200.0000	20<Am/V<30
R90	0.0000	0.0000	602.8100	14<Am/V<15
	-0.6761	50.7910	-40.0000	15<Am/V<30
R120	0.8283	57.6550	-15.0000	14<Am/V<30
	0.0000	1.5708	480.0000	14<Am/V<30

4.4- Fire effect on the concrete component

The effect of the fire on the concrete was determined by the 500 ºC isothermal, [1]. The external layer of concrete to be neglected may be calculated in both principal directions, defining $b_{c,fi,v}$ and $b_{c,fi,h}$. According to CEN - EN 1994-1-2, [1], the thickness of concrete to be neglected depends on section factor A_m/V, for standard fire resistance classes of R90 and R120. The new proposal demonstrates a strong dependence on the section factor for all fire rating.

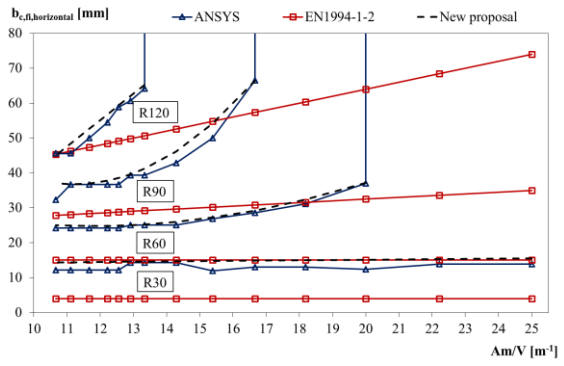

a) Horizontal reduction on HEB section.

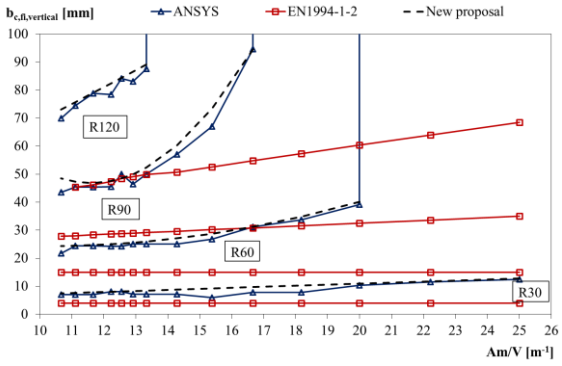

b) Vertical reduction on HEB section.

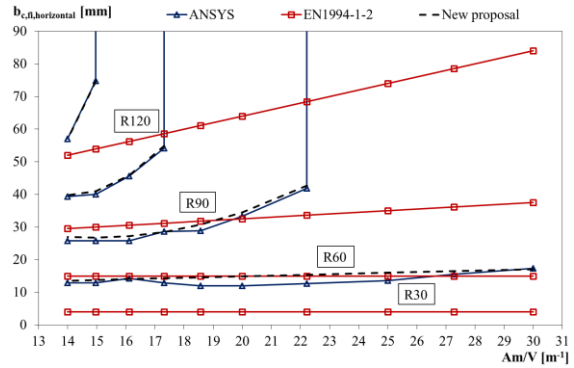

c) Horizontal reduction on IPE section.

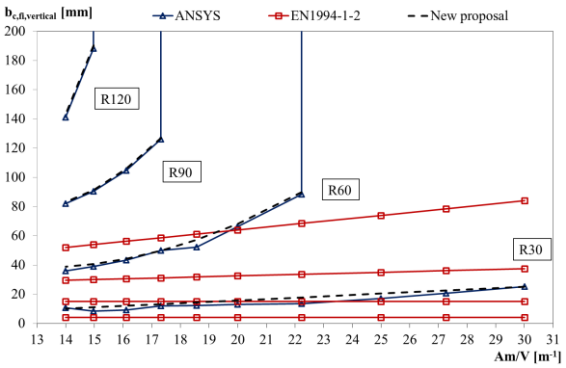

d) Vertical reduction on IPE section.

Figure 31 - Thickness reduction of the concrete area for HEB and IPE sections.

Figure 31present the new proposal for $b_{c,fi,v}$ and $b_{c,fi,h}$ for HEB and IPE sections. Table 21 and Table 22 provide the new formulae to determine the thickness of concrete to be neglected in fire design, based on the new Eq.(50) Which applies to both cross section types (HEB and IPE) and directions (horizontal and vertical). The new proposal defines the amount of concrete to be neglected in both principal directions. This value depends on the section factor for every fire rating class.

$$b_{c,fi} = a \times (A_m/V)^2 + b \times (A_m/V) + c \qquad (50)$$

Table 21 - Reduction in thickness of the concrete (HEB).

	$b_{c,fi} = a \times (A_m/V)^2 + b \times A_m/V + c$						
	$b_{c,fi,h}$			$b_{c,fi,v}$			
Resistance Standard fire	a	B	c	a	b	c	Section factor
R30	0,0	0,0809	13,5	0,0	0,372	3,5	$10 < A_m/V < 25$
R60	0,1825	-4,2903	50,0	0,1624	-3,2923	41,0	$10 < A_m/V < 20$
R90	1,0052	-22,575	163,5	1,8649	-43,287	298,0	$10 < A_m/V < 17$
R120	0,0	7,5529	-35,5	0,0	6,0049	9,0	$10 < A_m/V < 13$

Table 22 - Reduction in thickness of the concrete (IPE).

	$b_{c,fi} = a \times (A_m/V)^2 + b \times A_m/V + c$						
	$b_{c,fi,h}$			$b_{c,fi,v}$			
Resistance Standard fire	a	B	c	a	b	c	Section factor
R30	0,0	0,2206	10,5	0,0	0,9383	-3,0	$14 < A_m/V < 30$
R60	0,2984	-8,8924	93,0	0,5888	-15,116	135,0	$14 < A_m/V < 22$
R90	1,3897	-38,972	313,0	2,0403	-50,693	393,0	$14 < A_m/V < 17$
R120	0,0	18,283	-199,0	0,0	48,59	-537,0	$14 < A_m/V < 15$

The new proposal introduces a parametric approximation, based on the standard fire resistance and section factor, Eqs.(51)-(52). The application limits are presented in Table 23 and the temperature of the residual concrete is represented in Figure 32.

$$\theta_{c,t} = 3.1 \times t^{0.5} \times \left(A_m / V\right) + 0.003 \times t^{1.95} \tag{51}$$

$$\theta_{c,t} = 2.67 \times t^{0.5} \times \left(A_m / V\right) + 3.4 \times t^{0.61} \tag{52}$$

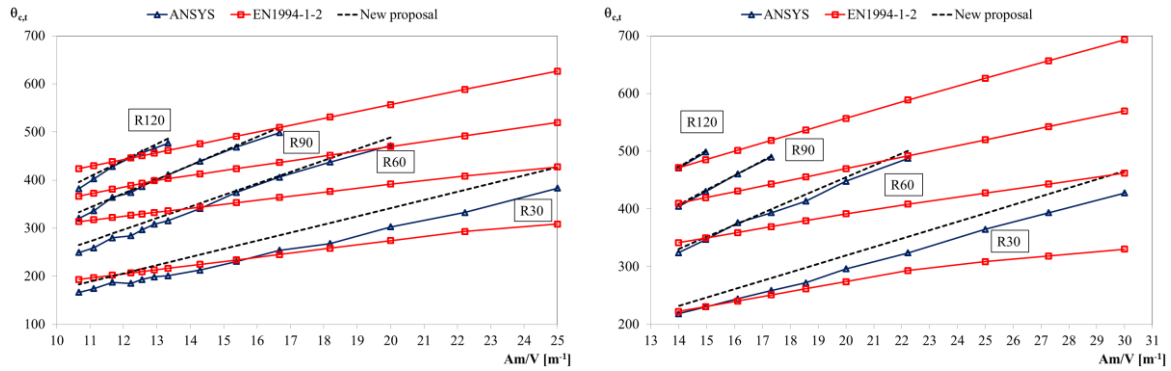

a) HEB sections b) IPE section

Figure 32 - Average temperature of residual concrete.

Table 23 - Application limits for average temperature of the concrete.

Standard fire resistance class	Section factor (HEB)	Section factor (IPE)
R30	Am/V<25	Am/V<30
R60	Am/V<20	Am/V<23
R90	Am/V<17	Am/V<18
R120	Am/V<14	Am/V<15

4.5- Fire effect on the reinforcement component

The effect of the fire into the reinforcement depends on the calculation of the average temperature of the material. The new parametric formula may be used to determine this effect.

Figure 33 depicts the average temperature of rebar determined by the numerical results. The results of the current version of CEN - EN 1994-1-2, [1], were indirectly determined through the most critical reduction factor used for the yielding stress and used for the elastic modulus. Alternatively, the new parametric formula is presented for the calculation of the average temperature of rebar. Eqs (53)-(54) were developed to the new proposal, based on the distance between rebar exposed surface (u), fire rating class (t) and section factor A_m/V .

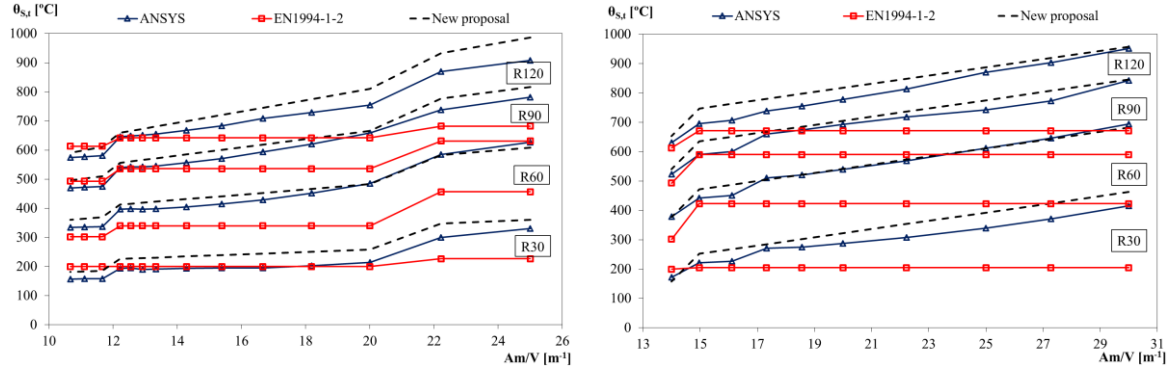

a) HEB sections b) IPE section

Figure 33 - Average temperature of rebar HEB and IPE

$$\theta_{s,t} = 0.1 \times t^{1.1} \times \left(A_m/V\right) + 7.5 \times t - 0.1 \times t^{1.765} - 8 \times u + 390 \quad ,(HEB) \tag{53}$$

$$\theta_{s,t} = 14.0 \times \left(A_m/V\right) + 11.0 \times t - 0.1 \times t^{1.795} - 8 \times u + 115 \quad ,(IPE) \tag{54}$$

This page was intentionally left in blank

CHAPTER.5 ADVANCED CALCULATION METHOD

The advanced calculation method, using the ANSYS software, based on the 3D modelling of the column with structural profiles IPE200 to IPE500 and HEB160 to HEB500. The Finite Element Method obtains the numerical results using different solution methods, including the incremental and interactive process. The numerical analysis is taken into account the thermal-structural uncoupled analysis, which is, not only the thermal action in the element totally involved by the fire, but also the static load to be supported in service conditions. The non-linearity of the material and the geometry are also considered. A four step, uncoupled thermal and mechanical analysis is required to determine the buckling resistance of partially encased columns.

The first step should be a nonlinear thermal analysis to define the temperature of the elements under fire.

The second step should be the elastic buckling analysis (static and Eigen buckling analysis) to define the elastic critical load and the stability mode for specific fire rating classes R30, R60, R90 and R120.

The third step should be the nonlinear geometric and material plastic analysis to find the plastic resistance of the cross section for specific fire rating classes R30, R60, R90 and R120.

The fourth step is the nonlinear geometric and material buckling analysis to find the buckling resistance of partially encased columns for specific fire rating periods R30, R60, R90 and R120.

The model is a full three dimensional model, based on perfect contact between materials.

5.1- Elements used in numerical models

Different types of elements are going to be applied to solve the thermal analysis and the mechanical analysis. These elements are defined in the data base of the software ANSYS. The elements were selected according to the simulation needs, using the lower order finite elements available.

5.1.1- Thermal model

Solid 70 has a 3D thermal conduction capability, the element has 8 nodes with a single degree of freedom, temperature, at each node. The element is used to a 3-D, transient thermal analysis see Figure 34. The element also can compensate for mass transport heat flow from a constant velocity field, [25].

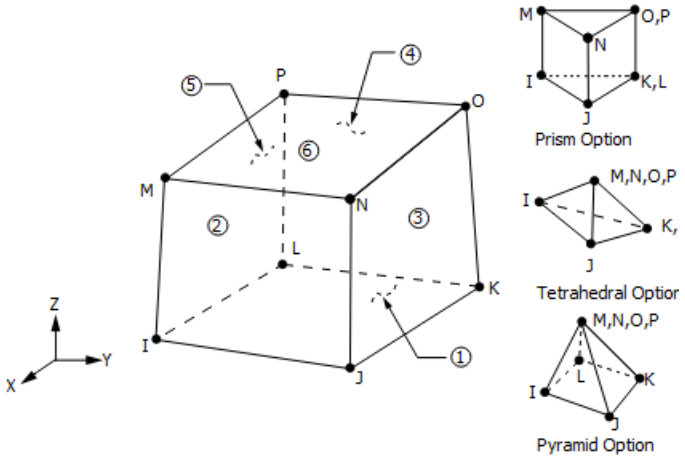

Figure 34 - SOLID70 Geometry (ANSYS16.2) [25].

The interpolating functions are linear and this element uses full integration points (2x2x2) to define conductivity matrix, [25]. This element is going to be applied to the volume material of steel, concrete and reinforcement.

5.1.2- Structural model

The three-dimensional model uses element SOLID 185 to model the hot rolled steel and the reinforcing bars. The finite element SOLID 65 is used to model concrete. SOLID 185 has eight nodes with three degrees of freedom at each node (displacements) and uses linear interpolating functions, [25]. The reduced integration method (Gauss point) was applied taking into consideration the comparison of the critical load with the analytical method.

Figure 35 represents the geometry of the finite element SOLID185 and the out surfaces used to apply the boundary conditions. This figure also represents some modified configurations that were avoided.

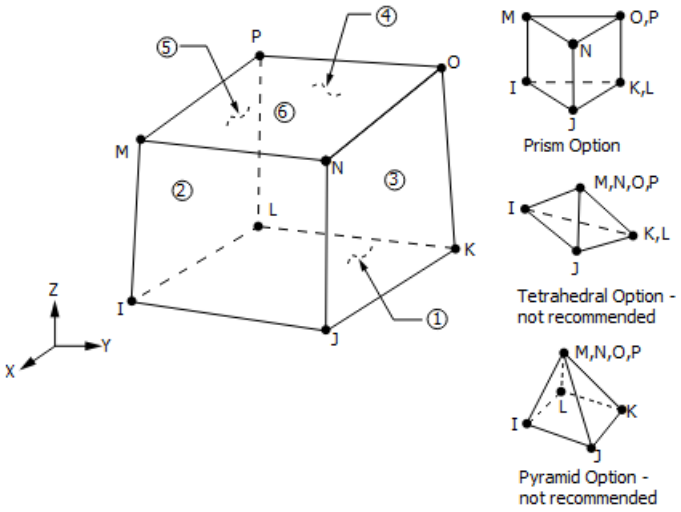

Figure 35 - SOLID185 Geometry (ANSYS16.2) [25].

SOLID65 was elected to model concrete, presents eight nodes with three degrees of freedom at each nodes (displacements) and uses linear interpolating functions with full integration scheme (2x2x2 Gauss point). This element was used to model the concrete part of the (PEC). The solid is capable of cracking in tension and crushing in compression see Figure 36, if the damage criterion is activated (not the case herein).

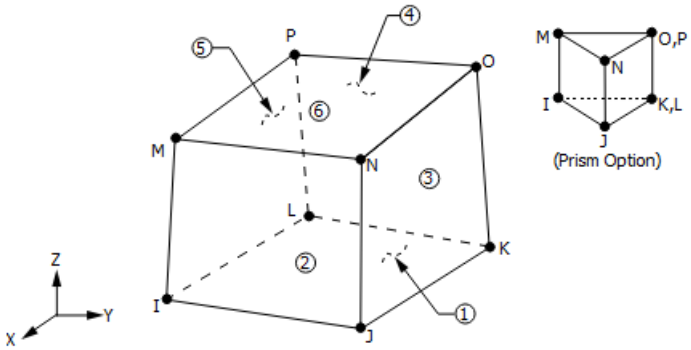

Figure 36 - Solid65 Geometry (ANSYS 16.2) [25].

The concrete is capable of cracking (in three orthogonal directions), crushing and achieve plastic deformation. The rebar are capable of tension and compression, but not able to resist shear, [25].

Perfect contact between the reinforcing bars and concrete is assumed with sharing nodes with the reinforcement and steel profile.

5.2- Convergence test

To know the best mesh applied to the PEC, a convergence test of the solution was done using different element sizes in Z, Y and X directions, see Figure 37. Current mesh considers 100 element divisions for height of 3m columns and 150 element divisions for height of 5m columns in Z direction. The size of the mesh applied to the cross section was based on a previous experience of the simulation for 2D analysis, [23].

Figure 38 presents a convergence test for cross section HEB 200 using three different sizes in Y, X and Z, the temperature was selected in the center of the rebars. Mesh 1 has 40299 nodes, Mesh 3 has 79083 and mesh 3 has 62721 nodes see Figure 37. As we can see there is no influence of the mesh applied, the results are close together.

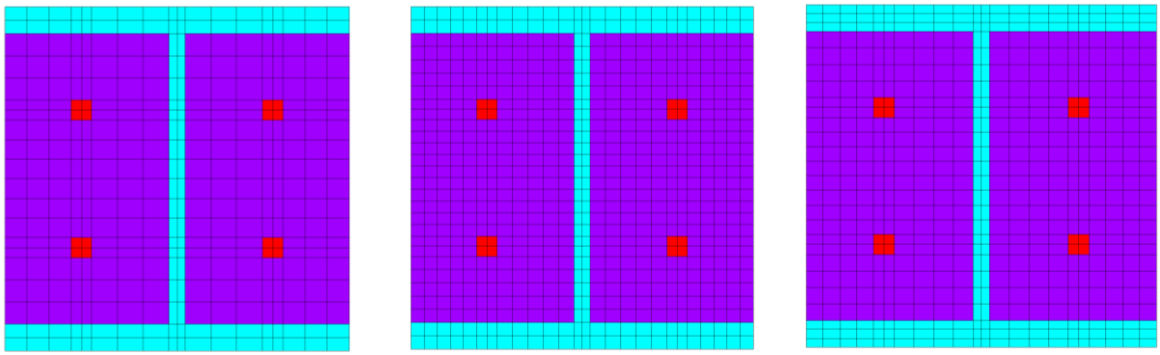

a) First mesh. b) Second mesh. c) Third mesh.

Figure 37 – Three different sizes of mesh for HEB180.

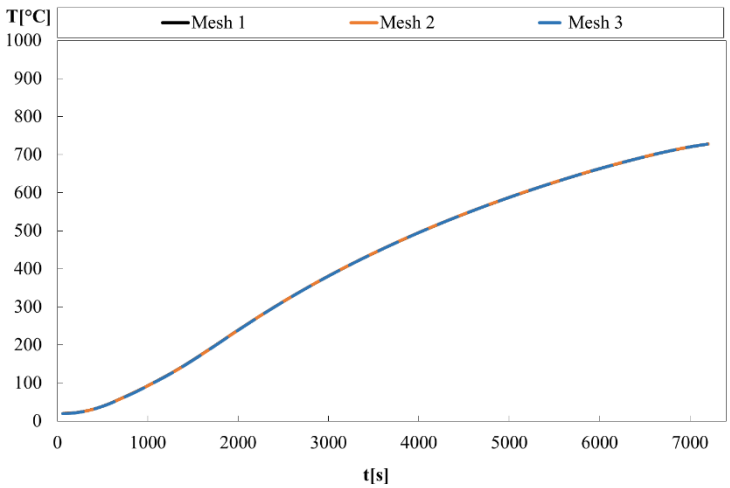

Figure 38 – Convergence test for cross section HEB 220 with three different mesh.

5.3- Nonlinear transient thermal analysis

The first step considers the nonlinear transient thermal analysis to calculate the temperature field. The finite element method requires the solution of Eq (55) in the internal domain of the partially encased column and Eq (56) in the external surface, when exposed to fire. In these equations: T represents the temperature of each material; $\rho(T)$ defines the specific mass; $C_p(T)$ defines the specific heat; $\lambda(T)$ defines the thermal conductivity; α_c specifies the convection coefficient; T_g represents the gas temperature of the fire compartment, using standard fire ISO 834, [13], around the cross section (4 exposed sides); Φ specifies the view factor; ε_m represents the emissivity of each material; ε_f specifies the emissivity of the fire; σ represents the Stefan-Boltzmann constant.

$$\nabla \cdot (\lambda_{(T)} \cdot \nabla T) = \rho_{(T)} \cdot C_{p(T)} \cdot \partial T / \partial t \qquad (\Omega) \tag{55}$$

$$(\lambda_{(T)} \cdot \nabla T) \cdot \vec{n} = \alpha_c (T_g - T) + \Phi \cdot \varepsilon_m \varepsilon_f \cdot \sigma \cdot (T_g^4 - T^4) \qquad (\partial\Omega) \tag{56}$$

SOLID70 has a 3D thermal conduction capability to model the profile, concrete and rebar's, which was presented before.

The nonlinear transient thermal analysis was defined with an integration time step of 60 s, which can decrease to 1 s and increase up to 120 s. The criterion for convergence uses a tolerance value of the heat flow, smaller than 0.1% with a minimum reference value of $1x10^{-6}$.

The temperature field was determined for the total time of 7200 s (R120). Figure 39 shows numerical thermal 2D results for column HEB300 and IPE200, Figure 41 present also numerical thermal 3D results for column HEB400 exposed to ISO834 fire, [13], after 30,60,90 and 120 minutes. The temperature field was recorded for the corresponding resistance class and applied as body load to the mechanical model. The mesh was defined after a solution convergence test. For the full results of the thermal effect in the (PEC) see ANNEX 1.

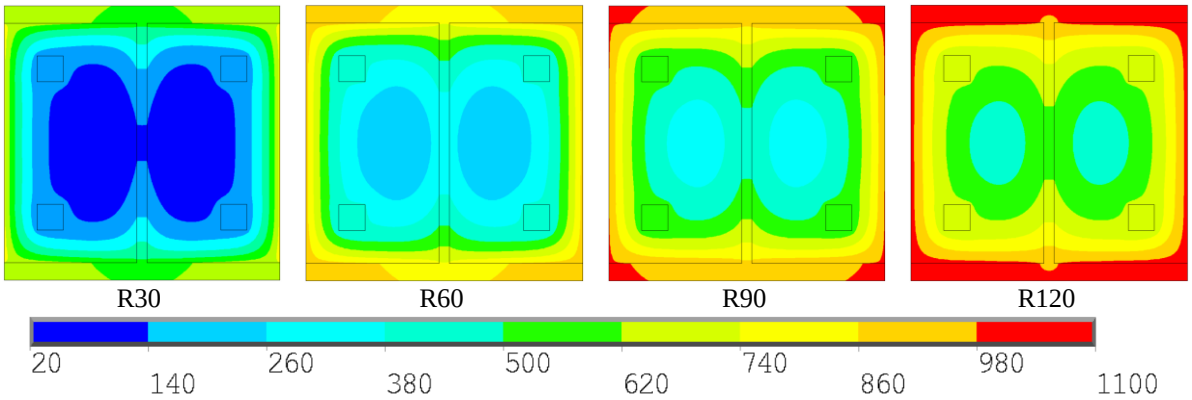

Figure 39 - Numerical thermal 2D results for column HEB300, for each fire rating

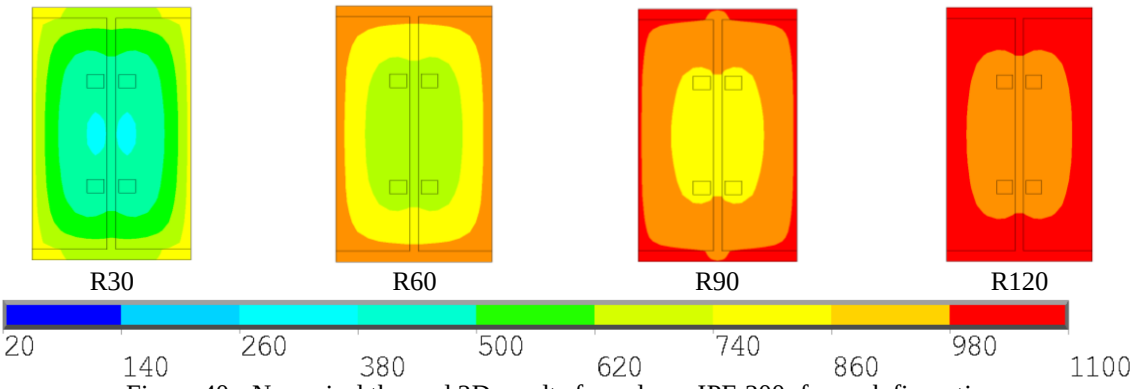

Figure 40 - Numerical thermal 2D results for column IPE 200, for each fire rating.

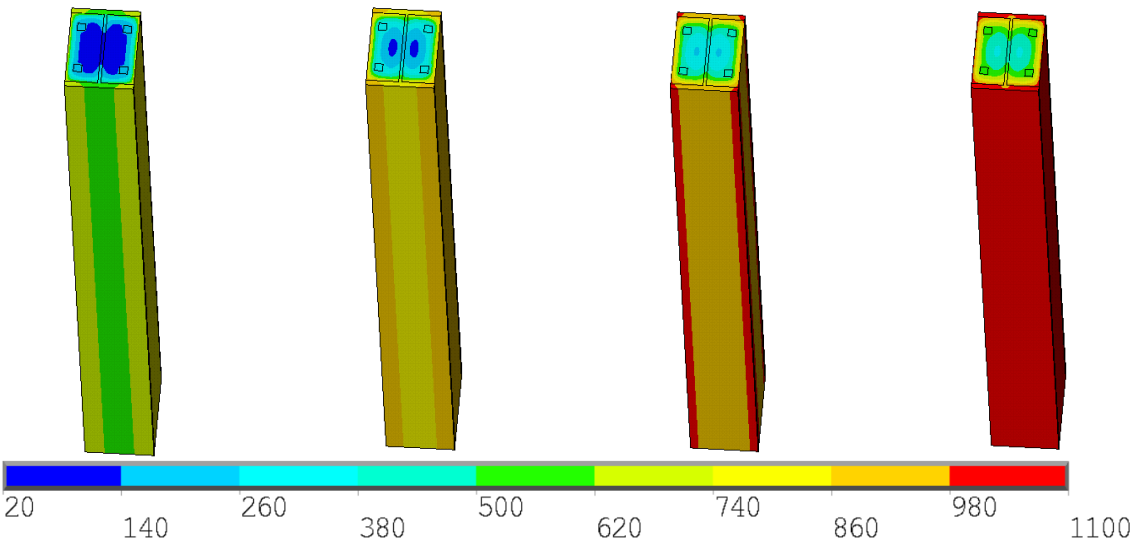

a) Time=30 min. a) Time=60 min. a) Time=90 min. a) Time=120 min.

Figure 41 - Numerical thermal 3D results for column HEB 400, for each fire rating.

Table 24 presents the thermal results from ANSYS, with the minimum (min) and maximum (max) value. The minimum temperature of profile decrease when the cross sections increase, mainly due to the decrease of the section factor. The results of the thermal analysis are presented in Annex1.

Table 24 - Thermal results from ANSYS [°C] (min-max).

Profile	A_m/V	R30	R60	R90	R120
HEB160	25,00	294-803	594-934	765-1000	889-1045
HEB180	22,22	220-802	517-933	699-1000	830-1044
HEB200	20,00	161-800	443-931	624-998	746-1044
HEB220	18,18	124-799	385-931	563-998	691-1043
HEB240	16,67	102-798	323-930	500-998	631-1043
HEB260	15,38	91-797	268-930	439-997	571-1043
HEB280	14,29	79-797	217-929	383-997	512-1043
HEB300	13,33	66-796	168-929	335-997	459-1042
HEB320	12,92	62-795	152-929	314-996	437-1042
HEB340	12,55	58-790	140-929	296-994	418-1040
HEB360	12,22	56-789	132-925	279-994	399-1040
HEB400	11,67	50-790	121-926	252-994	369-1041
HEB450	11,11	45-791	111-927	215-997	329-1042
HEB500	10,67	40-789	104-927	185-996	298-1042
IPE200	30,00	372-811	664-938	814-1002	933-1046
IPE220	27,27	320-808	606-935	742-1001	876-1045
IPE240	25,00	268-807	554-936	717-1001	831-1045
IPE270	22,22	201-806	479-935	652-1000	753-1044
IPE300	20,00	145-805	407-934	582-1000	703-1044
IPE330	18,56	120-804	356-934	529-1000	655-1044
IPE360	17,32	106-799	312-931	481-997	608-1043
IPE400	16,11	96-802	266-932	429-999	555-1044
IPE450	14,97	83-801	218-932	375-998	498-1043
IPE500	14,00	70-800	175-932	328-998	446-1044

5.4- Static and Eigen buckling analysis

The static linear analysis is the basis for the eigen buckling analysis. The solution of Eq (57) must be find primarily, assuming $\{F_{ref}\}$ is an arbitrary load to be applied on the Partially Encased Column (usually a unit force). $[K]$ Is its stiffness matrix and $\{d\}$ is the displacement vector. When the displacements are known, the stress field can be calculated for the reference load $\{F_{ref}\}$, which can be used to form the stress stiffness matrix $[K_{\sigma,ref}]$. Since the stress stiffness matrix is proportional to the load vector $\{F_{ref}\}$, an arbitrary stress stiffness matrix $[K_\sigma]$ and an arbitrary load vector $\{F\}$ may be defined by a constant λ as shown by Eqs (58)-(59).

The stiffness matrix is not changed by the applied load because the solution is linear. A relation between the stiffness matrices, the displacement and the critical load can then be presented as in Eq (60), which can be used to predict the bifurcation point. The critical load is defined as $\{F_{cri}\}$. Since the buckling mode is defined as a change in displacement for the same load, Eqs (60)-(61) are still valid, where $\{\delta d\}$ represents the incremental buckling displacement vector. The difference between Eq (60) and Eq (61) produces an eigenvalue problem, represented by Eq (62) where the smallest root defines the first buckling load, when bifurcation is expected.

$$[K]\{d\} = \{F_{ref}\} \tag{57}$$

$$[K_\sigma] = \lambda [K_{\sigma,ref}] \tag{58}$$

$$\{F\} = \lambda \{F_{ref}\} \tag{59}$$

$$\left[[K] + \lambda_{cri}[K_{\sigma,ref}]\right]\{d\} = \lambda_{cri}\{F_{ref}\} \tag{60}$$

$$\left[[K] + \lambda_{cri}[K_{\sigma,ref}]\right]\left(\{d\} + \{\delta d\}\right) = \lambda_{cri}\{F_{ref}\} \tag{61}$$

$$\left[[K] + \lambda\ [K_{\sigma,ref}]\right]\{\delta d\} = \{0\} \tag{62}$$

Figure 42 presents the elastic modulus used for all materials used in the Eigen buckling analysis at elevated temperature.

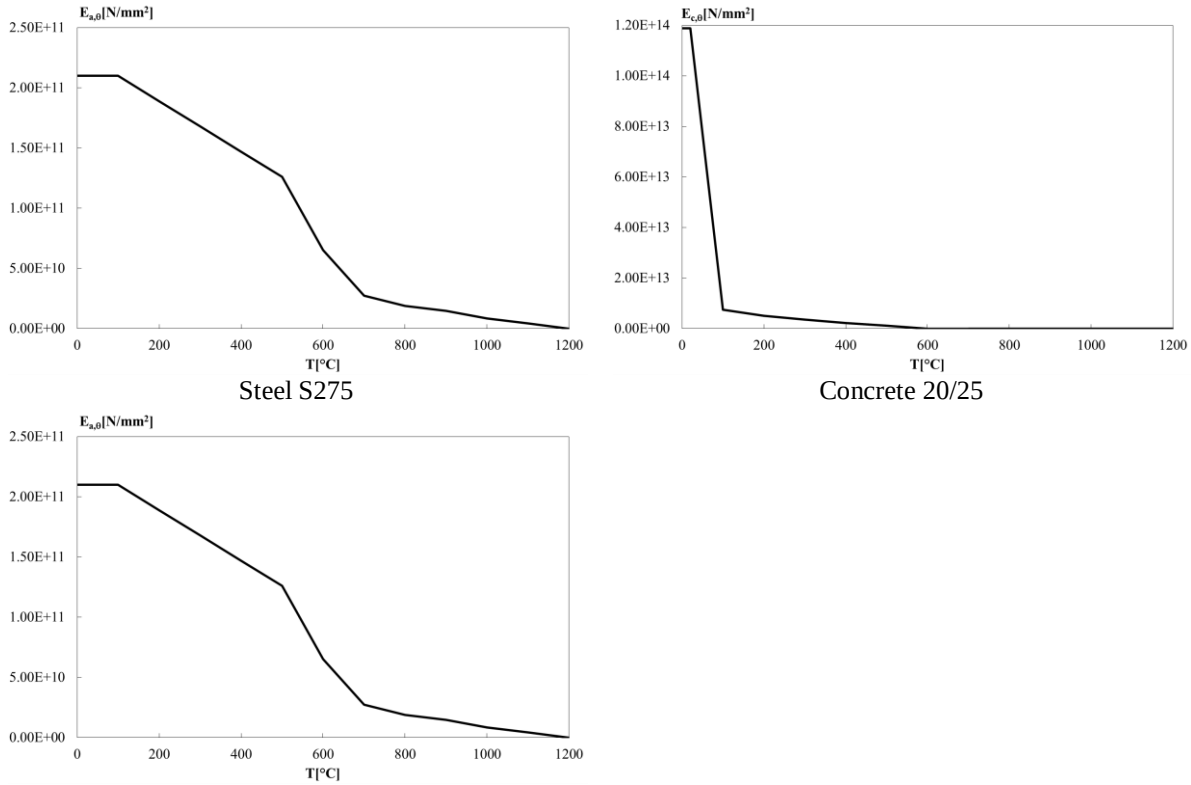

Figure 42 - Elastic modulus for the three materials at elevated temperature.

The trivial solution is not of interest, which means that the solution for λ is define for an algebraic equation, imposing the determinant of the global matrix equal to zero. The calculated eigenvalue is always related to an eigenvector $\{\delta d\}$ called a buckling mode shape, see Figure 43.

a) 1.0L. b) 0.7L. c) 0.5L.

Figure 43 - Buckling shape of three boundary conditions for HEB300 after R30.

This numerical solution of a linear buckling analysis assumes that everything is perfect and therefore the real buckling resistance will be lower than the calculated buckling load if the imperfections are taking into account.

Table 26, Table 27 and Table 28 presents the results of elastic critical load for both 3m and 5m of height using three different buckling length and four specific fire rating classes R30, R60, R90 and R120. As expected, partially encased columns based on HEB profile present higher critical load when compared with IPE profile. The critical load decreases with the relative slenderness in the fire situation.

Table 25 - Elastic critical load for 3m height after R30, R60.

	$N_{fi,cr,z,ANSYS}$ [N]					
	R30			R60		
Profile	0.5L	0.7L	1.0L	0.5L	0.7L	1.0L
HEB160	1710450	862823	425120	756905	363548	179333
HEB180	2850120	1447910	714097	1189010	613345	303489
HEB200	5533210	2908630	1446150	2412180	1321970	665935
HEB220	9782910	5323080	2669200	4407320	2536380	1297070
HEB240	13867700	7613460	3822930	6461320	3732390	1907690
HEB260	22789300	13136900	6689220	11071200	6786840	3539320
HEB280	29469700	17150300	8749830	14692900	9044590	4712810
HEB300	38058400	22307400	11398000	19112800	11811800	6154250
HEB320	40939300	23776800	12113900	20325300	12427000	6447800
HEB340	51291200	30411600	15834200	25822700	16389400	8657350
HEB360	53691800	31909800	16407700	26849400	16893700	8890350
HEB400	59740000	35145700	18011400	31528900	19694400	10325500
HEB450	65826800	38278100	19538900	33994100	20925500	10113000
HEB500	71591000	41227500	20978300	36258700	22058000	11461600
IPE200	218298	116206	56850	95340	51417	25163
IPE220	465156	252259	123599	180359	99140	48607
IPE240	777556	420869	206646	305079	167804	82599
IPE270	1820970	947980	468282	736244	393113	195670
IPE300	2835790	1500280	743268	1206100	659840	328337
IPE330	3810850	2030690	1007290	1671270	916430	458654
IPE360	6582720	3645910	1825850	2972470	1709150	867928
IPE400	8621540	4774130	2387850	4317830	2480820	1256197
IPE450	10961400	6089110	3047200	5582970	3208400	1624470
IPE500	15025700	8411240	4221590	8146720	4735830	2410380

Table 26 - Elastic critical load for 3m height after R90, R120.

	$N_{fi,cr,z,ANSYS}$ [N]					
	R90			R120		
Profile	0.5L	0.7L	1.0L	0.5L	0.7L	1.0L
HEB160	417492	210314	103530	308163	155851	76799
HEB180	660292	336085	165699	479893	245508	121194
HEB200	1226380	656510	328356	803119	424708	211551
HEB220	2213330	1268720	650152	1290200	705370	354627
HEB240	3316050	1941110	999870	1815180	1002950	504787
HEB260	5768880	3604570	1908240	3020740	1789830	924492
HEB280	7939250	4981400	2630180	4249790	2585060	1347330
HEB300	10667000	6703910	3531520	5870770	3619720	1892900
HEB320	11478700	7124730	3731820	6396210	3906730	2034140
HEB340	14612200	9426050	5042040	8074510	5123840	2723130
HEB360	15328500	9787080	5208420	8559780	5380520	2846500
HEB400	19313600	12345900	6566190	12106400	7559020	4057310
HEB450	21108600	13244500	6989840	13010000	8230330	4376710
HEB500	22705800	14040100	7372810	14237900	8856330	4679820
IPE200	60608	32800	16770	44655	24256	11875
IPE220	103250	56690	27778	75310	41710	20459
IPE240	159486	86683	42542	115592	63382	31156
IPE270	317046	163949	80855	230237	120421	59587
IPE300	503094	264967	131178	351434	186731	92677
IPE330	732762	392564	195199	474199	253714	126058
IPE360	1310640	739540	373768	782611	424759	218395
IPE400	2149410	1254390	640672	1031460	570420	285757
IPE450	2873660	1676310	855944	1389660	771249	386856
IPE500	4549151	2710810	1398400	2499671	1476500	760200

Table 27 - Elastic critical load for 5m height after R30, R60.

	$N_{fi,cr,z,ANSYS}$ [N]					
	R30			R60		
Profile	0.5L	0.7L	1.0L	0.5L	0.7L	1.0L
HEB160	671192	327045	160217	279780	136773	67035
HEB180	1113760	54431	266806	467898	230300	112999
HEB200	2211110	1094270	539295	997458	505452	249674
HEB220	3996180	2015480	993750	1890170	982690	488235
HEB240	5681200	2877290	1419390	2765470	1440990	715735
HEB260	9685960	5031110	2495050	4965170	2675860	1339620
HEB280	12594700	6573990	3262430	6593170	3558020	1780430
HEB300	16333200	8558030	4249060	8586850	4642240	2322610
HEB320	17439200	9092100	4509330	9052180	4860220	2426760
HEB340	22420400	11910000	5933640	11876900	6549300	3295050
HEB360	23326600	12336500	6139960	12262200	6721110	3376620
HEB400	25744600	13537600	6729200	14312000	7801630	3913480
HEB450	28097600	14677900	7284880	15254800	8240000	4124890
HEB500	30318600	15754200	7809470	16126600	8652030	4324960
IPE200	89124	45924	22450	37959	19660	9610
IPE220	188610	97996	47921	72870	38059	18615
IPE240	329486	170442	83389	130208	67823	33211
IPE270	728223	372109	182438	303128	156882	77126
IPE300	1124120	579484	284427	494408	258741	127409
IPE330	1505010	779070	382542	682487	358679	176691
IPE360	2645950	1400281	689999	1241010	671562	332665
IPE400	3444910	1823040	897890	1786670	966056	478013
IPE450	4375200	2320200	1142900	2303930	1246360	616655
IPE500	6035790	3215970	1586330	3392580	1850340	917328

Table 28 - Elastic critical load for 5m height after R90, R120.

	$N_{fi,cr,z,ANSYS}$ [N]					
	R90			R120		
Profile	0.5L	0.7L	1.0L	0.5L	0.7L	1.0L
HEB160	162006	78936	38660	119857	58506	28664
HEB180	256586	125570	61531	187175	91810	45009
HEB200	495812	248500	122422	321105	159960	78681
HEB220	945219	492031	244728	528259	267512	132047
HEB240	1436050	755575	376544	746987	379889	187579
HEB260	2636340	1446940	729146	1316490	697411	347898
HEB280	3630010	1991860	1002370	1891100	1017410	509303
HEB300	4872970	2671670	1342930	2638280	1429680	716536
HEB320	5190500	2820610	1414580	2853760	1535870	768447
HEB340	6836800	3827180	1636310	3729070	2065080	1042140
HEB360	7111600	3950070	1994330	3925130	2157910	1086960
HEB400	8968100	4980140	2513580	5500910	3085930	1564100
HEB450	9658940	5296080	2664670	6017200	3325700	1679020
HEB500	10277200	5584720	2804280	6503410	3555230	1790180
IPE200	24135	12516	6119	17780	9233	4515
IPE220	41327	21567	10547	30288	15867	7762
IPE240	66145	34265	16672	48197	25066	12270
IPE270	125655	64019	31371	91809	47062	23090
IPE300	200572	103133	50605	139710	72229	35477
IPE330	295625	153359	75368	188806	97957	48129
IPE360	544868	291381	144068	318875	169051	83394
IPE400	909233	496668	246569	419759	221682	109232
IPE450	1213140	662579	328879	570965	301890	148788
IPE500	1950240	1081980	539266	1074460	592085	294827

More detailed results are available in Annex 2.

5.5- Plastic resistance analysis

The plastic resistance was also evaluated, taking into consideration the criterion for the plastic behaviour of the column. A perfect geometry was elected for every type of cross section twenty four and for four fire ratings times 30, 60, 90 and 120 minutes, making a total of forty eight 3D simulations. The elements were prevented to move laterally and the bottom of the column was fixed to the ground. The incremental and iterative solution method (Newton Raphson) was used based on displacement. A compressive displacement was applied on the top of the column with a typical incremental displacement of 1 mm, with possibility to decrease up to 0.1 mm and to increase up to 0.2 mm. The reaction at the bottom of the column was used to calculate the plastic load.

The iterative and incremental simulation is material and geometric nonlinear, and used the criterion for convergence based on displacement, with a tolerance value of 5%. The mechanical properties of concrete follow the models defined in CEN - EN 1994-1-2, [1], for normal weight concrete, with the assumption of elastic perfectly plastic material under

compression and tension. The mechanical properties of the reinforcing steel follow the model of CEN - EN 1994-1-2, [1], and the mechanical properties of hot rolled steel follow the models of CEN - EN 1993-1-2, [14], both assuming the elastic perfectly plastic behaviour of materials.

Similar element types and meshes were used for this simulation taking into account the results of the previous simulations, being the reinforcement bars the last component to become plastic see Figure 45. Plastic resistance is defined by the reaction force when the reinforcement attains plastic strain. This was the criterion selected to define the plastic resistance of the cross section.

Figure 44 presents the materials properties used in finite elements for the nonlinear plastic resistance.

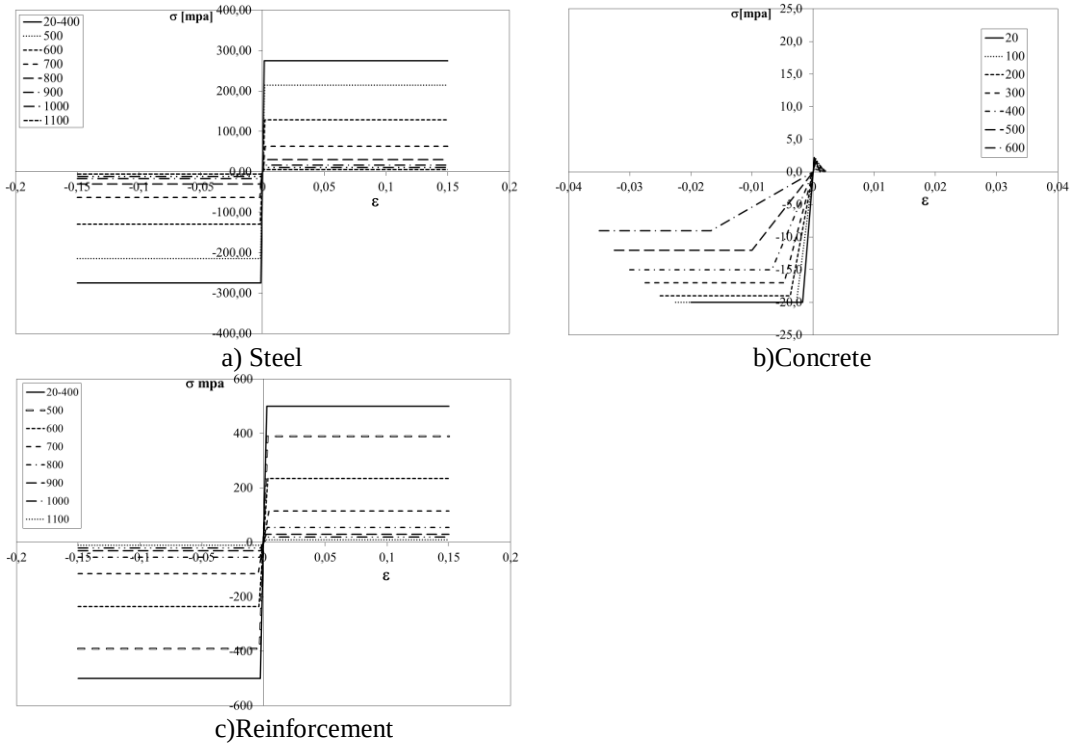

Figure 44 - Curve stress-strain of steel, concrete and reinforcement.

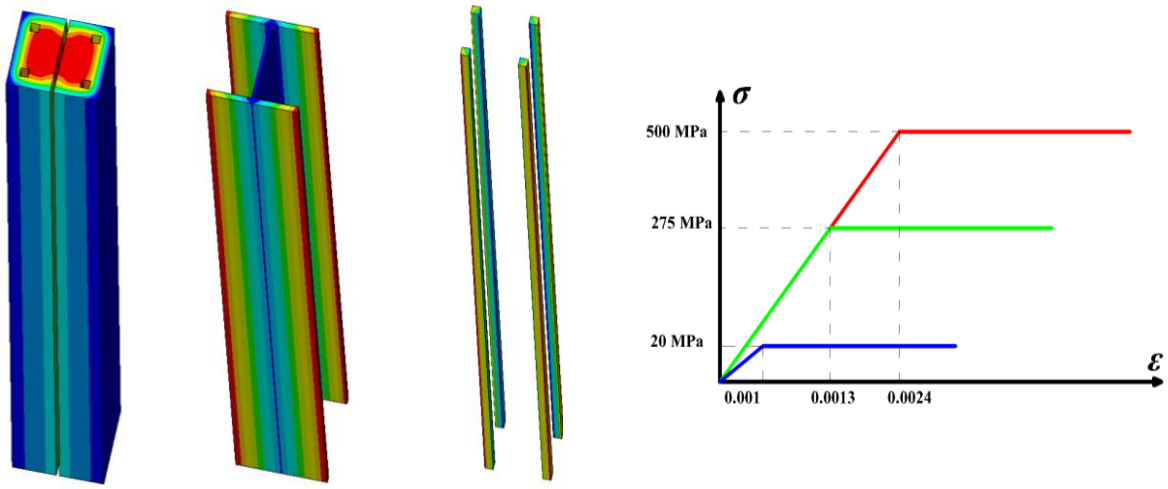

a) Concrete. b) Cross section. c) Reinforcement. d) Curve of stress strain.

Figure 45 - Plastic strain of HEB300 for R30 in three elements.

Table 29 presents the results of the plastic load for each cross section. .

Table 29 – Plastic resistance from ANSYS.

Profile	Am/V	$N_{fi,pl,Rd,ANSYS}$ [N]			
		R30	R60	R90	R120
HEB160	25.00	4496700	4267400	4156100	4082200
HEB180	22.22	5433500	5148500	5009900	4915200
HEB200	20.00	7121400	6789000	6605400	6482100
HEB220	18.18	8819200	8427200	8207900	8048500
HEB240	16.67	10039000	9593900	9333100	9144800
HEB260	15.38	12126000	11637000	11351000	11104000
HEB280	14.29	13329000	12794000	12474000	12196000
HEB300	13.33	14795000	14204000	13841000	13538000
HEB320	12.92	15815000	15188000	14796000	14480000
HEB340	12.55	18117000	17475000	17063000	16710000
HEB360	12.22	18949000	18284000	17849000	17483000
HEB400	11.67	20489000	19775000	19302000	18973000
HEB450	11.11	22331000	21566000	21047000	20692000
HEB500	10.67	24190000	23385000	22820000	22438000
IPE200	30.00	2649700	2556600	2443500	2394300
IPE220	27.27	3773900	3642500	3511100	3426700
IPE240	25.00	4212300	4027600	3916400	3825700
IPE270	22.22	5491100	5276400	5116800	5012000
IPE300	20.00	6228200	5969000	5783500	5664000
IPE330	18.56	7011400	6714100	6507500	6369600
IPE360	17.32	9074600	8742300	8490200	8315400
IPE400	16.11	9991200	9616100	9370300	9155600
IPE450	14.97	11350000	10928000	10650000	10406000
IPE500	14.00	14355000	14125500	13896000	13316000

5.6- Nonlinear buckling resistance analysis

The 3D model of Eigen buckling analysis was modified to include the geometric imperfections. Eigenvalue buckling analysis predicts the theoretical buckling strength (the bifurcation point) of an ideal linear elastic structure. The buckling resistance of each column was calculated by the incremental displacement and iterative solution model using (Newton Raphson) method. The imperfection of the geometry was based on the elastic buckling mode shape with updating of the nodal coordinates. This update was based on the mode shape and based on the maximum imperfection expected on the mid high of the column corresponding to $L/150$. Typical incremental displacement of 0,2 mm was applied, with minimum incremental displacement of 0,1 mm and maximum incremental displacement of 1 mm. The criterion for convergence is based on displacement with tolerance value of 5%. However, imperfections and nonlinearities prevent most real- world structures from achieving their theoretical elastic buckling strength. The nonlinear buckling analysis is a static analysis with large deflection (equilibrium in deformed configuration), extended to a point where the structure reaches its ultimate limit state (plasticity, modification into a mechanism). The buckling load is the maximum load determined for the curve plotted for load displacement curve see Figure 46.

A total of ninety six simulations were performed for the case of twenty four different cross section with one column length 3m using fixed end supports (buckling length equal to 0.5L) and for four fire resistance classes 30, 60 , 90 and 120 minutes.

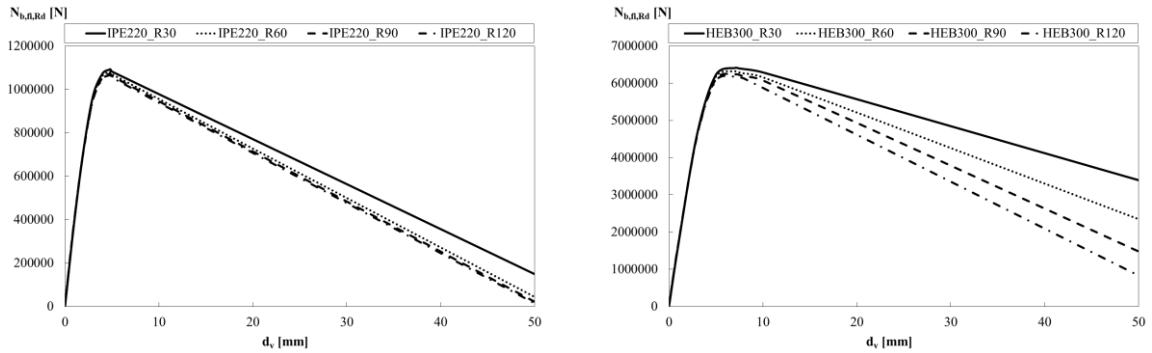

a) IPE220 for 3m of length. b) HEB300 for 3m of length.

Figure 46 – Curve load vertical displacement for each fire rating.

Table 30 present the results of buckling resistance obtained from ANSYS for 3m of height and for boundary condition 0.5L, using different fire ratings R30, R60, R90 and R120 minutes. The HEB profile has higher buckling resistance then IPE profile.

Table 30 – The design buckling resistance for each fire rating.

$N_{b,fi,Rd}$ [N] -3m- ANSYS-				
Profile	R30	R60	R90	R120
HEB160	1675685	1663100	1662200	1661400
HEB180	2075500	2075200	2074700	2074100
HEB200	2819000	2818500	2818000	2806000
HEB220	3592800	3591500	3591100	3590100
HEB240	4168400	4150900	4150600	4140800
HEB260	5187100	5108700	5076500	5021300
HEB280	5742600	5683800	5625800	5562800
HEB300	6410700	6321300	6241800	6180000
HEB320	6811900	6664900	6609600	6572900
HEB340	7943500	7874200	7773000	7690100
HEB360	8282900	8215200	8108200	8072300
HEB400	8919400	8853800	8744900	8647500
HEB450	9692600	9612900	9511700	9411200
HEB500	10472000	10399000	10282000	10180000
IPE200	738580	738530	738410	715180
IPE220	1090900	1079000	1071500	1065100
IPE240	1381700	1368200	1358800	1350800
IPE270	1996500	1977500	1961600	1950800
IPE300	2395800	2381400	2360200	2339000
IPE330	2776300	2747600	2719500	2355100
IPE360	3694700	3673600	3638100	3610800
IPE400	4559024	4524783	4490800	4432100
IPE450	4776474	4740600	4691100	4646000
IPE500	6119300	6060900	6060300	5959700

This page was intentionally left in blank

CHAPTER.6 COMPARISON OF RESULTS

Figure 47 present the comparison of the elastic buckling load, using the results obtained from the new proposal, for 30, 60, 90 and 120 minutes of fire exposure and for three different boundary conditions and also for both 3m and 5m of column height .

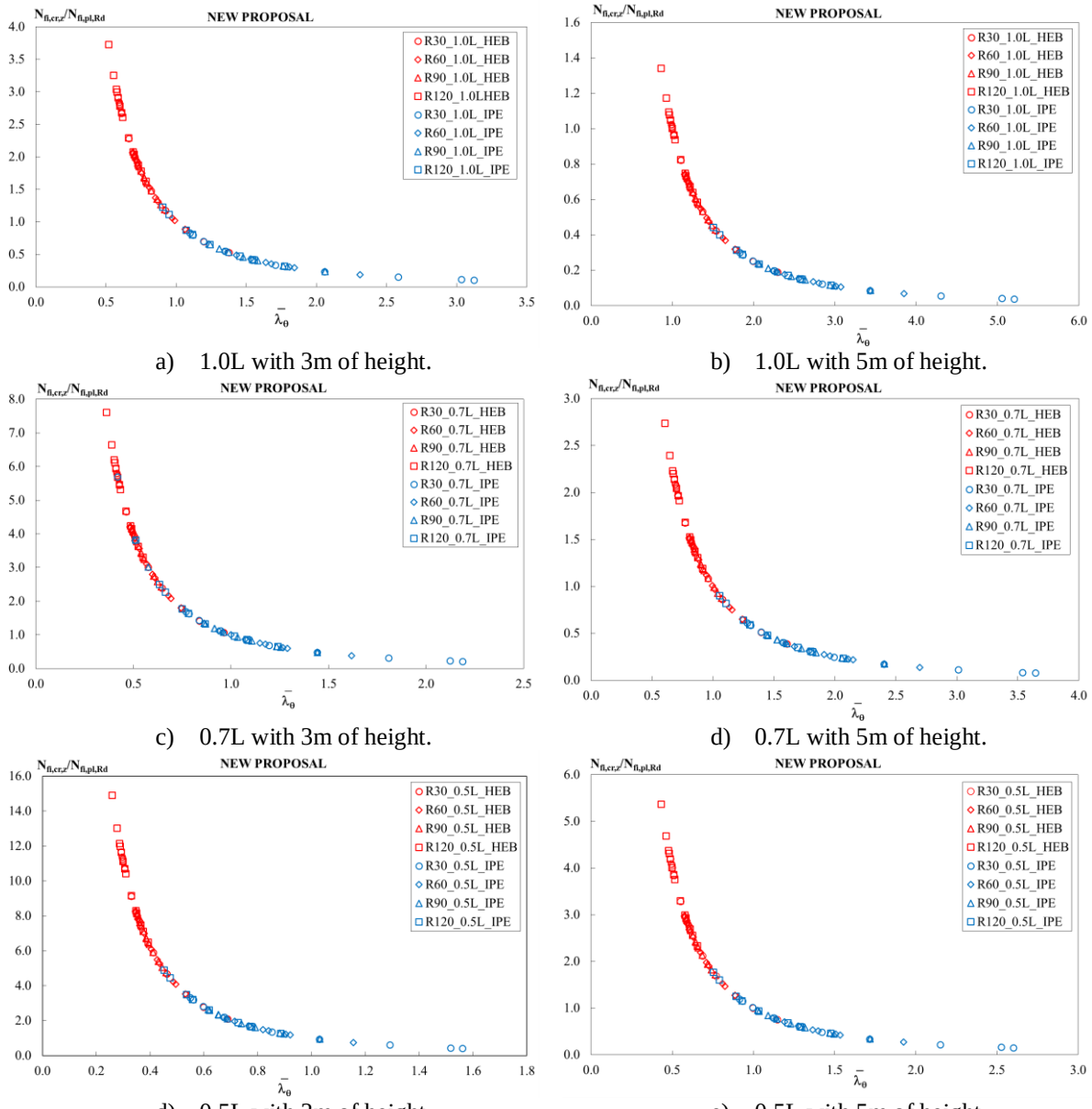

a) 1.0L with 3m of height.

b) 1.0L with 5m of height.

c) 0.7L with 3m of height.

d) 0.7L with 5m of height.

d) 0.5L with 3m of height.

e) 0.5L with 5m of height.

Figure 47 – Ratio between critical and plastic resistance for 3m and 5m of height.

The ratio between the critical load and the axial plastic resistance varies on the non-dimensional slenderness ratio and fits well with the new proposal used for the balanced summation model.

Figure 48 presents the comparison between the ratio of the critical load and plastic load obtained from analytical solutions and the results obtained from the numerical solutions for all the cross sections, for three boundary conditions and four rating times with 3m and 5m of length. The oblique line represents the perfect solution comparison between the simplified method and the numerical method. Two other limiting lines are defined by -10% and + 10%. The biggest difference of this ratio allowed is 10% represented above and below the oblique line. If the results achieved are below the oblique line for - 10% are considered unsafe because the analytical results is higher than the numerical solutions

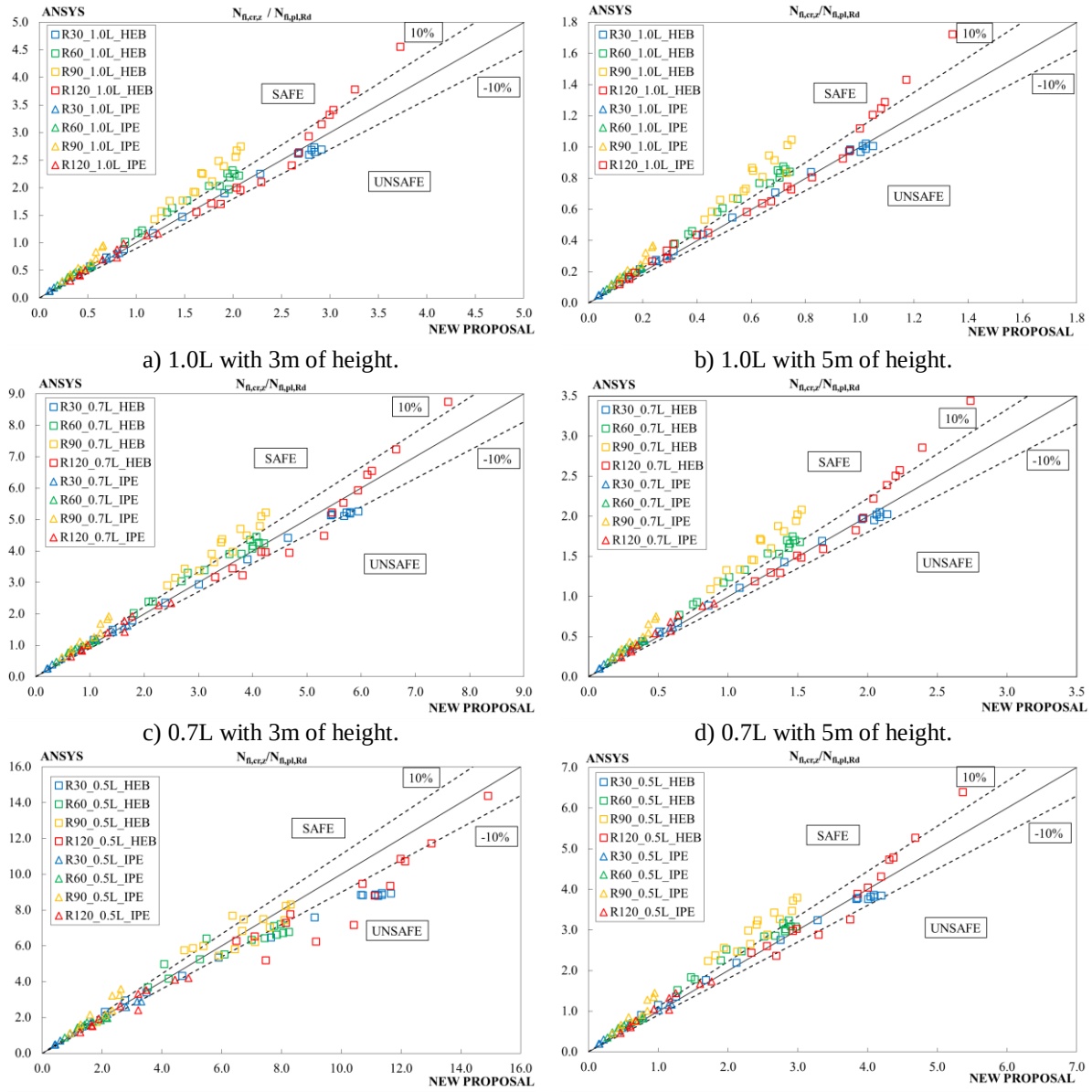

a) 1.0L with 3m of height.

b) 1.0L with 5m of height.

c) 0.7L with 3m of height.

d) 0.7L with 5m of height.

e) 0.5L with 3m of height.

f) 0.5L with 5m of height.

Figure 48 – Critical load (comparison between ansys and new proposal).

The numerical solution method is based on the elastic buckling analysis considering the full resistance of the four components, taking into account the update of the material properties and the full geometry of column. This fact justifies that the numerical results coming from ANSYS are always higher than the results coming from the new proposal.

Figure 49 present the comparison between the formulations prescribed on CEN - EN 1993-1-1[18] for the buckling curve and the results obtained from nonlinear analysis (ANSYS). The results are presented for 30, 60, 90, and 120 minutes of fire exposure and for the buckling length $L_\theta = 0.5l$.

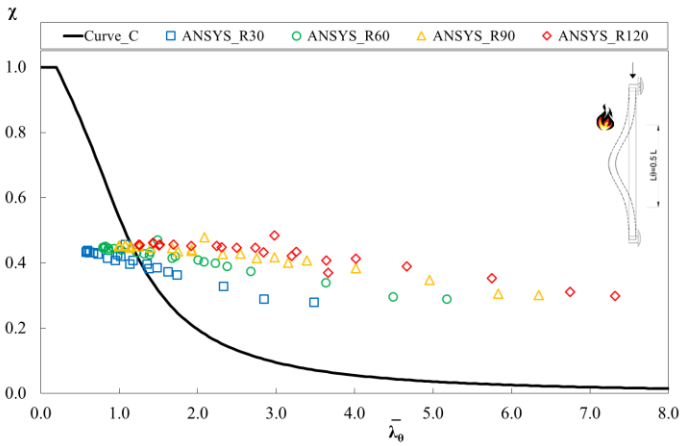

Figure 49 – Comparison of the buckling curve (ANSYS and Eurocode).

The results do not agree with the proposed curve of the Eurocode (curve c). More simulation are required to evaluate the buckling resistance and also to validate the numerical model.

The values of the non-dimensional slenderness are bigger than expected. This is due to the calculation of the plastic resistance.

The buckling resistance is decreasing with the non-dimensional slenderness, but far away from the design curve proposed by the Eurocode.

These results need more attention and reflexion for the future investigation.

This page was intentionally left in blank

CHAPTER.7 CONCLUSIONS

The fire resistance of partially encased columns depends on the temperature evolution during fire exposure, two different solution methods were applied to define the buckling resistance of partially encased columns in case of fire.

The New Proposal is based on the balanced summation method, for this reason, only some part of this resistance is taking into consideration comparing with the numerical method witch all the materials contribute for the global resistance of the column.

The advanced calculation method to achieve the results was based in four steps, the first one was the transient calculation of the temperature field of the cross-section in the column. The second step was the static calculation of elastic buckling analysis, taking into consideration the thermal analysis. The third step was the calculation of the plastic resistance of the column and the last one was the calculation of the buckling resistance, also taking into consideration the temperature field of the previous analysis.

The results of the thermal analysis shows agreement with the temperatures prescribed on the Eurocode 4 part 1.2, [1], and the New Proposal.

As expected, partially encased columns based on HEB profile present higher critical load when compared with IPE profile. The critical load decreases with the relative slenderness in the fire situation.

The results of the static calculations of elastic analysis also was in agreement with the values prescribed on Eurocode 4 part 1.2, [1], and the New Proposal, concluding that the new proposal is safe.

The results of the plastic analysis seems to give higher values than expected.

The results of the buckling resistance do not agree with the prescribed curve of Eurocode.

This page was intentionally left in blank

REFERENCES

[1] CEN - EN 1994-1-2; "Eurocode 4 - Design of composite steel and concrete structures- Part 1-2: General rules - Structural fire design"; Brussels, August 2005.

[2] J. A. Purkiss, Fire Safety Engineering: Design of Structures. Butterworth-Heinemann, second ed. 1996.

[3] Ministère de l'intérieur et des collectivités locales : « reglement de securite Contre les risques d'incendie et de panique dans les etablissement » Algérie, 1985.

[4] Malhotra H.L. and Stevens "Fire resistance of encased steel stanchions". Proceedings of the Institution of Civil Engineers - ICE; 27: 77-97, 1964.

[5] Schleich , JB. Computer Assisted analysis of the fire resistance of steel and composite concrete-steel structure, Luxembourg. Final Report EUR 10828, 1987

[6] Lie TT, Chabot M. ''A method to predict the fire resistance of circular steel columns filled hollow steel columns''. Journal of Fire Protection Engineering; 2(4):111–26, 1990.

[7] Stefan Winter and Jörg Lange, Behaviour of partially encased composite columns using high-strength steel – ultimate load and fire condition, Leipzig University, Steel and timber structures.2000.

[8] A.A. Marinopoulou, V.D. Balopoulos, C.N. Kalfas Simulation of partially encased composite steel–concrete columns with steel columns, Journal of Constructional Steel Research 63 (2006) 1058–1065.

[9] Ehab Ellobody, Ben Young. Investigation of concrete encased steel composite column at elevated tempeatures. Thin-Ealled Structures 2010; 48 (2010) 597-8: 597-608.

[10] Paulo A.G. Piloto, Ana B. R. Gavilan, Marco Zipponi, Alberto Marini, Luís M. R. Mesquita, Giovanni Plizzari; "Experimental Investigation of the Fire Resistance of Partially Encased Beams" journal of Constructional Steel Research Jan2013.

[11] Sadaoui Arezki, Illouli Said. Practical fire design of partially encased composite steel-concrete columns according to Eurocode 4. International Congress on Materials & Structural Stability, 2014. MATEC Web of Conferences 11, 01029: 1-8.

[12] A. Piquer , D. Hernández-Figueirido. Protected steel columns vs partially encased columns: Fire resistance and economic considerations. Journal of Constructional Steel Research 124 (2016) 47–56.

[13] ISO 834-1. "Fire-resistance tests - Elements of building construction – Part 1: general requirements". 1999.

[14] CEN - EN 1993-1-2; "Eurocode 3: Design of steel structures - Part 1-2: General rules - Structural fire design", European standards; Brussels, April 2005.

[15] CEN - EN 1991-1-2; "Eurocode 1: Actions on structures - Part 1-2: General actions on structures exposed to fire", European standards; Brussels, 2009.

[16] "Designing fire safety for steel – recent work", Proceedings of the ASCE Spring Convention, American Society of Civil Engineers, New York, 11-15 May, 16pp.

[17] T. Gernay, J.-M. Franssen, A performance indicator for structures under natural fire, Engineering Structures, Volume 100, 2015, Pages 94-103, ISSN 0141-0296

[18] CEN - EN 1992-1-2; "Eurocode 2: Design of concrete structures - Part 1-2: General rules structural fire design." European standards; Brussels, 2004.

[19] CEN - EN 1993-1-1; "Eurocode 3: Design of steel structures - Part 1-1: General rules - Rules for buildings." European standards; Brussels, 2005.

[20] CEN - EN 1992-1-1; "Eurocode 2: Design of concrete structures - Part 1-1: General rules and rules for buildings." European standards; Brussels, 2004.

[21] EN 1363-1 ‘’Fire resistance tests-Part 1: General Requirements” Europen standards; Brussels, 2012.

[22] O. Jungbluth, Optimierte Verbandbauteile, Stahlbau Handbuch 1, Stahlbeau-Verglas-Gmbh, Köeln, 1982.

[23] Paulo Piloto, David Almeida, A. B Ramos-Gavilán, Luís M. R. Mesquita; “Partially Encased Section: Strength and Stiffness Under Fire Conditions”; pp: 15-18, Book of Abstracts of the IFireSS – International Fire Safety Symposium, ISBN 978-989-98435-3-0, pp: 29-38, Book of full papers ISBN 978-989-98435-5-4, ISSN 2412-2629, University of Coimbra, Portugal, 20th-22nd April 2015.

[24] Cajot Louis-Guy, Gallois Louis, Debruyckere Rik, Franssen Jean-Marc, Simplified design method for slim floor beams exposed to fire, Proceedings of the Nordic Steel Construction Conference, Oslo, Norway, 5-7 September, 2012.

[25] ANSYS® Academic Research, Release 16.2, Help System, Element reference, ANSYS, Inc.

This page was intentionally left in blank

ANNEX

ANNEX

COLUMN UNDER FIRE

1-THERMAL ANALYSIS FOR 3M OF HEIGHT (ANSYS) HEB AND IPE.

- **Profil HEB 160**

R30

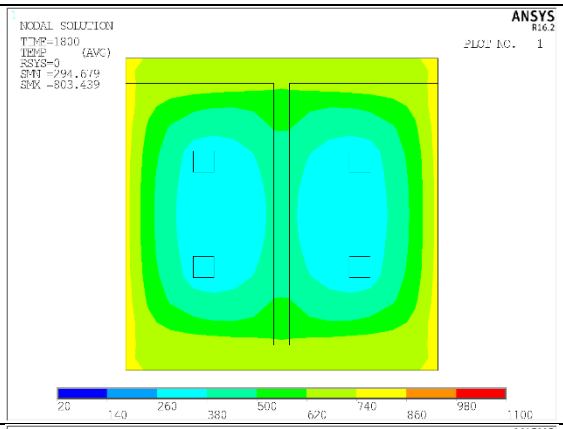

R60

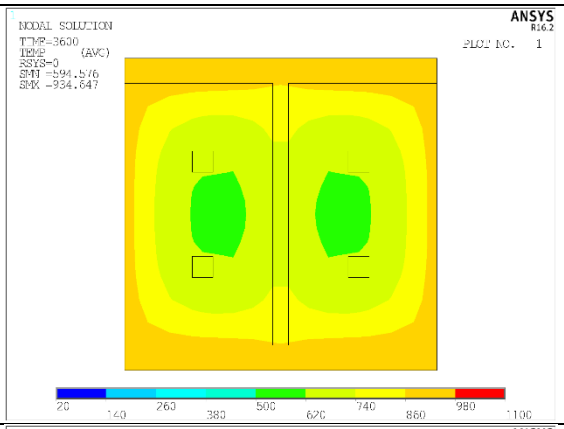

R90

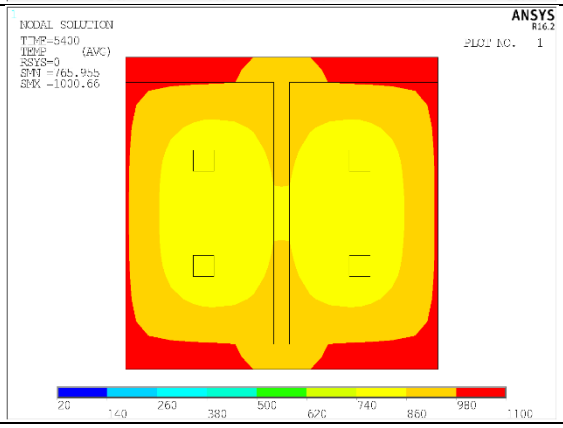

R120

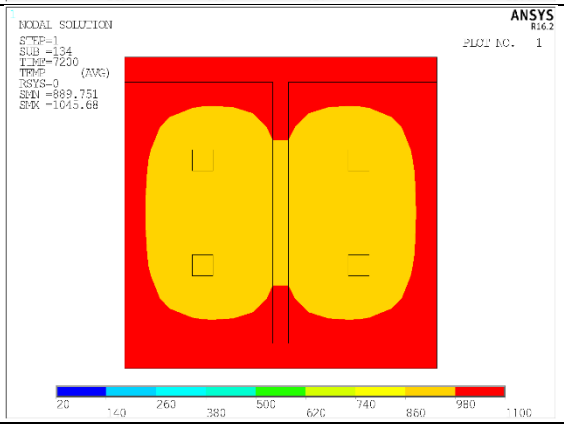

- **Profil HEB 180**

R30

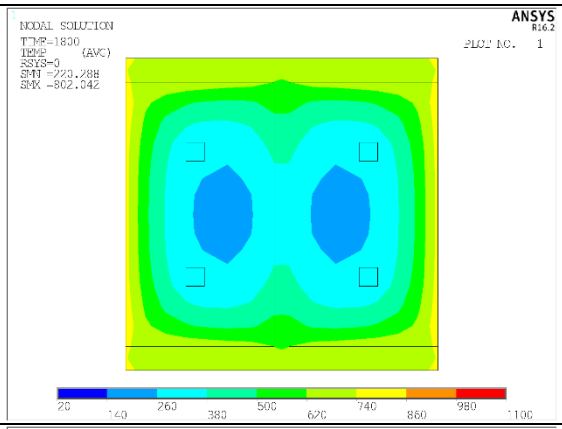

R60

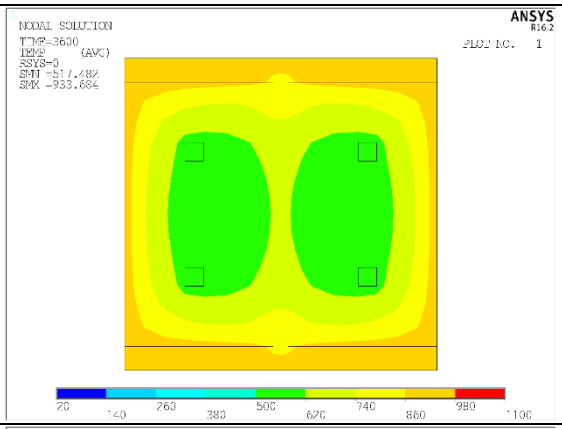

R90

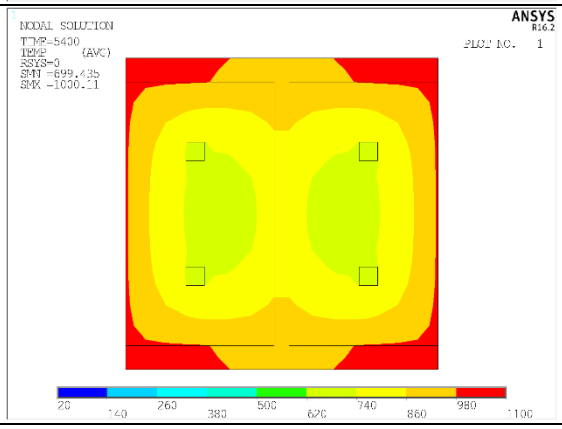

R120

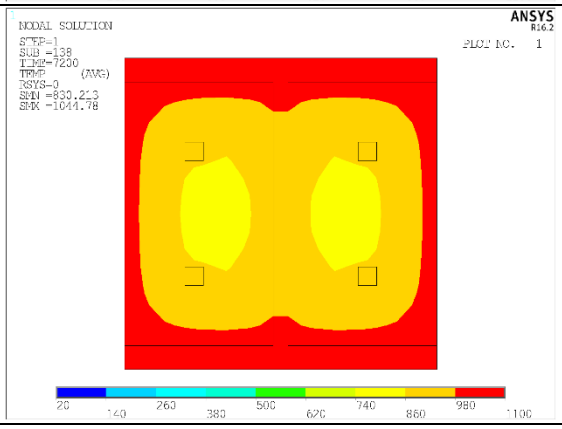

- **Profil HEB 200**

R30

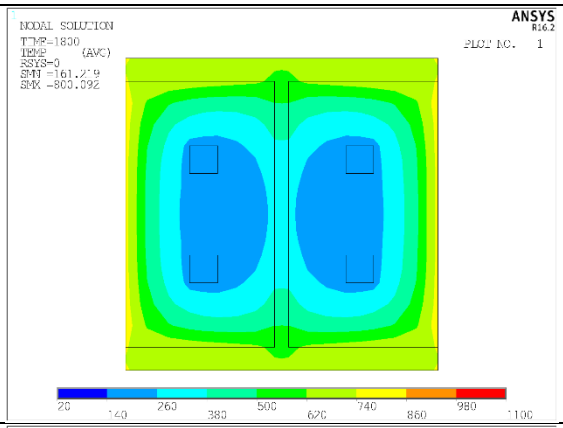

R60

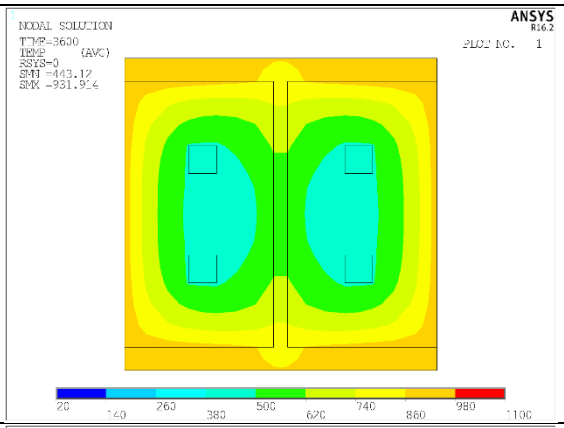

R90

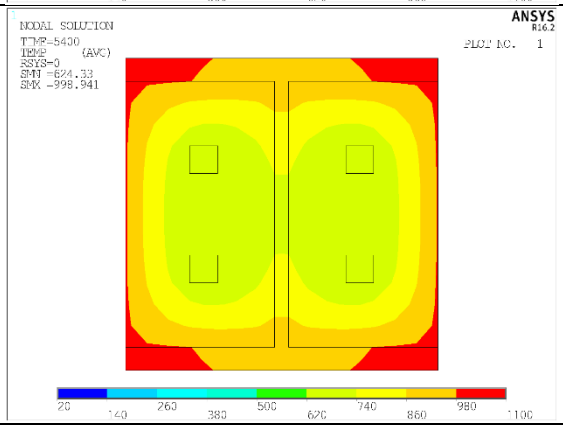

R120

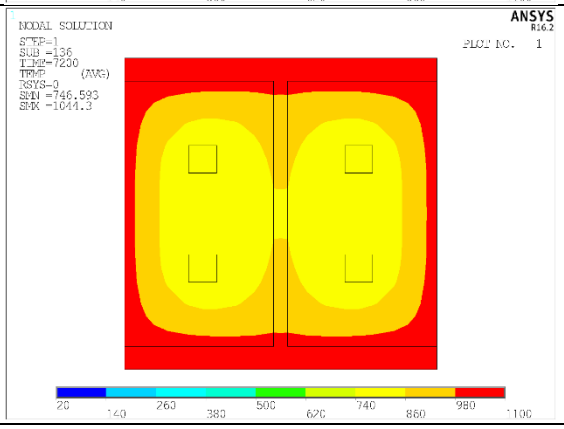

- **Profil HEB 220**

R30

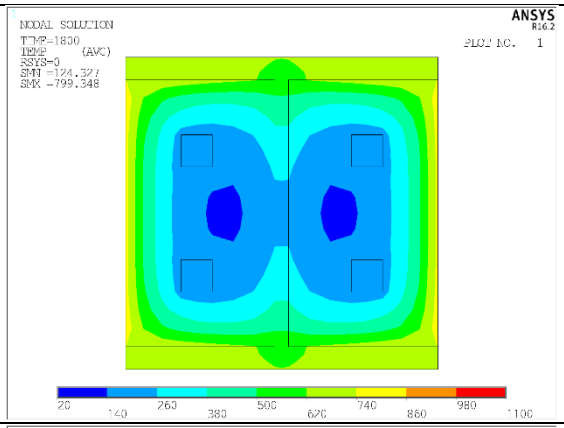

R60

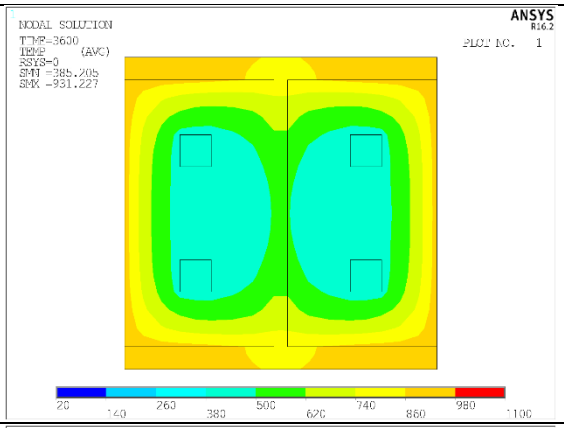

R90

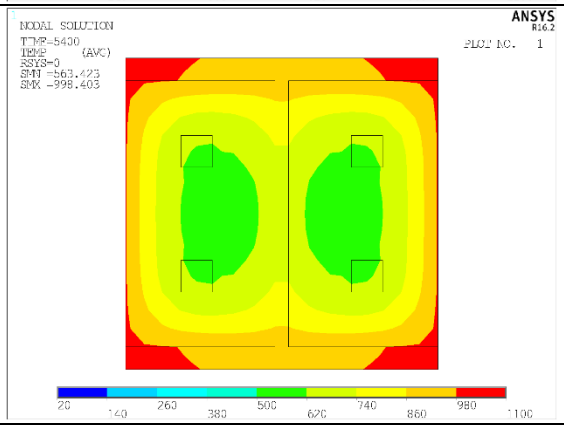

R120

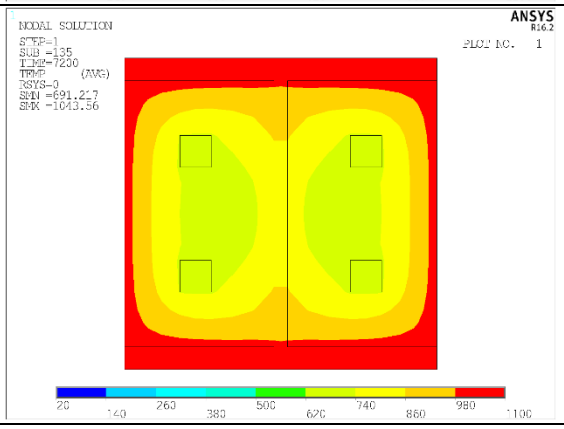

- **Profil HEB 240**

R30

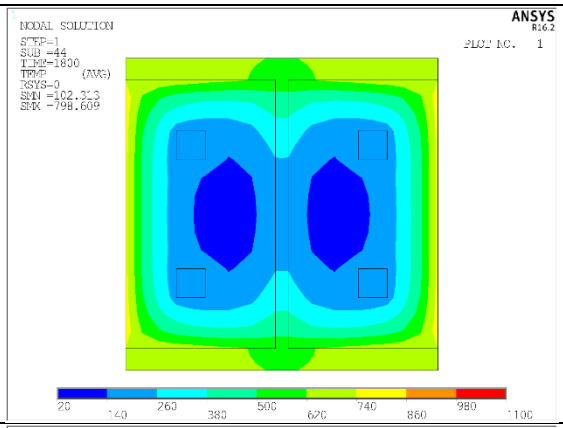

R60

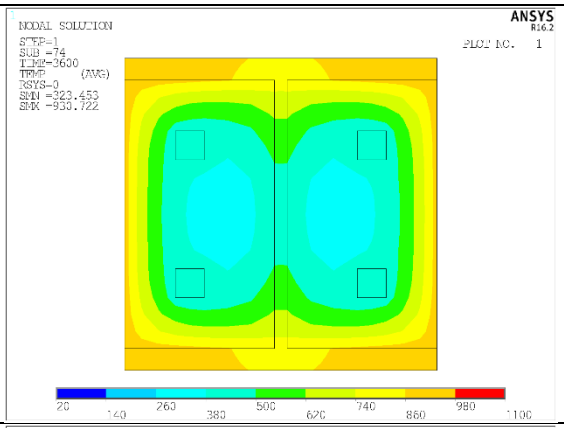

R90

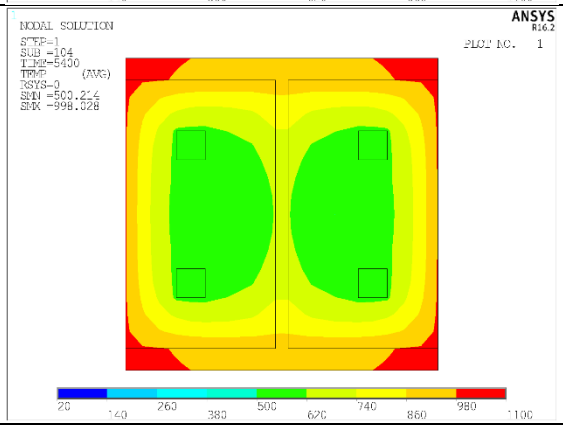

R120

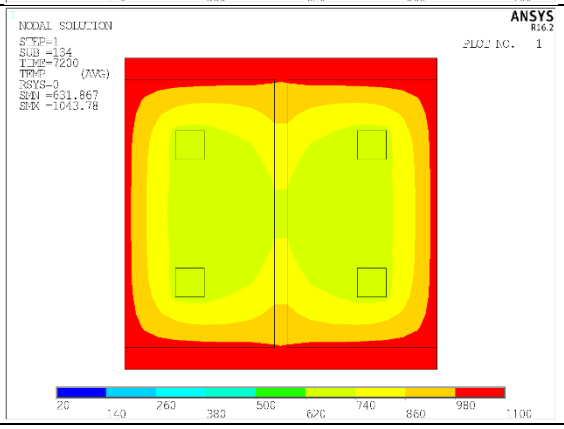

- **Profil HEB 260**

R30

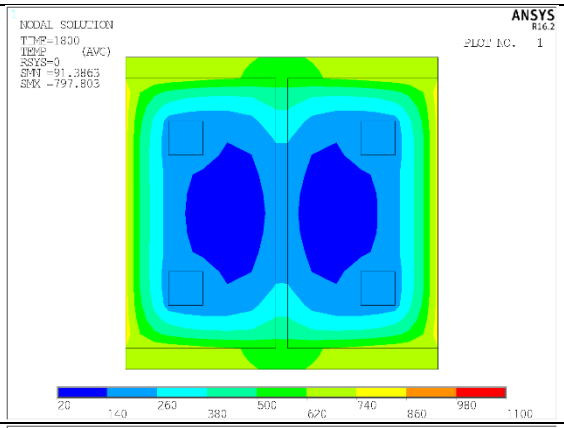

R60

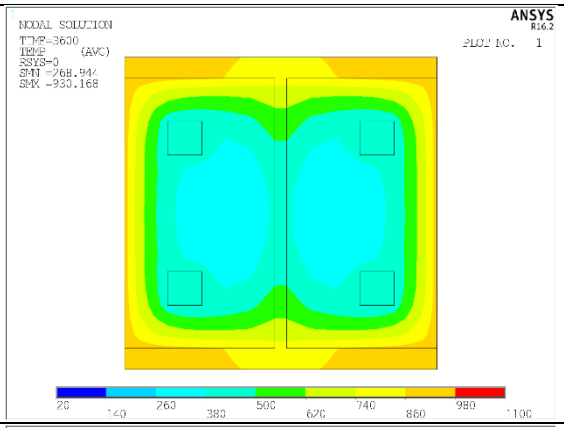

R90

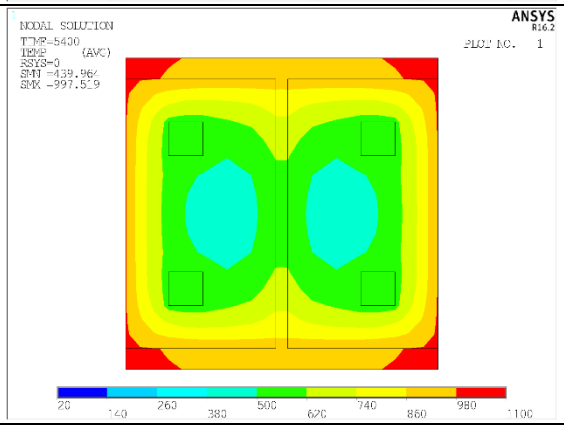

R120

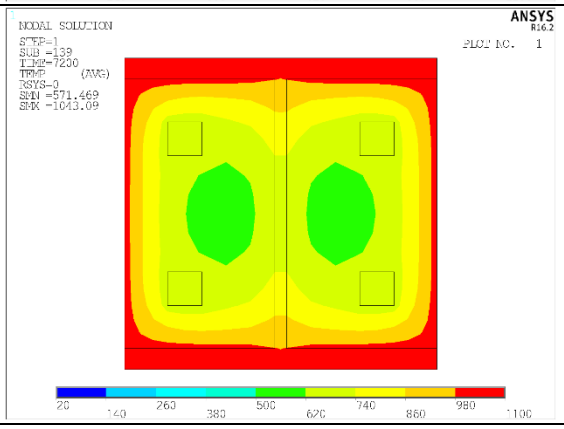

- **Profil HEB 280**

R30

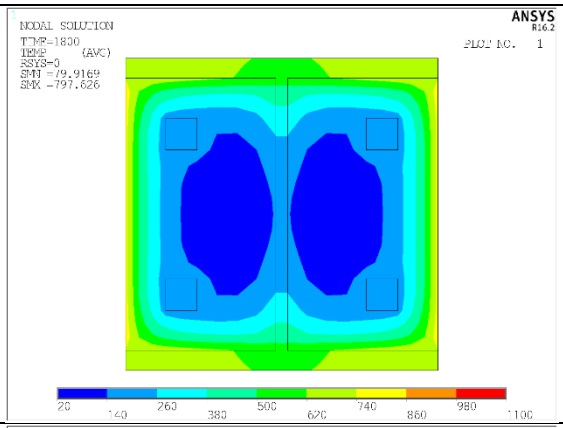

R60

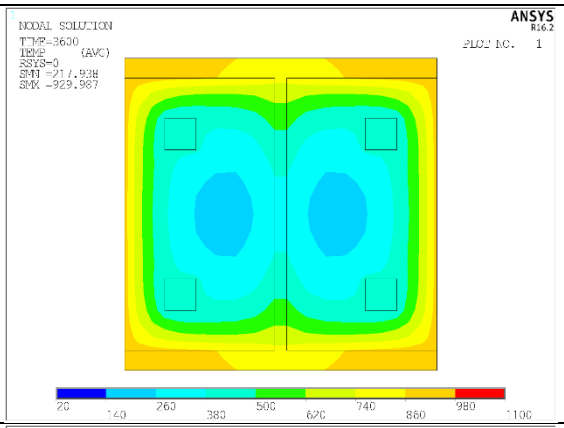

R90

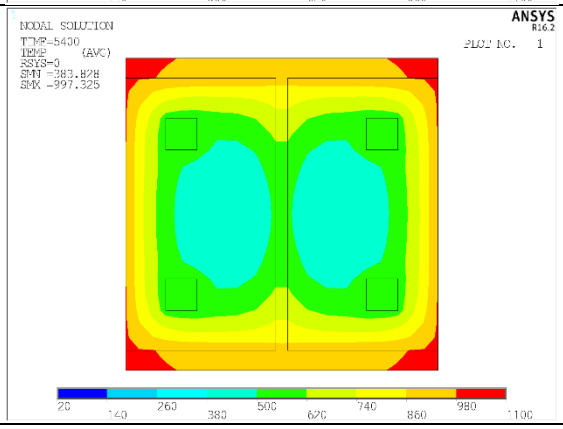

R120

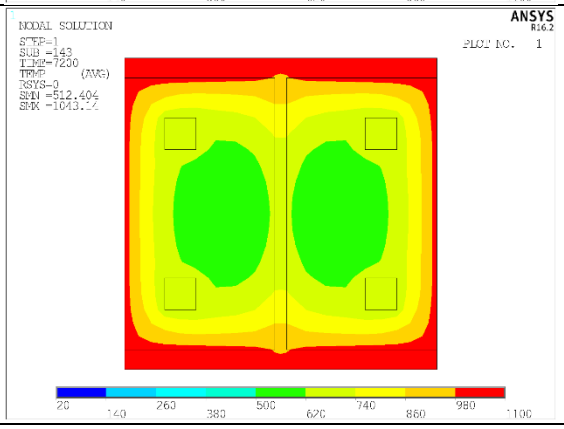

- **Profil HEB 300**

R30

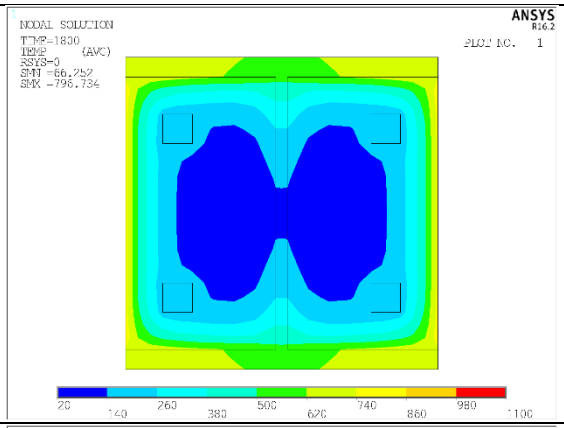

R60

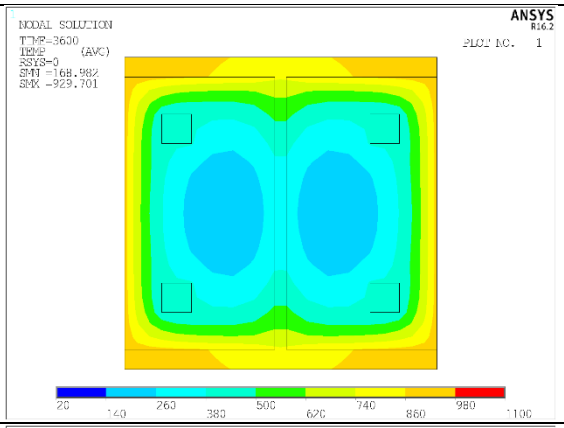

R90

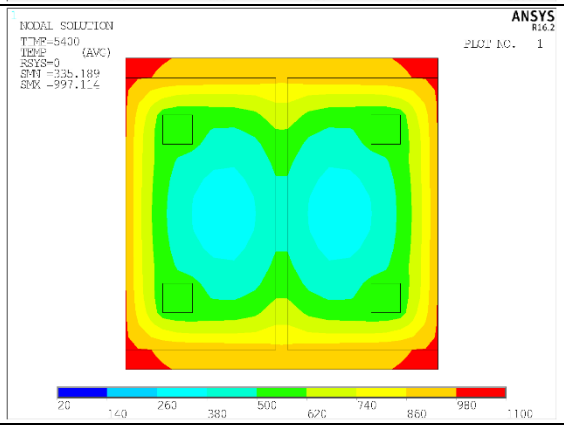

R120

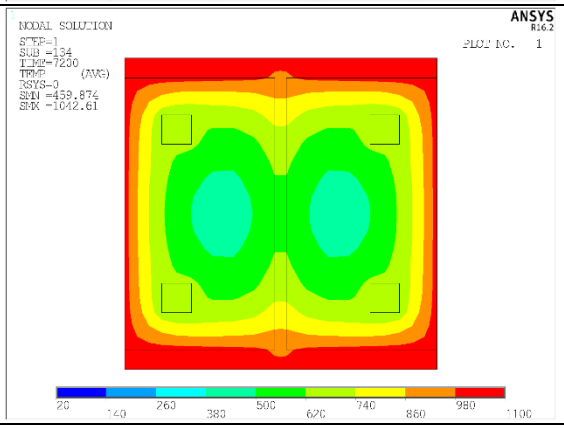

- **Profil HEB 320**

R30

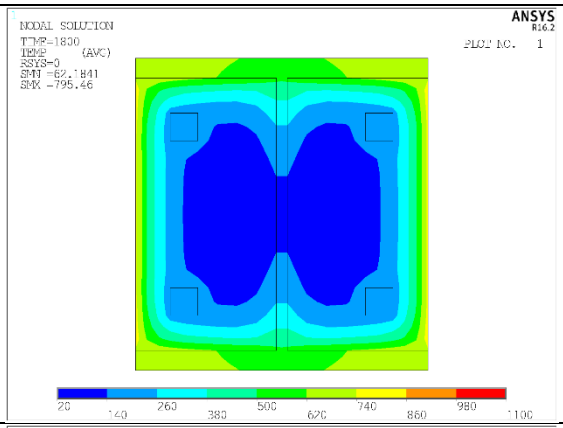

R60

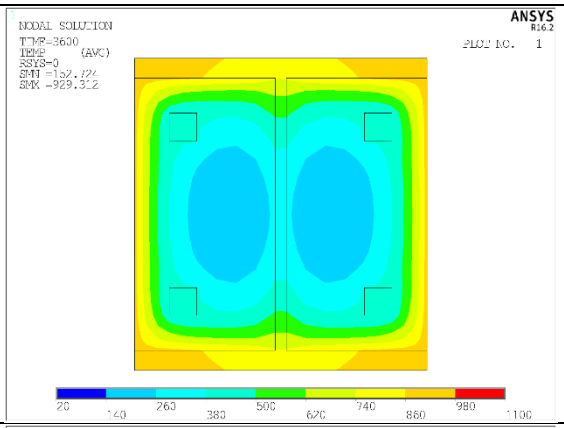

R90

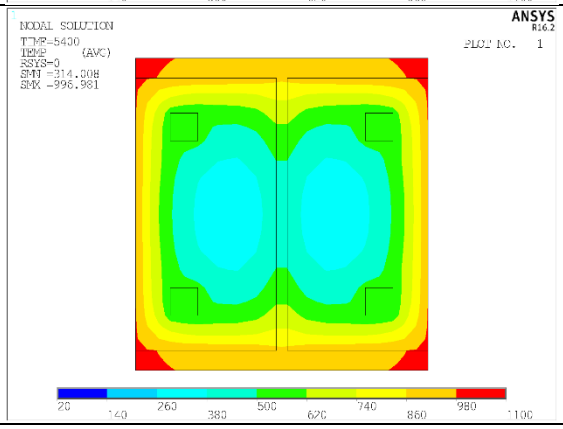

R120

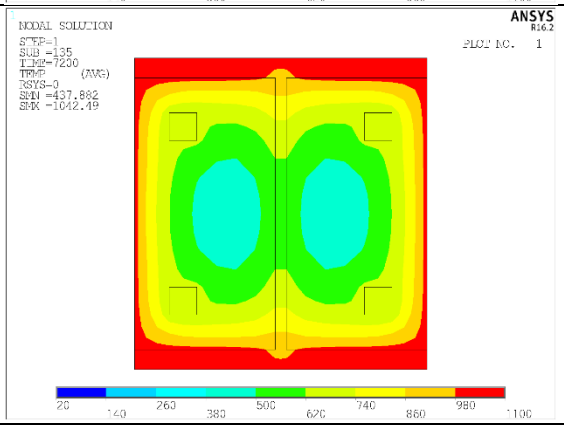

- **Profil HEB 340**

R30

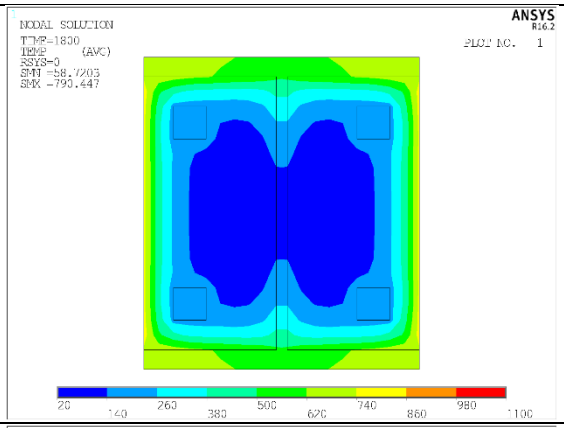

R60

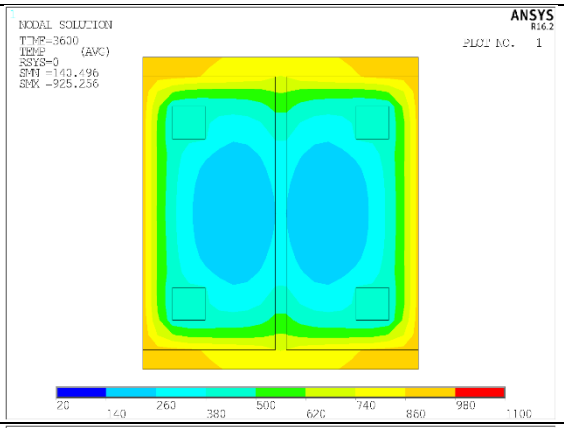

R90

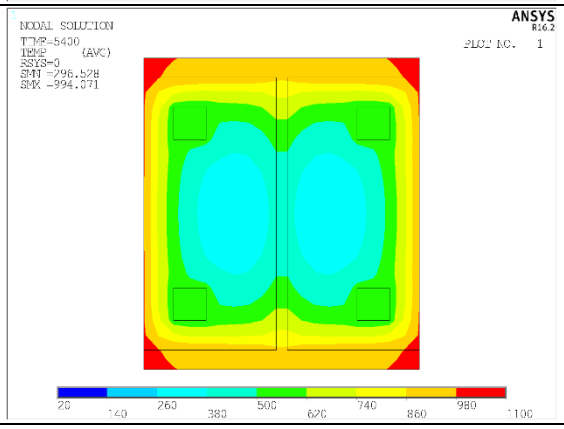

R120

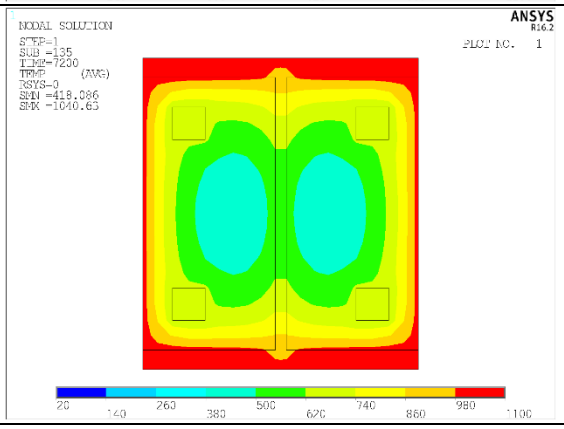

- **Profil HEB 360**

R30

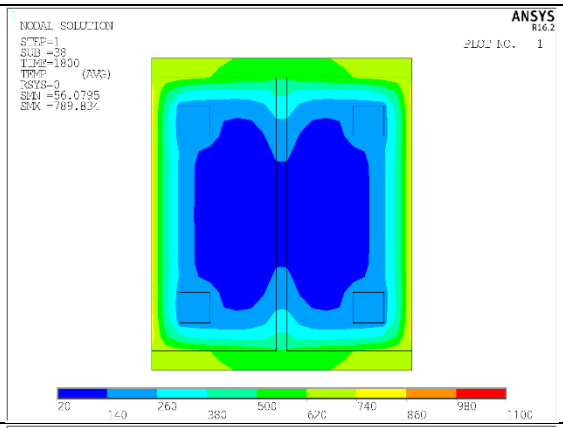

R60

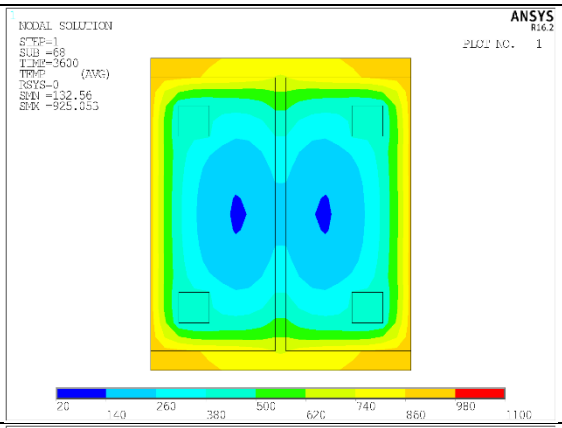

R90

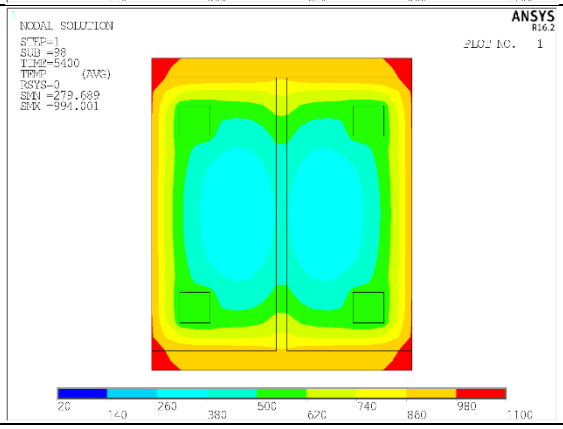

R120

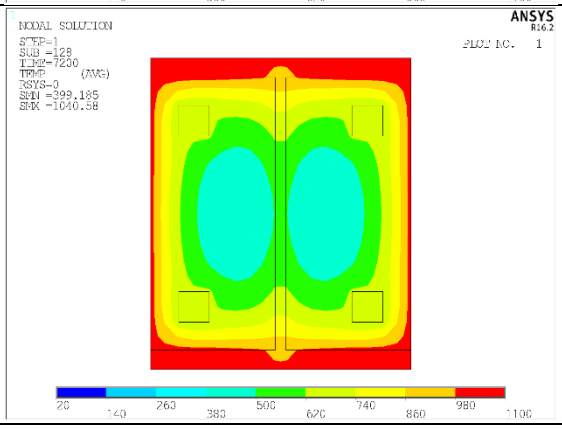

- **Profil HEB 400**

R30

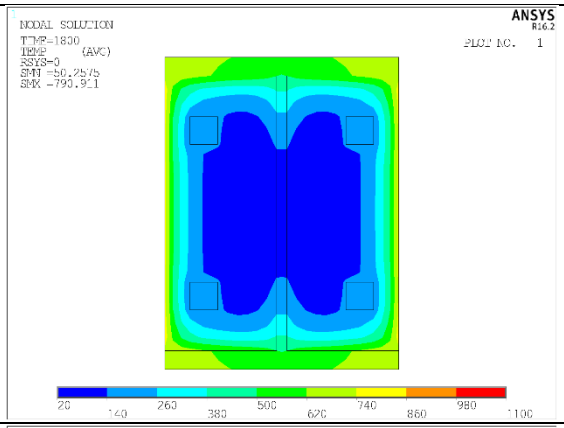

R60

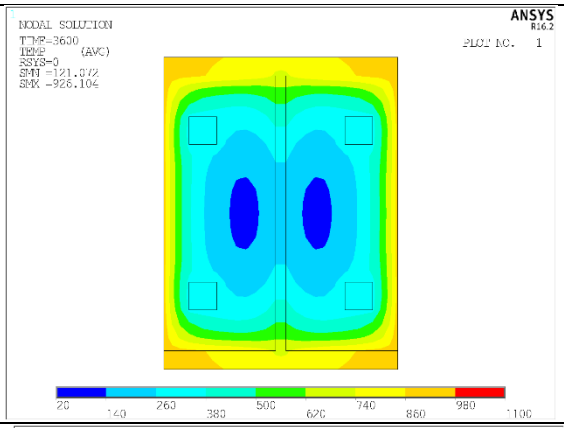

R90

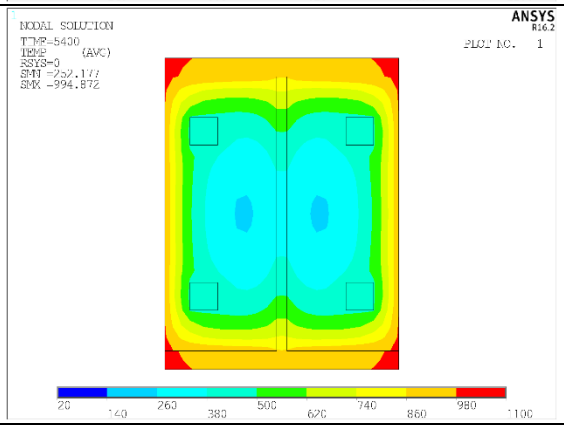

R120

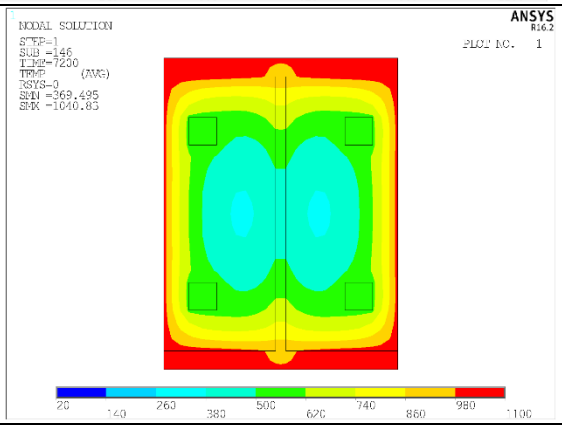

- **Profil HEB 450**

R30

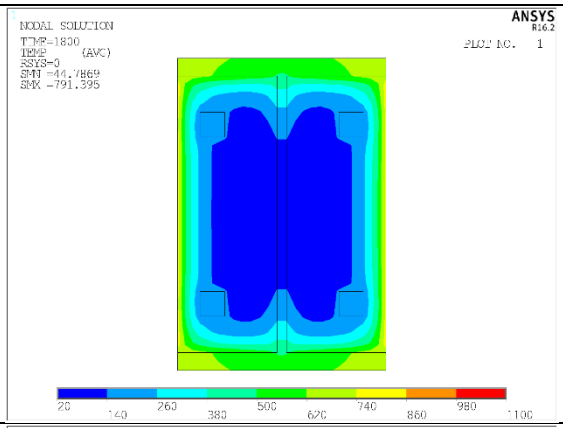

R60

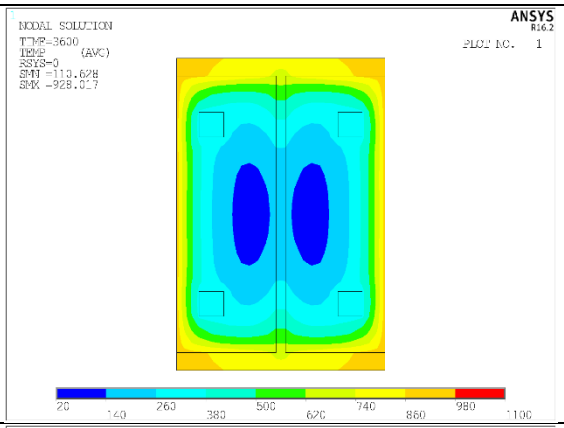

R90

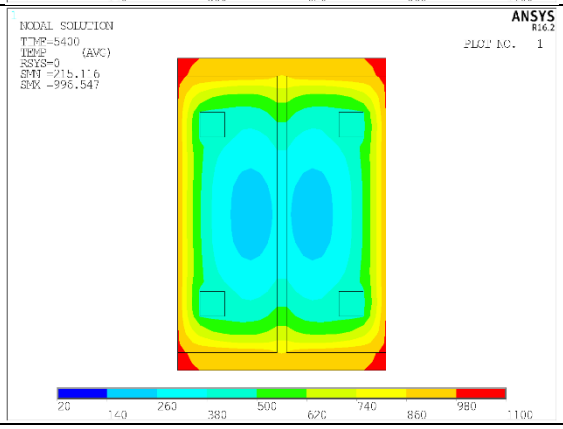

R120

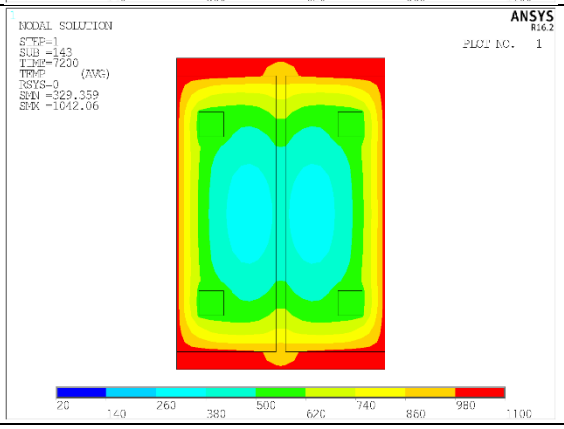

- **Profil HEB 500**

R30

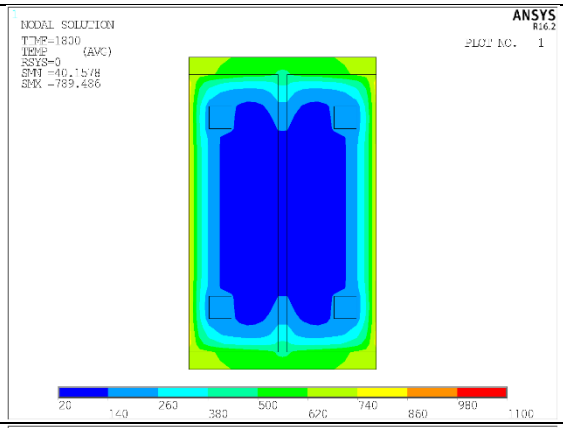

R60

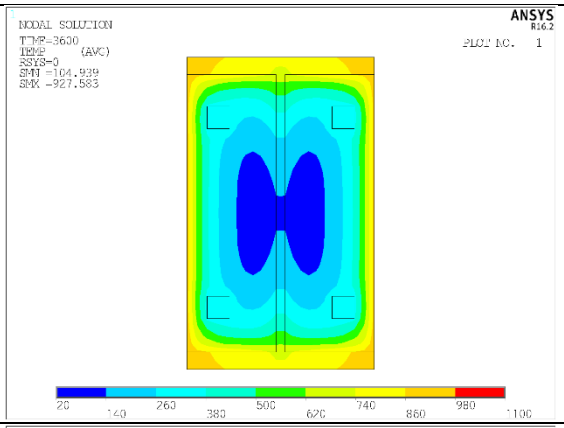

R90

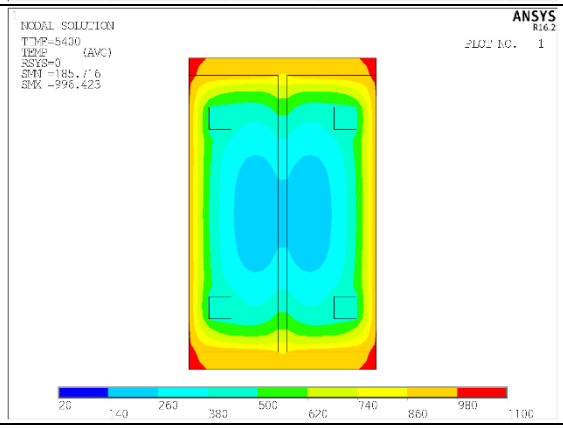

R120

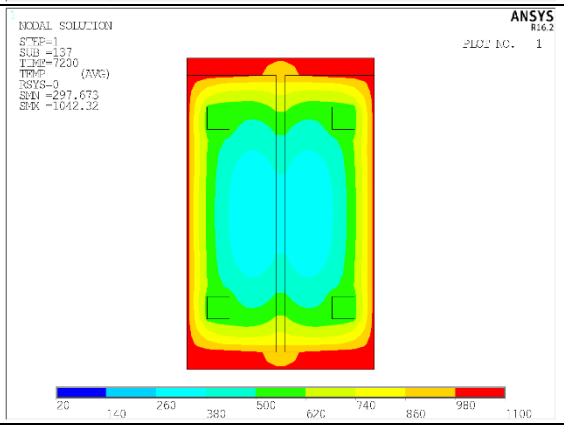

- **Profil IPE 200**

R30

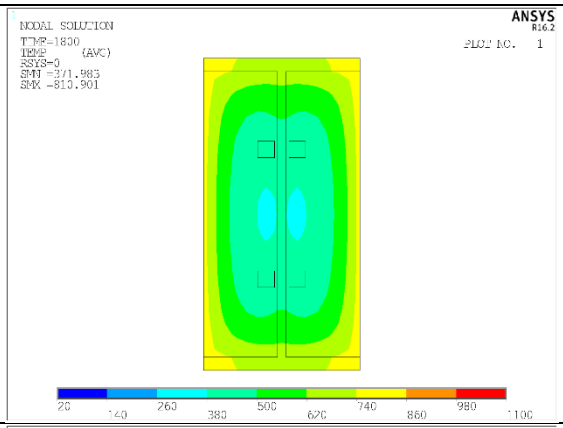

R60

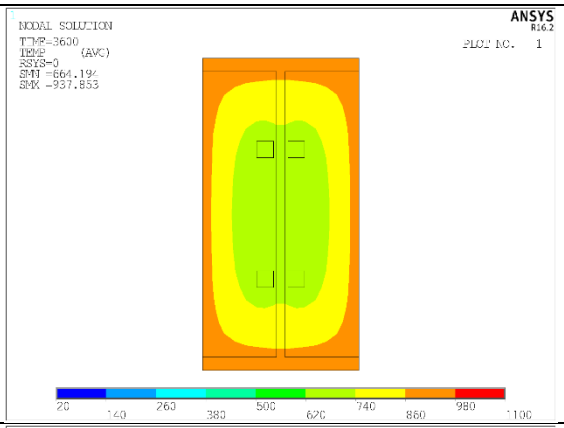

R90

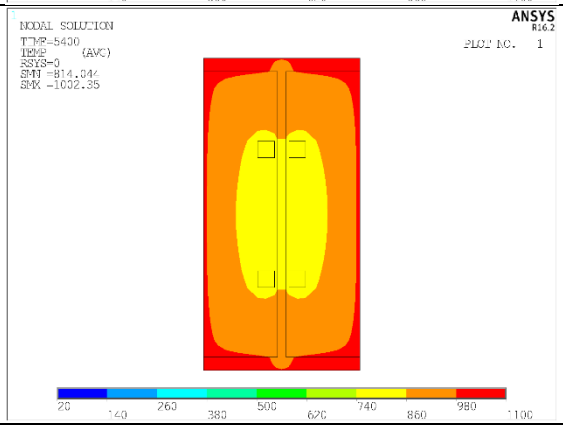

R120

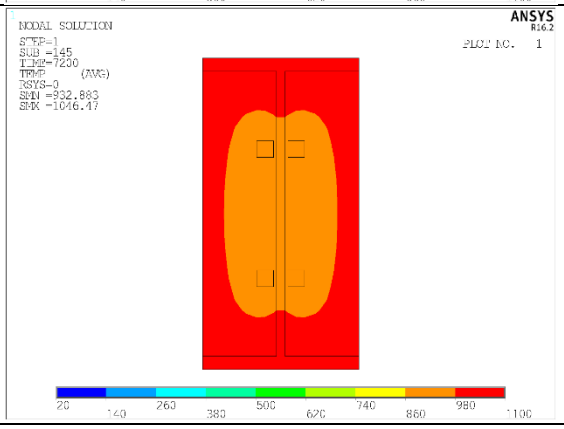

- **Profil IPE 220**

R30

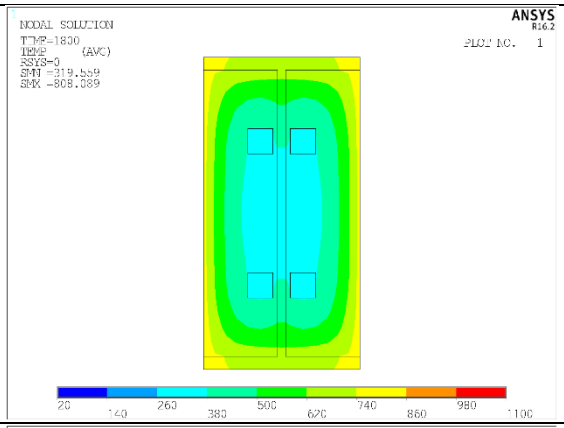

R60

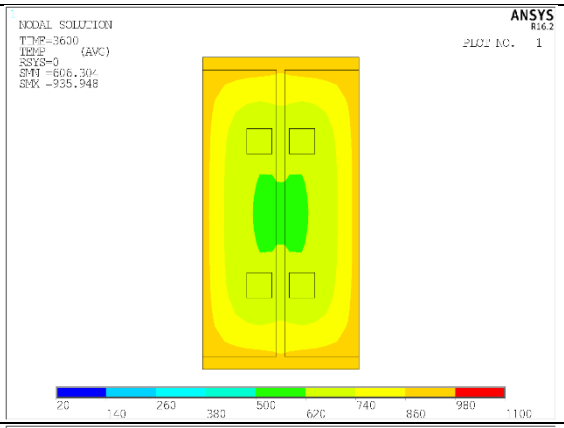

R90

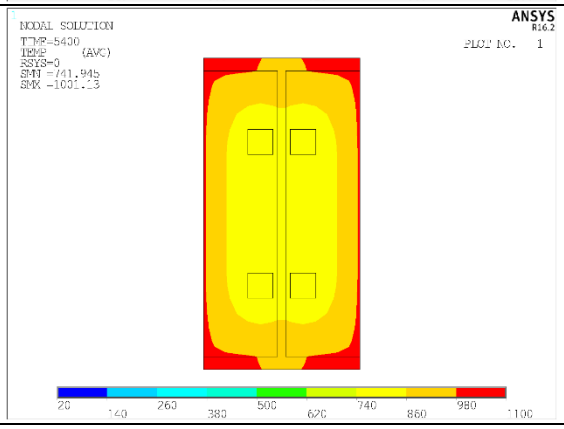

R120

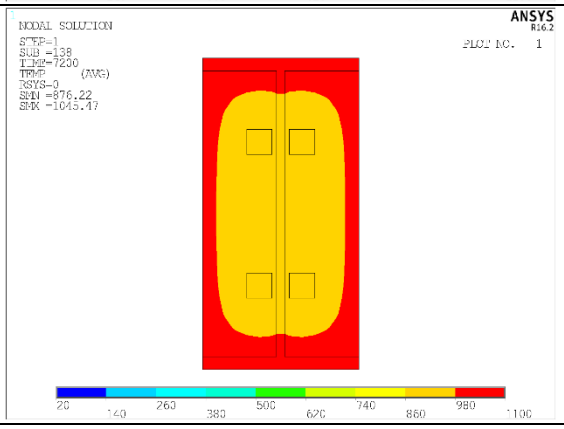

- **Profil IPE 240**

R30

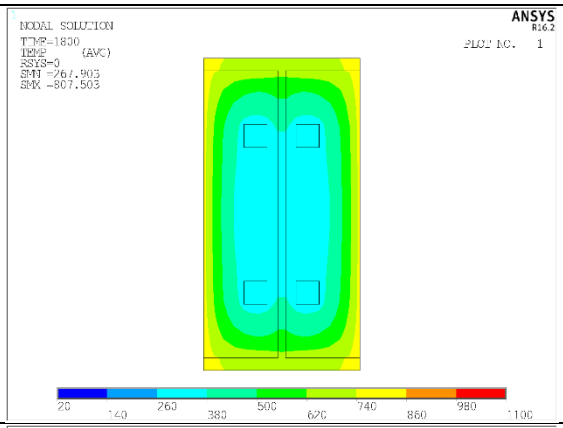

R60

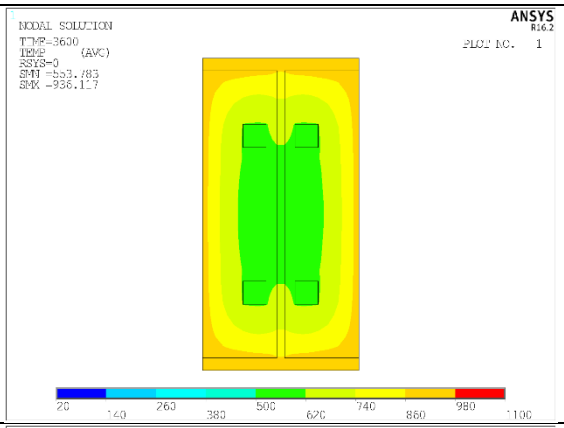

R90

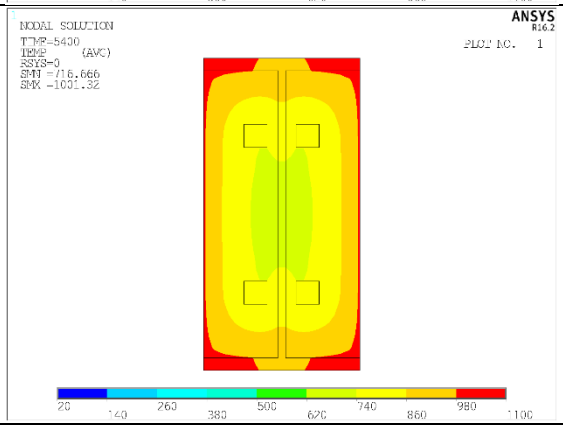

R120

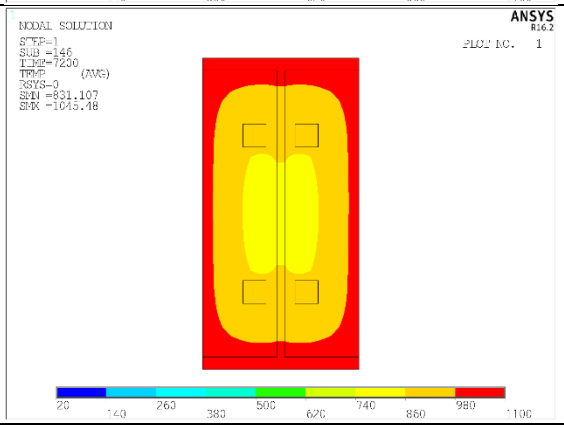

- **Profil IPE 270**

R30

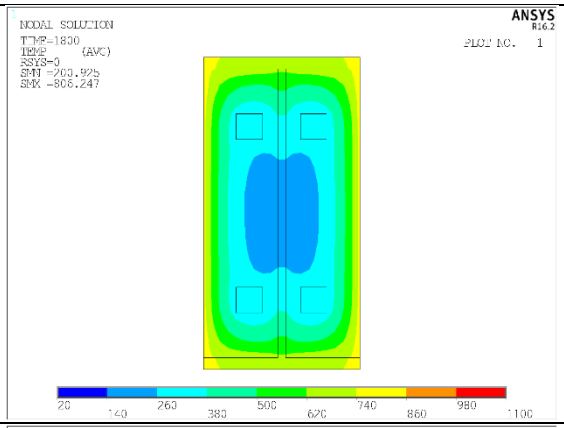

R60

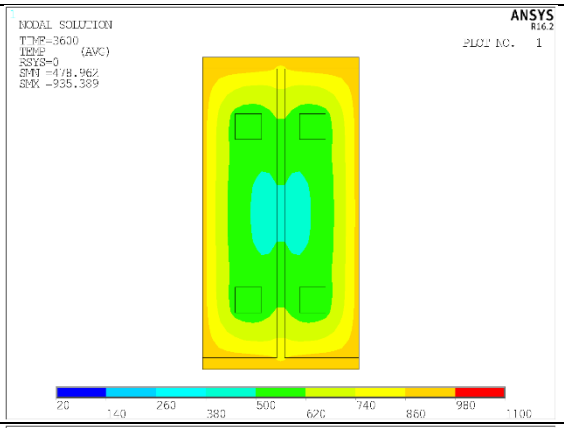

R90

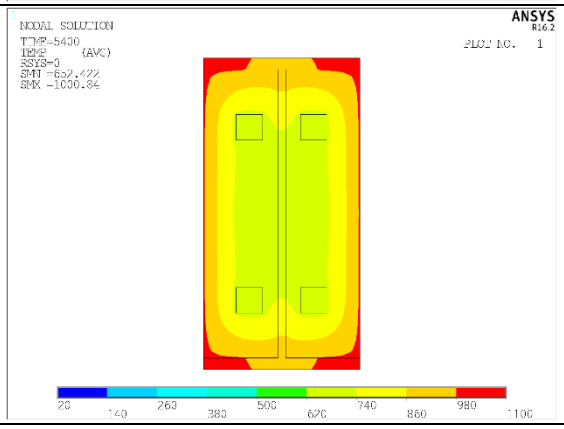

R120

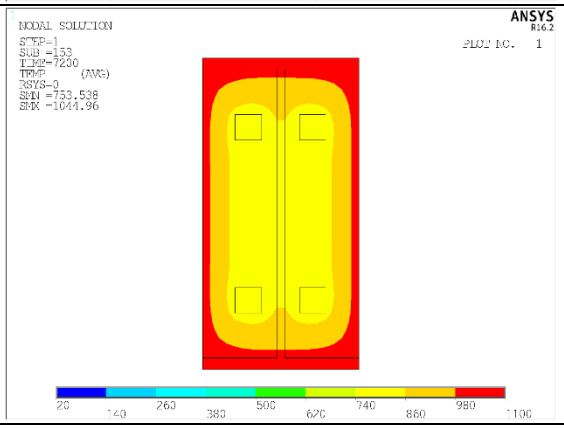

- **Profil IPE 300**

R30

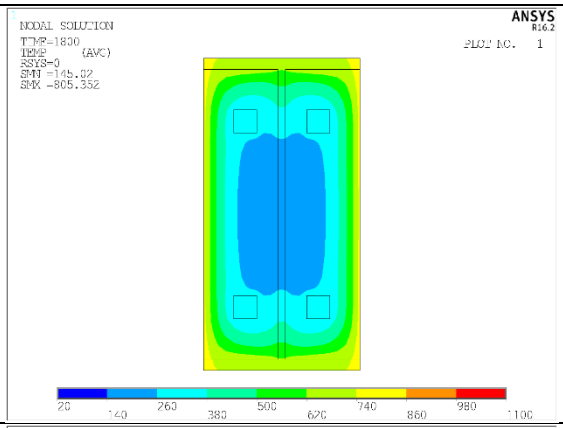

R60

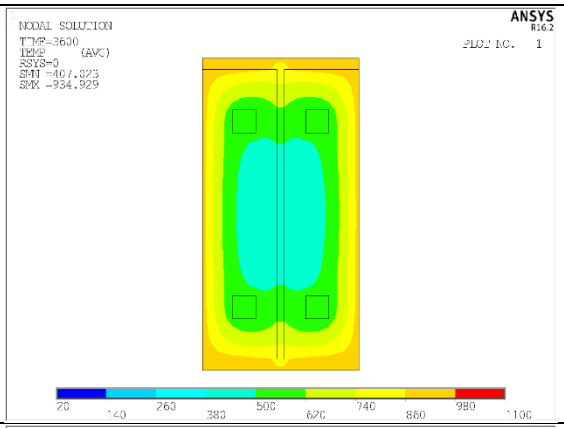

R90

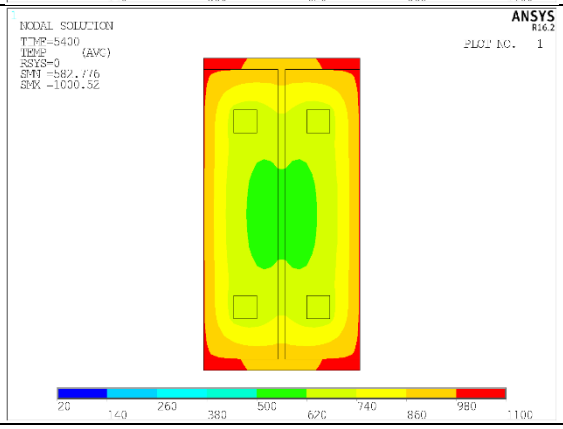

R120

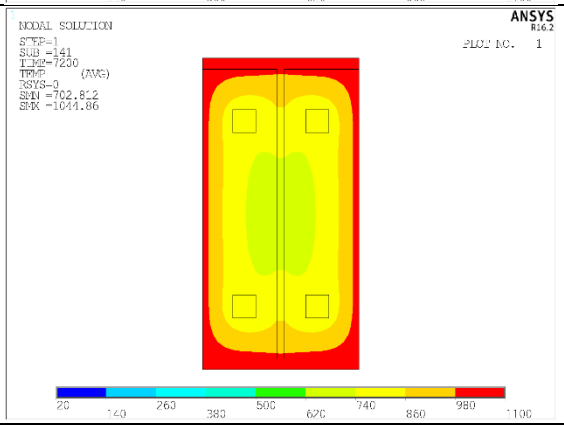

- **Profil IPE 330**

R30

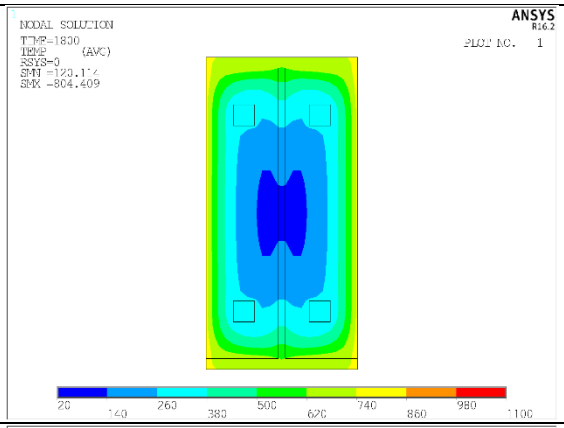

R60

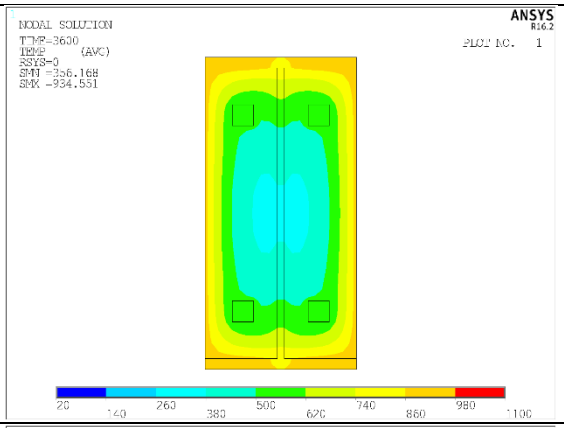

R90

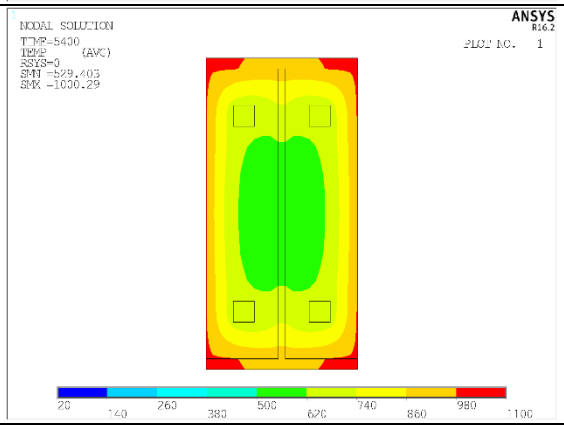

R120

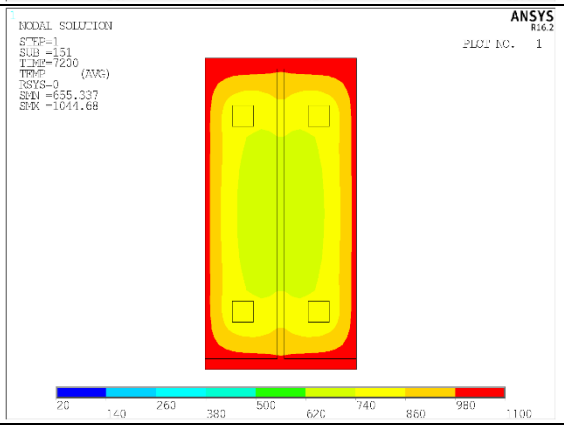

- **Profil IPE 360**

R30

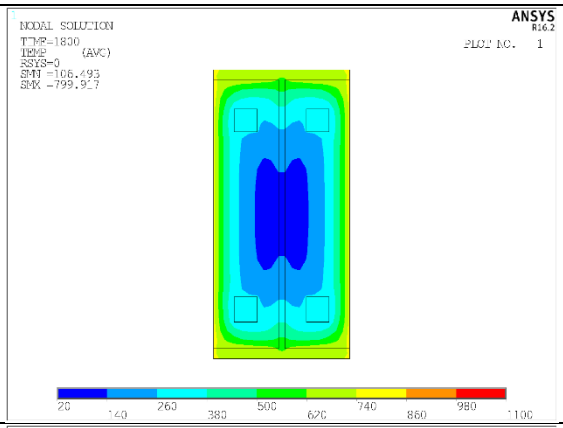

R60

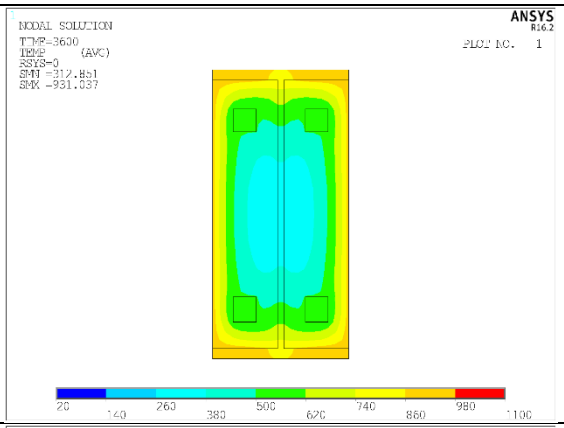

R90

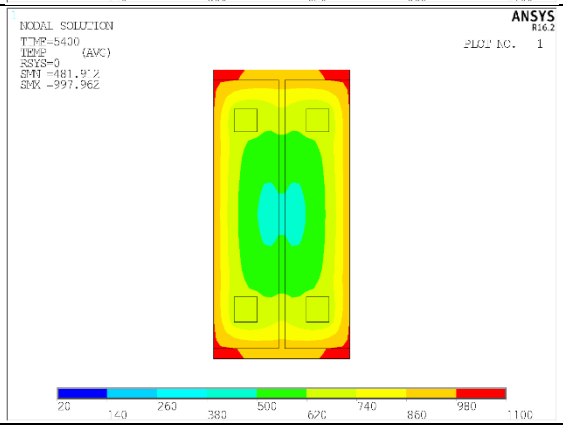

R120

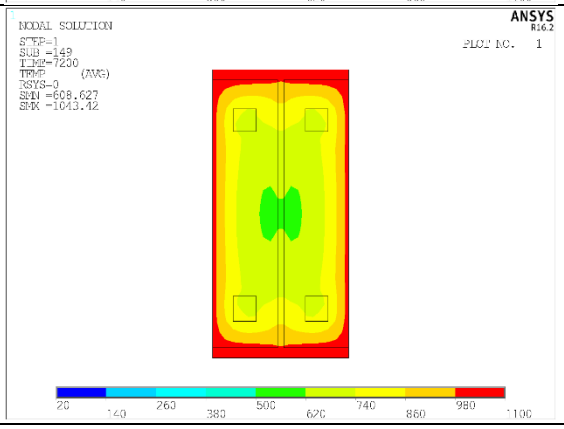

- **Profil IPE 400**

R30

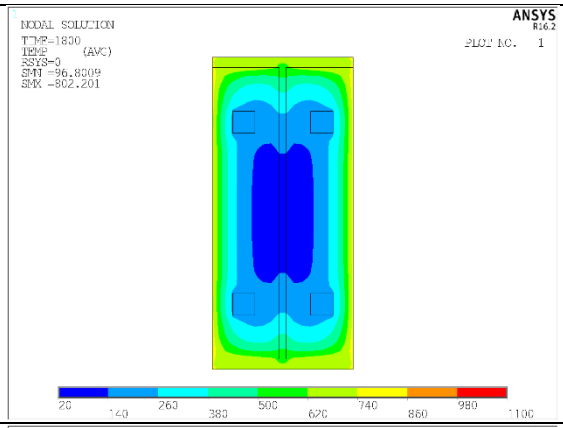

R60

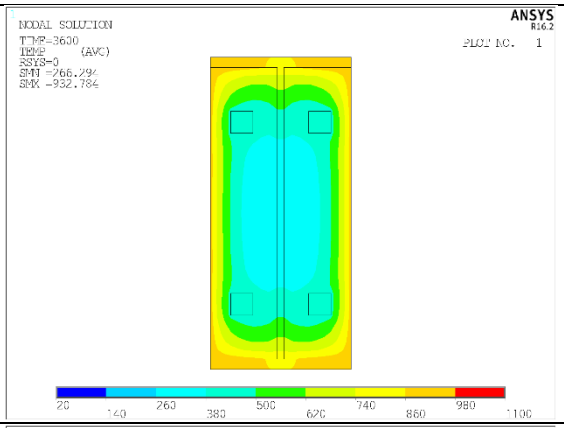

R90

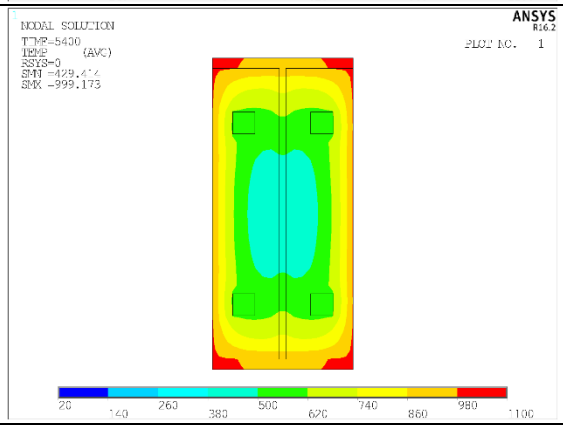

R120

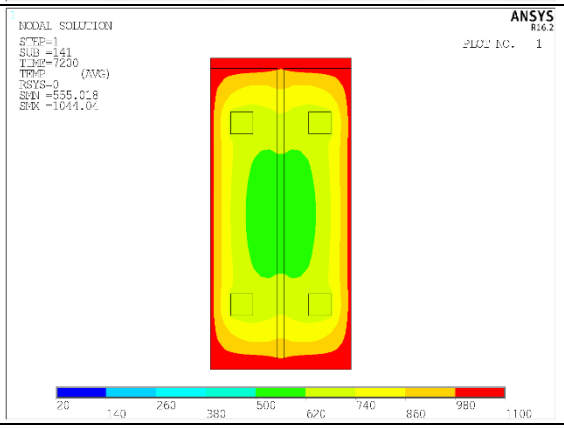

- **Profil IPE 450**

R30

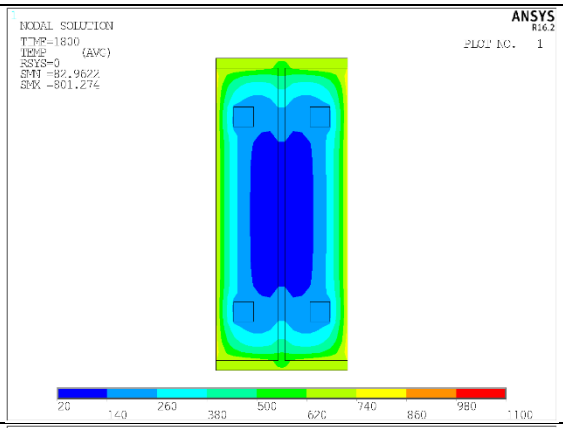

R60

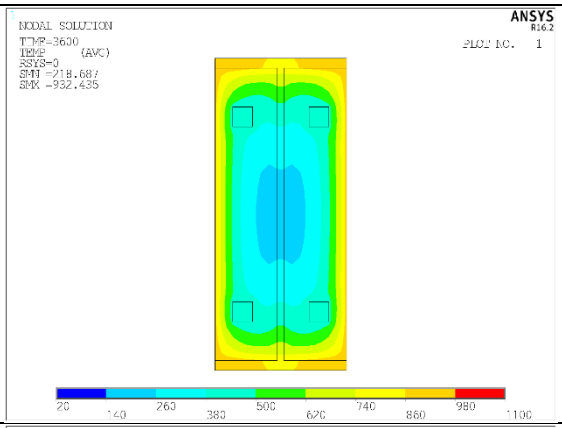

R90

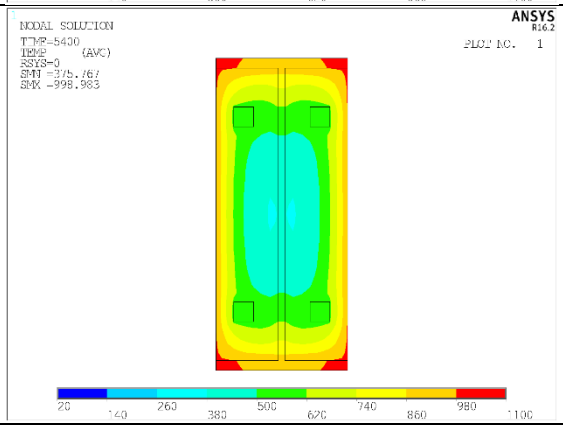

R120

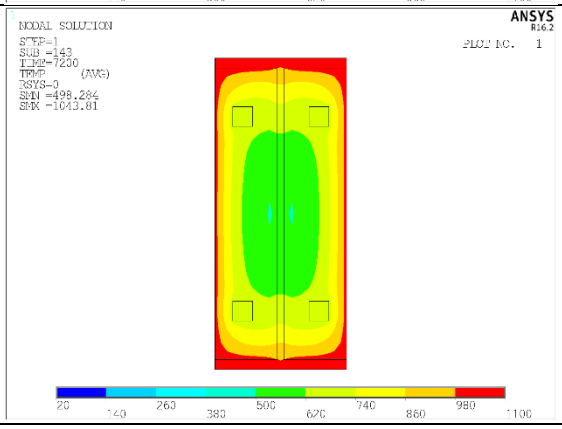

- **Profil IPE 500**

R30

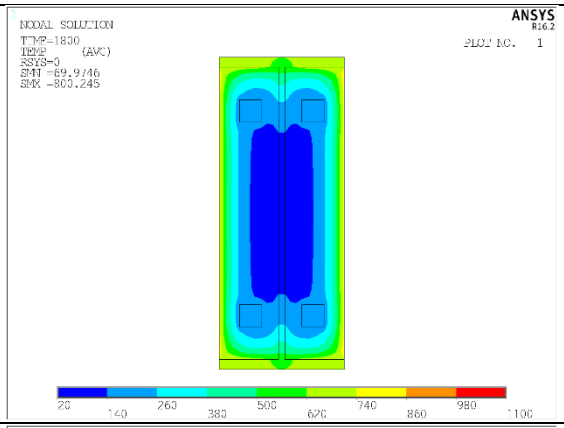

R60

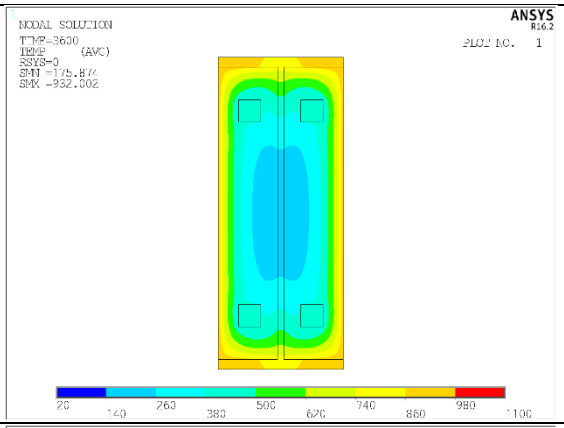

R90

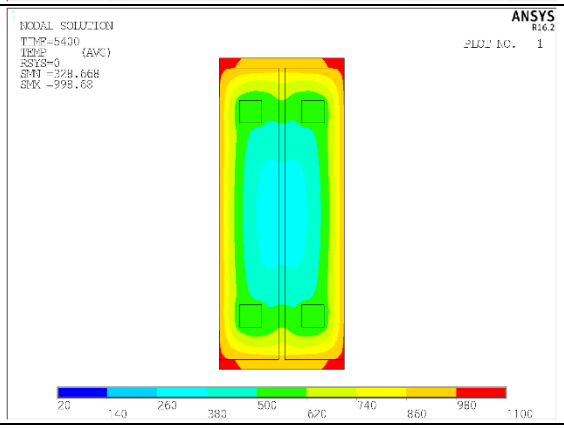

R120

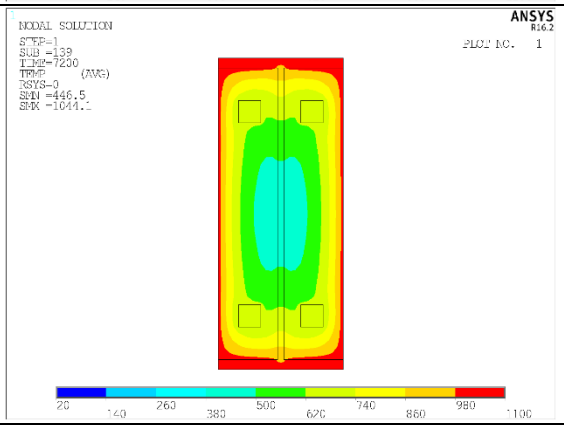

2-EIGEN BUCKLING ANALYSIS FOR 3M OF HEIGHT HEB-IPE PROFILE.

Table 1 – Critical load and linear buckling of HEB 160 for R30, R60, R90 and R120.

	R30	R60	R90	R120
1.0L				
$N_{fi,cr,z}$	425120 N	179333 N	103530 N	76799 N
0.7L				
$N_{fi,cr,z}$	862823 N	363548 N	210314 N	155851 N
0.5L				
$N_{fi,cr,z}$	1710450 N	756905 N	417492 N	308163 N

Table 2 - Critical load and linear buckling of HEB 180 for R30, R60, R90 and R120.

	R30	R60	R90	R120
1.0L				
$N_{fi,cr,z}$	714097 N	303489 N	165699 N	121194 N
0.7L				
$N_{fi,cr,z}$	1447910 N	613345 N	336085 N	245508 N
0.5L				
$N_{fi,cr,z}$	2850120 N	1189010 N	660292 N	479893 N

Table 3 - Critical load and linear buckling of HEB 200 for R30, R60, R90 and R120.

	R30	R60	R90	R120
1.0L				
$N_{fi,cr,z}$	1446150 N	665935 N	328356 N	211551 N
0.7L				
$N_{fi,cr,z}$	2908630 N	1321970 N	656510 N	424708 N
0.5L				
$N_{fi,cr,z}$	5533210 N	2412180 N	1226380 N	803119 N

Table 4 - Critical load and linear buckling of HEB 220 for R30, R60, R90 and R120.

	R30	R60	R90	R120
1.0L				
$N_{fi,cr,z}$	2669200 N	1297070 N	650152 N	354627 N
0.7L				
$N_{fi,cr,z}$	5323080 N	2536380 N	1268720 N	705370 N
0.5L				
$N_{fi,cr,z}$	9782910 N	4407320 N	2213330 N	1290200 N

Table 5 - Critical load and linear buckling of HEB 240 for R30, R60, R90 and R120.

	R30	R60	R90	R120
1.0L				
$N_{fi,cr,z}$	3822930 N	1907690 N	999870 N	504787 N
0.7L				
$N_{fi,cr,z}$	7613460 N	3732390 N	1941110 N	1002950 N
0.5L				
$N_{fi,cr,z}$	13867700 N	6441320 N	3316050 N	1815180 N

Table 6 - Critical load and linear buckling of HEB 260 for R30, R60, R90 and R120.

	R30	R60	R90	R120
1.0L				
$N_{fi,cr,z}$	6689220 N	3539320 N	1908240 N	924492 N
0.7L				
$N_{fi,cr,z}$	13136900 N	6786840 N	3604570 N	1789730 N
0.5L				
$N_{fi,cr,z}$	22789300 N	11071200 N	5768880 N	3020740 N

Table 7 - Critical load and linear buckling of HEB 280 for R30, R60, R90 and R120.

	R30	R60	R90	R120
1.0L				
$N_{fi,cr,z}$	8749830 N	4712810 N	2630180 N	1347330 N
0.7L				
$N_{fi,cr,z}$	17150300 N	9044590 N	7984100 N	2585060 N
0.5L				
$N_{fi,cr,z}$	29469700 N	14692900 N	7939250 N	4249790 N

Table 8 - Critical load and linear buckling of HEB 300 for R30, R60, R90 and R120.

	R30	R60	R90	R120
1.0L				
$N_{fi,cr,z}$	11398000 N	6154250 N	3531520 N	1892900 N
0.7L				
$N_{fi,cr,z}$	22307400 N	11811800 N	6703910 N	3619720 N
0.5L				
$N_{fi,cr,z}$	38058400 N	19112800 N	10667000 N	5870770 N

Table 9 - Critical load and linear buckling of HEB 320 for R30, R60, R90 and R120.

	R30	R60	R90	R120
1.0L				
$N_{fi,cr,z}$	12113900 N	6447800 N	3731820 N	2043140 N
0.7L				
$N_{fi,cr,z}$	23776800 N	12427000 N	7124730	3906730 N
0.5L				
$N_{fi,cr,z}$	40939300 N	20325300 N	11478700 N	6396210 N

Table 10 - Critical load and linear buckling of HEB 340 for R30, R60, R90 and R120.

	R30	R60	R90	R120
1.0L				
$N_{fi,cr,z}$	15834200 N	8657350 N	5042040 N	2723130 N
0.7L				
$N_{fi,cr,z}$	30411600 N	16389400 N	9426050 N	5123840 N
0.5L				
$N_{fi,cr,z}$	51291200 N	25822700 N	14612200 N	8074510 N

Table 11 - Critical load and linear buckling of HEB 360 for R30, R60, R90 and R120.

	R30	R60	R90	R120
1.0L				
$N_{fi,cr,z}$	16407700 N	8890350 N	5208420 N	2846500 N
0.7L				
$N_{fi,cr,z}$	31909800 N	16893700 N	9787080 N	5380520 N
0.5L				
$N_{fi,cr,z}$	53691800 N	26849400 N	15328500 N	8559780 N

Table 12 - Critical load and linear buckling of HEB 400 for R30, R60, R90 and R120.

	R30	R60	R90	R120
1.0L				
$N_{fi,cr,z}$	18011400 N	10325500 N	6566190 N	4057310 N
0.7L				
$N_{fi,cr,z}$	35145700 N	19694400 N	12345900 N	7559020 N
0.5L				
$N_{fi,cr,z}$	59740000 N	31528900 N	19313600 N	12106400 N

Table 13 - Critical load and linear buckling of HEB 450 for R30, R60, R90 and R120.

	R30	R60	R90	R120
1.0L				
$N_{fi,cr,z}$	19538900 N	10113000 N	6989840 N	4376710 N
0.7L				
$N_{fi,cr,z}$	38278100 N	20925500 N	13244500 N	8230330 N
0.5L				
$N_{fi,cr,z}$	65826800 N	33994100 N	21108600 N	13010000 N

Table 14 - Critical load and linear buckling of HEB 500 for R30, R60, R90 and R120.

	R30	R60	R90	R120
1.0L				
$N_{fi,cr,z}$	20978300 N	11461600 N	7372810 N	4679820 N
0.7L				
$N_{fi,cr,z}$	41227500 N	22058000 N	14040100 N	8856330 N
0.5L				
$N_{fi,cr,z}$	71591000 N	36258700 N	22705800 N	14237900 N

Table 15 - Critical load and linear buckling of IPE200 for R30, R60, R90 and R120.

	R30	R60	R90	R120
1.0L				
$N_{fi,cr,z}$	56850 N	25163 N	16770 N	11875N
0.7L				
$N_{fi,cr,z}$	116206 N	51417 N	32800 N	24256 N
0.5L				
$N_{fi,cr,z}$	218298 N	95340 N	60608 N	44655 N

Table 16 - Critical load and linear buckling of IPE220 for R30, R60, R90 and R120.

	R30	R60	R90	R120
1.0L				
$N_{fi,cr,z}$	123599 N	48607 N	27778 N	20459 N
0.7L				
$N_{fi,cr,z}$	252259 N	99140 N	56690 N	41710 N
0.5L				
$N_{fi,cr,z}$	465156 N	180359 N	103250 N	75310 N

Table 17 - Critical load and linear buckling of IPE240 for R30, R60, R90 and R120.

	R30	R60	R90	R120
1.0L				
$N_{fi,cr,z}$	206646 N	82599 N	42542 N	31156 N
0.7L				
$N_{fi,cr,z}$	420869 N	167804 N	86683 N	63382 N
0.5L				
$N_{fi,cr,z}$	777556 N	305079 N	159486 N	115592 N

Table 18 - Critical load and linear buckling of IPE270 for R30, R60, R90 and R120.

	R30	R60	R90	R120
1.0L	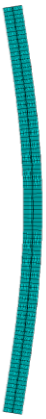	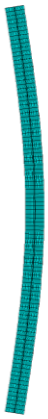	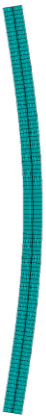	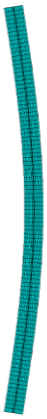
$N_{fi,cr,z}$	468282 N	195670 N	80855 N	59587 N
0.7L				
$N_{fi,cr,z}$	947980 N	393113 N	163948 N	120421 N
0.5L				
$N_{fi,cr,z}$	1820970 N	736244 N	317046 N	230237 N

Table 19 - Critical load and linear buckling of IPE300 for R30, R60, R90 and R120.

	R30	R60	R90	R120
1.0L				
$N_{fi,cr,z}$	743268 N	328337 N	131178 N	92677 N
0.7L				
$N_{fi,cr,z}$	1500280 N	656840 N	264967 N	186731 N
0.5L				
$N_{fi,cr,z}$	2835790 N	1206100 N	503094 N	351434 N

Table 20 - Critical load and linear buckling of IPE330 for R30, R60, R90 and R120.

	R30	R60	R90	R120
1.0L				
$N_{fi,cr,z}$	1007290 N	458654 N	195199 N	126058 N
0.7L				
$N_{fi,cr,z}$	2030690 N	916430 N	392564 N	253714 N
0.5L				
$N_{fi,cr,z}$	3810850 N	1671270 N	732762 N	474199 N

Table 21 - Critical load and linear buckling of IPE360 for R30, R60, R90 and R120.

	R30	R60	R90	R120
1.0L				
$N_{fi,cr,z}$	1825850 N	867928 N	373768 N	218395 N
0.7L				
$N_{fi,cr,z}$	3645910 N	1709150 N	739540 N	424759 N
0.5L				
$N_{fi,cr,z}$	6582720 N	2972470 N	1310640 N	782611 N

Table 22 - Critical load and linear buckling of IPE400 for R30, R60, R90 and R120.

	R30	R60	R90	R120
1.0L				
$N_{fi,cr,z}$	2387850 N	1256197 N	640672 N	285757 N
0.7L				
$N_{fi,cr,z}$	4774130 N	2480820 N	1254390 N	570420 N
0.5L				
$N_{fi,cr,z}$	8621540 N	4317830 N	2149410 N	1031460 N

Table 23 - Critical load and linear buckling of IPE450 for R30, R60, R90 and R120.

	R30	R60	R90	R120
1.0L				
$N_{fi,cr,z}$	3047200 N	1624470 N	855944 N	386856 N
0.7L				
$N_{fi,cr,z}$	6089110 N	3208400 N	1676310 N	771249 N
0.5L				
$N_{fi,cr,z}$	10961400 N	5582970 N	2873660 N	1389660 N

Table 24 - Critical load and linear buckling of IPE500 for R30, R60, R90 and R120.

	R30	R60	R90	R120
1.0L				
$N_{fi,cr,z}$	4221590 N	2410380 N	1398400 N	760200N
0.7L				
$N_{fi,cr,z}$	8411240 N	4735830 N	2710810 N	1476500N
0.5L				
$N_{fi,cr,z}$	15025700N	8146720 N	4549151 N	2499671 N

3- EIGEN BUCKLING ANALYSIS FOR 5M OF HEIGHT HEB-IPE PROFILE

Table 25 - Critical load and linear buckling of HEB 160 for R30, R60, R90 and R120.

	R30	R60	R90	R120
1.0L				
$N_{fi,cr,z}$	160217 N	67035 N	38660 N	28664 N
0.7L				
$N_{fi,cr,z}$	327045 N	136773 N	78936 N	58506 N
0.5L				
$N_{fi,cr,z}$	671192 N	279780 N	162006 N	119857 N

Table 26 - Critical load and linear buckling of HEB 180 for R30, R60, R90 and R120.

	R30	R60	R90	R120
1.0L	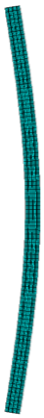	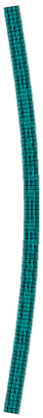	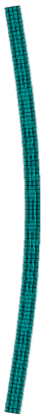	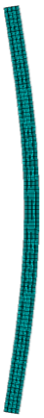
$N_{fi,cr,z}$	266806 N	112999 N	61531 N	45009 N
0.7L				
$N_{fi,cr,z}$	544431 N	230300 N	125570 N	91810 N
0.5L				
$N_{fi,cr,z}$	1113760 N	467896 N	256586 N	187175 N

Table 27 - Critical load and linear buckling of HEB 200 for R30, R60, R90 and R120.

	R30	R60	R90	R120
1.0L	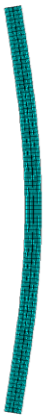	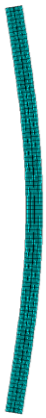	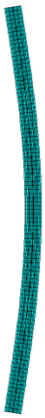	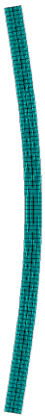
$N_{fi,cr,z}$	539295 N	249674 N	122422 N	78681 N
0.7L				
$N_{fi,cr,z}$	1094270 N	505452 N	248500 N	159960 N
0.5L				
$N_{fi,cr,z}$	2211110 N	997458 N	495812 N	321105 N

Table 28 - Critical load and linear buckling of HEB 220 for R30, R60, R90 and R120.

	R30	R60	R90	R120
1.0L				
$N_{fi,cr,z}$	993750 N	488235 N	244728 N	132047 N
0.7L				
$N_{fi,cr,z}$	2015480 N	982690 N	492031 N	267512 N
0.5L				
$N_{fi,cr,z}$	3996180 N	1890170 N	945219 N	528259 N

Table 29 - Critical load and linear buckling of HEB 240 for R30, R60, R90 and R120.

	R30	R60	R90	R120
1.0L		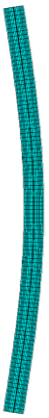		
$N_{fi,cr,z}$	1419390 N	715735 N	376544 N	187579 N
0.7L				
$N_{fi,cr,z}$	2877290 N	1440990 N	755575 N	379889 N
0.5L				
$N_{fi,cr,z}$	5681200 N	2765470 N	1436050 N	746987 N

Table 30 - Critical load and linear buckling of HEB 260 for R30, R60, R90 and R120.

	R30	R60	R90	R120
1.0L				
$N_{fi,cr,z}$	2495050 N	1339620 N	729146 N	347898 N
0.7L				
$N_{fi,cr,z}$	5031110 N	2675860 N	1446940 N	697411 N
0.5L				
$N_{fi,cr,z}$	9685960 N	4965170 N	2636340 N	1316490 N

Table 31 - Critical load and linear buckling of HEB 280 for R30, R60, R90 and R120.

	R30	R60	R90	R120
1.0L				
$N_{fi,cr,z}$	3262430 N	1780430 N	1002370 N	509303 N
0.7L				
$N_{fi,cr,z}$	6573990 N	3558020 N	1991860 N	1017410 N
0.5L				
$N_{fi,cr,z}$	12594700N	6593170 N	3630010 N	1891100 N

Table 32 - Critical load and linear buckling of HEB 300 for R30, R60, R90 and R120.

	R30	R60	R90	R120
1.0L				
$N_{fi,cr,z}$	4249060 N	2322610 N	1342930 N	716536 N
0.7L				
$N_{fi,cr,z}$	8558030 N	4642240 N	2671670 N	1429680 N
0.5L				
$N_{fi,cr,z}$	16333200 N	8586850 N	4872970 N	2638280 N

Table 33 - Critical load and linear buckling of HEB 320 for R30, R60, R90 and R120.

	R30	R60	R90	R120
1.0L				
$N_{fi,cr,z}$	4509330 N	2426760 N	1414580 N	768447 N
0.7L				
$N_{fi,cr,z}$	9092100 N	4860220 N	2820610 N	1535870 N
0.5L				
$N_{fi,cr,z}$	17439200 N	9052180 N	5190500 N	2853760 N

Table 34 - Critical load and linear buckling of HEB 340 for R30, R60, R90 and R120.

	R30	R60	R90	R120
1.0L				
$N_{fi,cr,z}$	5933640 N	3295050 N	1636310 N	1042140 N
0.7L				
$N_{fi,cr,z}$	11910000 N	6549300 N	3827180 N	2065080 N
0.5L				
$N_{fi,cr,z}$	22420400 N	11876900 N	6836800 N	3729070 N

Table 35 - Critical load and linear buckling of HEB 360 for R30, R60, R90 and R120.

	R30	R60	R90	R120
1.0L				
$N_{fi,cr,z}$	6139960 N	3376620 N	1994330 N	1086960 N
0.7L				
$N_{fi,cr,z}$	12336500 N	6721110 N	3950070 N	2157910 N
0.5L				
$N_{fi,cr,z}$	23326600 N	12262200 N	7111600 N	3925130 N

Table 36 - Critical load and linear buckling of HEB 400 for R30, R60, R90 and R120.

	R30	R60	R90	R120
1.0L				
$N_{fi,cr,z}$	6729200 N	3913480 N	2513580 N	1564100 N
0.7L				
$N_{fi,cr,z}$	13537600 N	7801630 N	4980140 N	3085930 N
0.5L				
$N_{fi,cr,z}$	25744600 N	14312000 N	8968100 N	5500910 N

Table 37 - Critical load and linear buckling of HEB 450 for R30, R60, R90 and R120.

	R30	R60	R90	R120
1.0L				
$N_{fi,cr,z}$	7284880 N	4124890 N	2664670 N	1679020 N
0.7L				
$N_{fi,cr,z}$	14677900 N	8240000 N	5296080 N	3325700 N
0.5L				
$N_{fi,cr,z}$	28097600 N	15254800 N	9658940 N	6017200 N

Table 38 - Critical load and linear buckling of HEB 500 for R30, R60, R90 and R120.

	R30	R60	R90	R120
1.0L				
$N_{fi,cr,z}$	7809470 N	4324960 N	2804280 N	1790180 N
0.7L				
$N_{fi,cr,z}$	15754200 N	8652030 N	5584720 N	3555230 N
0.5L				
$N_{fi,cr,z}$	30318600 N	16126600 N	10277200 N	6503410 N

Table 39 - Critical load and linear buckling of IPE200 for R30, R60, R90 and R120.

	R30	R60	R90	R120
1.0L				
$N_{fi,cr,z}$	22450 N	9610 N	6119 N	4515 N
0.7L				
$N_{fi,cr,z}$	45924 N	19660 N	12516 N	9233 N
0.5L				
$N_{fi,cr,z}$	89124 N	37959 N	24135 N	17780 N

Table 40 - Critical load and linear buckling of IPE220 for R30, R60, R90 and R120.

	R30	R60	R90	R120
1.0L				
$N_{fi,cr,z}$	47921 N	18615 N	10547 N	7762 N
0.7L				
$N_{fi,cr,z}$	97996 N	38059 N	21567 N	15867 N
0.5L				
$N_{fi,cr,z}$	188610 N	72870 N	41327 N	30288 N

Table 41 - Critical load and linear buckling of IPE240 for R30, R60, R90 and R120.

	R30	R60	R90	R120
1.0L				
$N_{fi,cr,z}$	83389 N	33211 N	16672 N	7762 N
0.7L				
$N_{fi,cr,z}$	97996 N	38059 N	21567 N	15867 N
0.5L				
$N_{fi,cr,z}$	188610 N	72870 N	41327 N	30288 N

Table 42 - Critical load and linear buckling of IPE270 for R30, R60, R90 and R120.

	R30	R60	R90	R120
1.0L				
$N_{fi,cr,z}$	182438 N	77126 N	31371 N	23090 N
0.7L				
$N_{fi,cr,z}$	372109 N	156882 N	64019 N	47062 N
0.5L				
$N_{fi,cr,z}$	728223 N	303128 N	125655 N	91809 N

Table 43 - Critical load and linear buckling of IPE300 for R30, R60, R90 and R120.

	R30	R60	R90	R120
1.0L	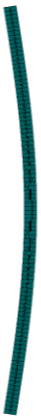	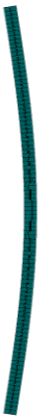		
$N_{fi,cr,z}$	284427 N	127409 N	50605 N	35477 N
0.7L				
$N_{fi,cr,z}$	372109 N	258741 N	103133 N	72229 N
0.5L				
$N_{fi,cr,z}$	1124120 N	494408 N	200572 N	139710 N

Table 44 - Critical load and linear buckling of IPE330 for R30, R60, R90 and R120.

	R30	R60	R90	R120
1.0L				
$N_{fi,cr,z}$	382542 N	176691 N	75368 N	48129 N
0.7L				
$N_{fi,cr,z}$	779070 N	358679 N	153359 N	97957 N
0.5L				
$N_{fi,cr,z}$	1505010 N	682487 N	295625 N	188806 N

Table 45 - Critical load and linear buckling of IPE360 for R30, R60, R90 and R120.

	R30	R60	R90	R120
1.0L				
$N_{fi,cr,z}$	689999 N	332665 N	144068 N	83394 N
0.7L				
$N_{fi,cr,z}$	1400281 N	671562 N	291381 N	169051N
0.5L				
$N_{fi,cr,z}$	2645950 N	1241010 N	544868 N	318875 N

Table 46 - Critical load and linear buckling of IPE400 for R30, R60, R90 and R120.

	R30	R60	R90	R120
1.0L				
$N_{fi,cr,z}$	897890 N	478013 N	246569 N	109232 N
0.7L				
$N_{fi,cr,z}$	1823040 N	966056 N	496668 N	221682 N
0.5L				
$N_{fi,cr,z}$	344910 N	1786670 N	909233 N	419756 N

Table 47 - Critical load and linear buckling of IPE450 for R30, R60, R90 and R120.

	R30	R60	R90	R120
1.0L				
$N_{fi,cr,z}$	1142900 N	616655 N	328879 N	148788 N
0.7L				
$N_{fi,cr,z}$	2320200 N	1246360 N	662579 N	301890 N
0.5L				
$N_{fi,cr,z}$	4375200 N	2303930 N	1213140 N	570965 N

Table 48 - Critical load and linear buckling of IPE500 for R30, R60, R90 and R120.

	R30	R60	R90	R120
1.0L				
$N_{fi,cr,z}$	1586330 N	917328 N	539266 N	294827 N
0.7L				
$N_{fi,cr,z}$	3215970 N	1850340 N	1081980 N	592085 N
0.5L				
$N_{fi,cr,z}$	6035790 N	3392580 N	1950240 N	1074460 N